DESIGN AND DEVELOPMENT OF OFFSHORE MOBILE ELECTRICITY GENERATION SYSTEM USING DAMPING WAVE ENERGY CONVERTER

WONG YI HONG

MASTER OF ENGINEERING SCIENCE

LEE KONG CHIAN FACULTY OF ENGINEERING AND SCIENCE
UNIVERSITI TUNKU ABDUL RAHMAN
JUNE 2019

DESIGN AND DEVELOPMENT OF OFFSHORE MOBILE ELECTRICITY GENERATION SYSTEM USING DAMPING WAVE ENERGY CONVERTER

By

WONG YI HONG

A dissertation submitted to the
Lee Kong Chian Faculty of Engineering and Science,
Universiti Tunku Abdul Rahman,
In partial fulfillment of the requirements for the degree of
Master of Engineering Science
June 2019

DECLARATION

I hereby declare that the dissertation is based on my original work except for quotations and citations which have been duly acknowledged. I also declare that it has not been previously or concurrently submitted for any other degree at UTAR or other institutions.

Name _____

Date _____

APPROVAL SHEET

This thesis entitled "**DESIGN AND DEVELOPMENT OF OFFSHORE MOBILE ELECTRICITY GENERATION SYSTEM USING DAMPING WAVE ENERGY CONVERTER**" was prepared by WONG YI HONG and submitted as partial fulfillment of the requirements for the degree of Master of Engineering Science at Universiti Tunku Abdul Rahman.

Approved by:

_____
(Dr. Lai An Chow)
Date:……..
Supervisor
Department of Electrical and Electronic
Lee Kong Chian Faculty of Engineering Science
Universiti Tunku Abdul Rahman

_____
(Prof. Chong Kok Keong)
Date:……..
Co-supervisor
Department of Electrical and Electronic
Lee Kong Chian Faculty of Engineering Science
Universiti Tunku Abdul Rahman

LEE KONG CHIAN FACULTY OF ENGINEERING AND SCIENCE

UNIVERSITI TUNKU ABDUL RAHMAN

Date: _____

SUBMISSION OF DISSERTATION

It is hereby certified that Wong Yi Hong (ID No: 1506764) has completed this dissertation entitled "Design And Development Of Offshore Mobile Electricity Generation System Using Damping Wave Energy Converter" under the supervision of Dr. Lai An Chow (Supervisor) from the Department of Electrical and Electronic Engineering, Lee Kong Chian Faculty Of Engineering And Science, and Prof. Chong Kok Keong (Co Supervisor) from the Department of Electrical and Electronic Engineering, Lee Kong Chian Faculty Of Engineering And Science.

I understand that University will upload softcopy of dissertation in pdf format into UTAR Institutional Repository, which may be made accessible to UTAR community and public.

Yours truly,

_____

(*Wong Yi Hong*)

ACKNOWLEDGEMENT

First and foremost, I would like to express my earnest gratitude to my research supervisor, Dr. Lai An Chow for his guidance and invaluable insights that have been immensely helpful throughout the research development as well as my research co-supervisor Prof. Chong Kok Keong for the continuous support and advises over the course of the research progress.

In addition, I would like to specially thank Mr. King Yeong Jin for his technical knowledge supports and provided important hardware for the research purpose.

Also, I would like to thank the UTAR Center of Risk Reduction for providing access to the shaking table equipment for purpose of research and Mr. Lim Jun Xian for aiding me with guiding and operating the said equipment for the length of research.

Moreover, I would like to thank UTAR for providing the Research Scholar Scheme during the research period with the number: IPSR/RMC/UTAR RF/2014-C2/L01.

Last but not least, my sincere thanks go to everyone who have helped with the research and my beloved family as well.

ABSTRACT

Design and Development of Offshore Mobile Electricity Generation System using Damping Wave Energy Converter

Wong Yi Hong

This research is intended to study the feasibility of harnessing ocean wave energy using a damping wave energy converter (DWEC), a type of passive damping device that operates similarly to a tuned liquid column damper (TLCD) that is designed to reduce externally induced vibration at a designated frequency range, albeit with the ability to harvest wave energy simultaneously. The proposed DWEC can be integrated with a floating offshore structure to operate as a vibration suppressing device through reduction of dynamic response of the structure due to wave impact and simultaneously generating electricity through the oscillating flow of stored liquid within the DWEC. The constructed DWEC prototype is tuned according to the theoretical study and tested with two different sets of design using a shaking table with a set of predetermined frequency range and a third set that is simulated using commercial CFD software ANSYS Fluent. With that, the amount of energy extractable from the oscillating water motion within the DWEC column are studied as well.

TABLE OF CONTENTS

LIST OF TABLES

LIST OF FIGURES

CHAPTER 1

INTRODUCTION

1.1 Background of Study

Ocean wave energy is a highly concerned renewable energy resource to be harnessed worldwide since over 70% of Earth's surface is covered by ocean. Despite that wave power varies depending on locations, the estimated global ocean average wave power is above 2 TW (Gunn et al., 2012). As of now, there are four common categories of wave energy converter (WEC) technologies that have been tested and deployed: the oscillating water column (OWC) terminators, attenuators, point absorbers, and overtopping terminators.

The operating principle of OWC is further discussed since it is one of the mechanism that is adopted by the author as part of the hardware design. An OWC can be installed onshore (LIMPET by WaveGen), near-shore (Oceanlix by Energetch) and offshore (OE Buoy by Ocean energy Ltd) individually depending on the availability of locations, but the general working principle is basically identical: a partially-submerged hollow structure that capture ocean energy from the impacted ocean wave at the opening beneath through compression and decompression of confined air within the structure which are

forced through an air turbine that is coupled with a generator. In comparison to most other types of WECs, OWC provides a significant advantage due to its simplicity where the rotor of the turbine is the only moving part in the structure.

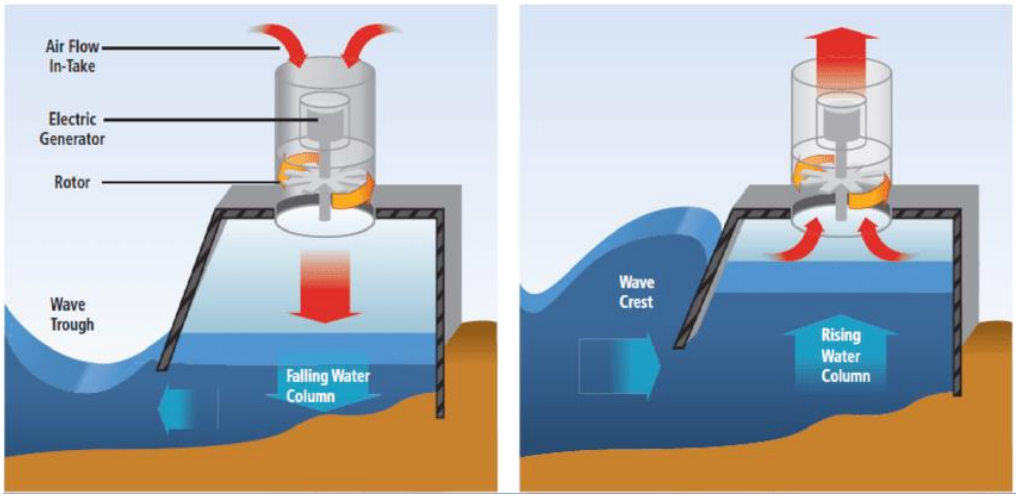

(a) (b)

Figure 1. 1: An oscillating wave column and its operation visualized (a) air flows into the chamber as wave leaves (b) air pushes out of the chamber as wave impacts. (Lewis et al. 2011)

A Tuned Liquid Column Damper (TLCD) is one of the liquid damper devices that capable of suppressing vibration by introducing damping force through the motion of liquid movement stored within the TLCD column (Xu et al., 1992). It is selectively tuned at a specific frequency so that the liquid within the TLCD oscillates out of phase with the mounted structure's motion, and effectively dissipates the externally induced motion energy acting on the structure (Connor J., 2003). The TLCD has been implemented in numerous high-rise buildings around the world, for instant, the One Wall Centre in Vancouver, Random House Tower in Manhattan, Comcast Center in

Philadelphia and other buildings to protect the buildings from damage caused by wind-induced excitation force.

In recent past, due to the increasing growth in the development and exploration of offshore structures for various kinds of applications, TLCD has been explored as a vibration mitigating device that can be installed within offshore structure such as tension-leg platform (TLP) to dissipate structural vibration induced by the ocean waves. A group of researchers, Lee et al. have studied that implementing an underwater TLCD device that is accurately tuned on an offshore floating structure is able to reduce its dynamic response to the sea waves effectively (Lee et al., 2012). In year 2015, Jianbing et al. have conducted several experiments with numerical analysis showing that a TLCD is capable of reducing the structural dynamic response of the offshore wind turbine system effectively, hence improving its serviceability and safety (Jianbing et al., 2015).

Therefore, the study here presents an endeavor to design and develop a novel type of WEC known as the DWEC (Damping wave energy converter), that adapts the energy generating mechanism of an OWC using a modified closed-circuit liquid damper that can be installed in an offshore floating platform to maintain structural stability by absorbing motion induced by ocean wave while simultaneously harness energy from the oscillating motion of contained water within the DWEC. The DWEC differs itself from other types of WEC as it can works not only as a standalone ocean wave energy harvesting

device, but serves as an auxiliary compartment of an operational floating platform too.

1.2 Problem Statement

The problem to be addressed in this study is that how the ocean wave energy can be harnessed using the tuned liquid column damper (TLCD) vibration damping mechanism. This study is to determine the feasibility of harnessing ocean wave energy through the use of a novel damping wave energy converter (DWEC) that is designed based on TLCD, a type of passive damping device that is used to suppress externally induced vibration within a specific frequency range. The proposed DWEC can be integrated with a floating offshore structure to serve as a vibration mitigating device by reducing the dynamic response of the floating structure and simultaneously utilize the oscillating flowing motion of liquid within the DWEC for generating electricity. The designed DWEC prototype is tuned accordingly to a specific frequency and tested using a shaking table with a set of predetermined frequency range. The oscillating motion of water within the DWEC and the potential of installation of hydro turbine generator in term of recoverable amount of energy are studied.

1.3 Objectives

1) To design and construct a damping wave energy converter (DWEC) based on TLCD.
2) To study the performance of the DWEC in terms of vibration mitigation.

3) To devise a feasible energy generating method using pre-existing mechanism of TLCD.
4) To evaluate the performance of designed and constructed DWEC.

1.4 Hypothesis

The designed and developed novel DWEC prototype is capable of suppressing externally induced vibration when effectively tuned in accordance to its operating condition as well as having the capability to harness power from the vibrating motion by means of installed turbine.

1.5 Significance of Study

The findings of this research will be contributing to further exploration and development of harnessing ocean wave energy particularly in Malaysia waters as part of the nation's effort to propagate the progress of utilizing the renewable energy resources that are available in the country in lieu of fossil fuels. In addition, the novelty of using a pre-existing vibration damping device as the underlying mechanism of harnessing wave energy can serve as an insight or study material for other researchers to develop new ideas or methods to extract renewable energy using technologies from different engineering fields.

1.6 Structure of Dissertation

The dissertation is structured as follows:

1. Chapter 1 provides the introductory details of the study and its problem statement, objectives, the involved hypothesis and the significance of study.
2. Chapter 2 discusses the literature reviews of ocean wave energy and its respective challenges, WECs, the wave energy perspective in Malaysia, TLCD and CFD Simulations.
3. Chapter 3 describes the methodology of how the research study is taken approach and the procedure of doing so.
4. Chapter 4 discusses the data collected from the previously established methodology and the results obtained from it.
5. Finally, chapter 5 concludes the study on how the set goals are achieved through the research works.

CHAPTER 2

LITERATURE REVIEW

2.1 Ocean Wave Energy

In today's world, renewable energy is on the rise to overtake the fossil fuels as the next primary energy source due to its availability and environmental friendliness. Such trend is especially noteworthy in the developed western countries as the EU called for an increase in electricity generated by renewable energy from 12.2% in 2002 to 20% by 2020 (Blažauskas et al., 2015) and as of 2016, 17% of energy consumed in the EU is produced by renewable energy (Ec.europa.eu, 2018). With rapid technological advancement in the energy sector, the world progressively transitioning into the golden age of low-carbon new energy source as their cost for development declines over the year. As one of the highly regarded source of renewable energy, ocean covers more than 70% of Earth's surface and carries a tremendous amount of energy that is exploitable in several forms, namely marine current, tides, salinity gradient, temperature gradient and waves.

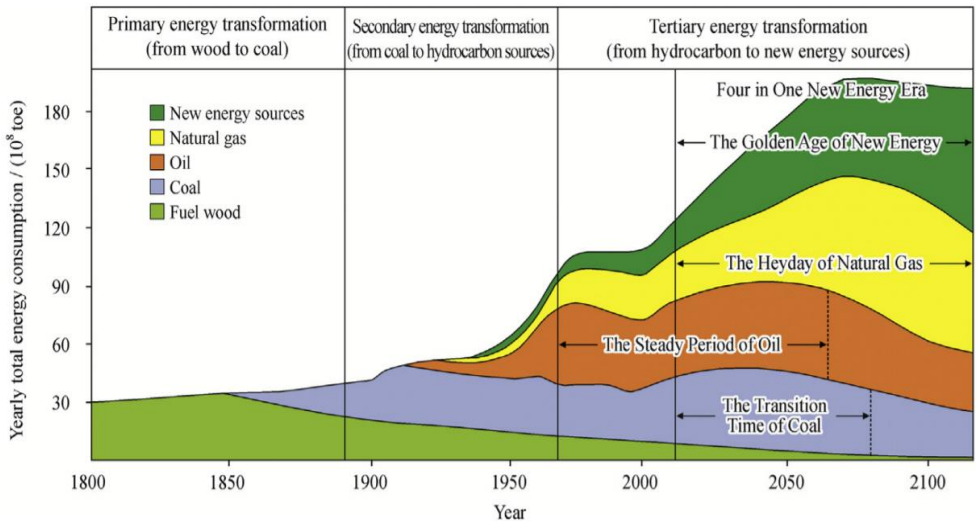

Figure 2.1: Trends and forecasts of global energy consumption (Caineng et al., 2016).

Ocean wave, alongside with ocean tides are two of the most exploitable form in the field of ocean renewable energy harvesting. The wave is created as wind blows over the surface of the ocean and the continual disturbance creates waves that can travel long distance with enough wind force and consistency. Ocean wave has greater power density (2-3kW/m^2) in comparison to wind (0.4-0.6kW/m^2) and solar (0.1-0.2kW/m^2). Although wave power varies substantially in different locations, the estimated theoretical potential wave energy is up to 29,500 TWh/yr according to IRENA (International Renewable Energy Agency) (Melikoglu M., 2018). Asides from being highly predictable, limited environmental interference and widely available from shoreline to deep waters, wave energy is also available throughout the day and thus allowing wave energy converters to generate power up to 90% of the time (Drew et al., 2009).

2.2 Development Challenges

However, exploiting ocean wave energy bring about different sets of challenges that hampers its progress on becoming a commercially viable and competitive source of electricity. For starters, in terms of design challenge, conversion of low frequency and irregular wave oscillatory motion into usable electricity requires some energy conversion stages that converts the said motion into useful motion that is capable of driving a generator to produce acceptable output. Waves can have different height and period as the sea states varies from moment to moment, carrying a different power level accordingly. Thus a wave energy harvesting device may need to operate in tandem with an external energy storage to obtain a steady power output over time (Czech et al., 2012).

For certain geographical areas, extreme ocean condition also poses a major challenge for wave energy harvesting device as well. Such device needs be over-designed to be able to withstand drastic loading especially during harsh weather that are not encountered during normal sea state to prevent catastrophic structural failure. Last but not least, one of the toughest barrier to wave energy harvesting development is the availability of funding. Despite having great potential, a new technology has to compete with the other more mature technology such as solar and wind and such endeavor can proved to be hard due to a very large sum of capital may be needed for a successful development of wave energy harvesting technology. The primary cost of developing a wave energy plant are as follows:

(i) pre-operating cost

(ii) construction costs

(iii) operational expenditure (OPEX)

(iv) decommissioning costs.

It is deduced that the cost of equipment and installation for a wave energy converter is within the range of 2.5 to 6.0 M€ per installed MW and the estimated final cost for a conveter with installed rated power of 1MW is about 3000,000 € (Astariz et al., 2015).

2.3 Wave Energy Converter (WEC)

Devices that are developed to capture ocean wave energy are commonly known as wave energy converters (WECs). There are four major types of known WEC technologies that are currently being tested and deployed around the globe, few have been built as full-scaled model in which most are found in European countries. Figure 2.2 shows the examples of WECs as compiled by Lopez et al. Each of these WECs are distinguished by their working principles as follow:

- **Oscillating water column (OWC) terminators**: comprises of two primary compartments, a partially-submerged collector chamber, where power from the waves is transfer to the air volume within the chamber, and a power take off (PTO) system that converts the air compression power into electricity typically with the use of a bi-directional axial turbine (Heath T. V., 2012).

- **Point absorbers**: generate electricity from the bobbing or pitching action of the device regardless of wave direction, by converting the up-and-down pitching motion of the waves into rotary or oscillatory movements depends on the design.
- **Attenuators**: long slim device aligned in parallel with wave direction in which energy is harnessed through the attenuation of wave amplitude with swinging motion of flexible joints that linked together a series of cylindrical section.
- **Overtopping terminators**: water is forced over the top of a reservoir that is above sea level by wave motion, and the water within is released back to the sea through turbines at the bottom.

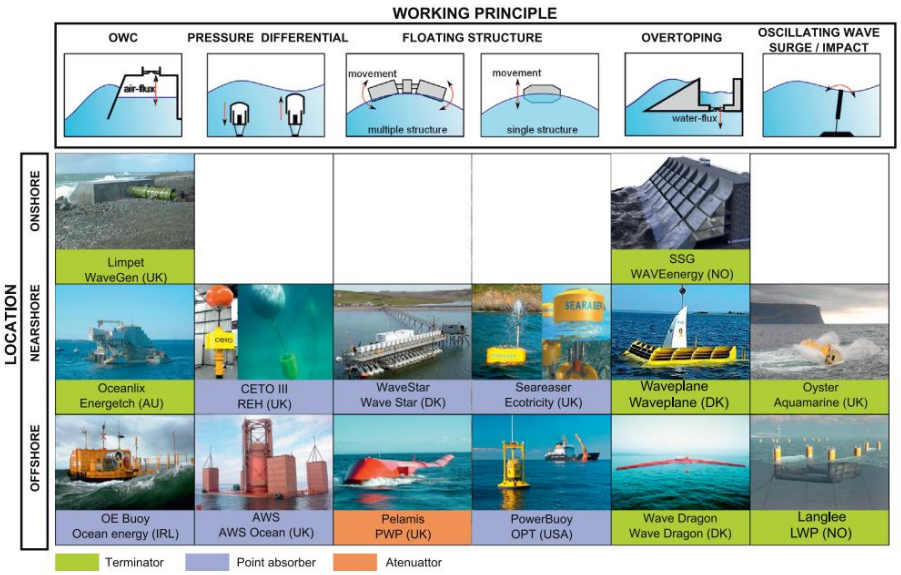

Figure 2.2: Examples of WECs with their respective working principles and examples (López et al., 2018).

The characteristics of the sea state are substantial to the design and development of a successful WEC. Therefore, localized prerequisite analysis

and resource assessment must be carried out during pre-deployment phase to obtain crucial information such as wave amplitude, period and direction beforehand as a WEC needs to be design in tuned with the sea states for maximum wave energy absorption. WECs such as the Pelamis attenuator and Wave Dragon terminator need to align themselves with the wave direction as well to capture as much wave energy as possible. As previously mentioned in the challenges for developing wave energy harvesting technology, vigorous testing and structural performance evaluation is also important for developing a WEC with high reliability to be able to survive the impact and loading from offshore natural elements.

2.4 Oscillating Wave Column (OWC)

The development progress and operating principle of OWC are further discussed as the underlying mechanism is adopted by the author as part of the prototype design which will be shown in the methodology section.

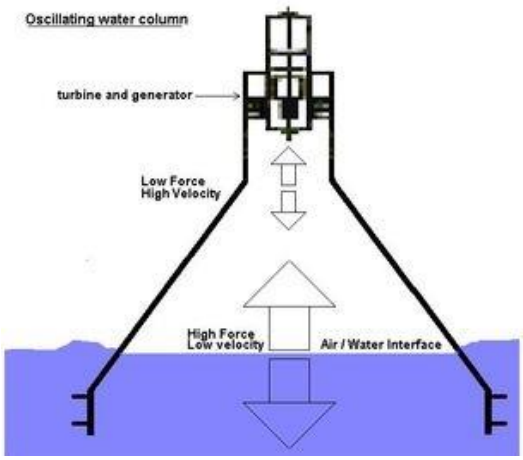

Figure 2.3: 2D illustration of an OWC (Nicole et al., 2010).

As one of the more successful type of WECs, the OWC has been consistently under development for many years past. The earliest unit of OWC was developed by a Japanese navy officer, Yoshio Masuda as a wave-powered navigation buoy that went commercial in Japan since 1965 and later on, he developed the first large-scale WEC, Kaimei, an 820 tons barge with thirteen built-in open-bottomed OWC for the Japan Marine Science and Technology Centre (JAMSTEC). The barge was deployed at the western coast of Japan in 1978-80 and again in 1985-86 for the testing of unidirectional air turbines with various rectifying valve arrangement and self-rectifying air turbines respectively. In the meantime, the study of OWC is also initiated in European countries such as United Kingdom, Scotland and Norway as more and more large-scale WEC projects took place for R&D purpose (Antonio et al., 2015). Some of the examples of large-scale OWCs are as follow:

(i) Islay LIMPET (Land Installed Marine Power Energy Transmitter): constructed in year 2000 with a proposed capacity of 500kW which later on downscaled to 250kW, developed by Queen's University of Belfast and WaveGen at the Scottish island of Islay.

(ii) Mutriku wave energy plant: built in 2006 at the Bay of Biscay in Spain and began commercial operation in 2011. With sixteen air chamber turbines installed, it produces 300kW to power two hundred and fifty household (Power Technology, 2011).

(iii) European Pico OWC plant: first built in 1995 and started autonomous operation in 2012 after various issues took place. Located at Pico Island, Portugal and with an installed capacity of 400kW (Brito-Melo et al., 2007).

Even though an OWC can be installed onshore (LIMPET by WaveGen), near-shore (Oceanlix by Energetch) and offshore (OE Buoy by Ocean energy Ltd) depending on location availability, the general working principle remains identical as previously shown.

In comparison to most other type of WECs, OWC offers a significant advantage due to its simplicity where the rotor of the turbine is the only moving part in the structure, thus making it reliable due to reduced possibility of mechanical issues and maintenance cost. Not to mention that the concept of OWC is adaptable for deployment in various forms such as on the shoreline, near shore and offshore as well.

2.5 Wave Energy Perspective in Malaysia

With an estimated coastline of 4,675km long, Malaysia is presented with ample opportunity to explore the potential of harvesting ocean wave energy. Some ocean wave studies have been carried out by different parties to assess the amount of wave resources available. Based on the assessment carried out by the Universiti Kebangsaan Malaysia using data such as satellite images within the timeline of year 1992 to 2007, it was concluded that the average annual wave energy in the Malaysian waters is within the range of 2.8kW/m to 8.6kW/m and

with the waters of Sarawak and Terrenganu having the best opportunity for wave energy development (Nasir et al., 2016).

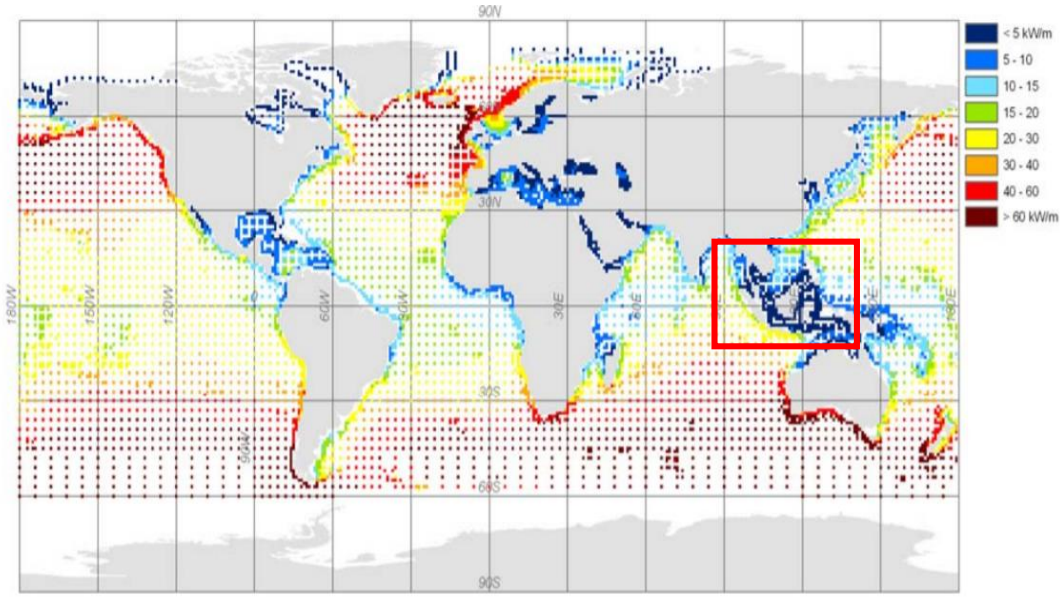

Figure 2.4: Annual global gross theoretical wave power for all WorldWaves grid points worldwide, with the red square highlighting the waters surrounding Malaysia (Mork et al., 2010).

The detail ocean wave characteristics and climate prediction of territorial waters surrounding the Peninsular Malaysia is also studied by University of Terengganu Malaysia in 2011. Although ocean waves in general are almost always irregular as multiple regular waves with different frequencies and amplitudes superimpose over each other, the representative wave condition in a given area can be determined using meteorological data. It is discovered that with a total wave energy density of 17.69MWh/m, more than 60% of the annual wave energy is generated by waves of height between 0.2 to 1.2m and more than 70% of those is accounted by wave with peak period of 2 to 8s (Muzathik et al., 2011). These information are essential to the design and development of wave energy harvesting device that are set to deploy to the said

areas. The wave energy resource particularly at the coast of Terengganu shown great potential for wave power exploitation especially during northeast monsoon season where the general wave direction is to the North and the occurrence of wave heights higher than 2m are between 32-44% (Muzathik et al., 2011).

However, the general consensus for the development of ocean wave energy in Malaysia is deemed to be difficult as an average wave power of equal or more than 15kW/m is required to be economically viable for commercial scale development with current WEC technologies, while the available average wave power in Malaysia waters is only 8.5kW/m (Samrat et al., 2014). Hence, despite the exploitation of resource in water areas with relatively lower wave power density is still a challenge, but it can be overcomed with the deployment of small-scale or isolated wave energy harvesting devices that are capable of utilizing the said low power density.

To that end, some OWC prototypes have been built and tested by local researchers with emphasis on conceptual feasibility. A 1:5 OWC model is design and constructed by Marine Technology Centre in Universiti Technologi Malaysia to study its operating performance in Malaysia sea waters condition. Although no actual values on power generation is provided, the model was shown to be capable of harvesting wave energy using a two-stage Savonius turbine through wave tank experiment at wave period of 2-3s that corresponds to the characteristic of Malaysia waters (Yaakob et al., 2013). Inspired by the Powerbuoy and Islay LIMPET, another WEC prototype known as the UMT Evo

Wave Power that utilizes oscillating bodies technology is being built by Universiti Malaysia Terengganu (UMT) and tested off the coast of Terrenganu (Akmal et al., 2016). The WEC prototypes reviewed here are developed solely for energy generation while the proposed DWEC can do the same and provide stabilization simultaneously.

2.6 Tuned Liquid Column Damper (TLCD)

First proposed by Sakai et al. in 1989, a tuned liquid column damper is one of the passive damper type that can reduce vibration force by introducing damping through the motion of moving liquid contained within the column (Xu et al., 1992). It is technically a modification from an existing damping mechanism known as the tuned mass damper (TMD), a widely used damper which installed as a system's auxiliary mass to absorb undesired vibration, albeit filled with liquid instead of solid mass. A TLCD is tuned at a specific frequency so the liquid contained within oscillates in such a way that is out of phase with the structure's motion, thus counteracting and dissipating externally induced energy acting on the structure (Connor J., 2003).

Structural vibration control is essential to tall buildings as they are more susceptible to environmental loadings due to greater structural response towards uncontrolled wind loading and seismic activity, which may bring discomfort to the occupants within and even leads to structural failure. Aside from using base isolation method, one of the more commonly used solution is the inclusion of TMD within the building to suppress the structural response caused by these

dynamic loadings, some of the well-known examples are Shanghai Tower in China, Taipei 101 in Taiwan, Fernsehturm Berlin in Germany and etc.

The TLCD's performance in terms of structural vibration reduction has been thoroughly studied and analyzed over the course of decades and it is known to be as effective as the TMD (Gao et al., 2006) and even offers some advantages in different aspects in comparison to the TMD. Apart from both TLCD and TMD are capable of operating in passive mode, the TLCD has a well understood mathematical model, which enables the precise tuning of damping based on user requirement. One of the advantages of TLCD also includes the absence of active mechanism within, thus leads to lower cost and maintenance work, high adaptability and versatility due to the arbitrariness of damper's shape, and also ease of parameter controlling since the natural frequency of the TLCD can be easily tuned by adjusting the water level within the damper (Min et al., 2005) (Ve et al., 2015). In recent study, the TLCD also can be utilized as a mean to control the seismic response of a base-isolated structure, thus further improves the building's structural stability especially against earthquake motion (Di et al., 2016).

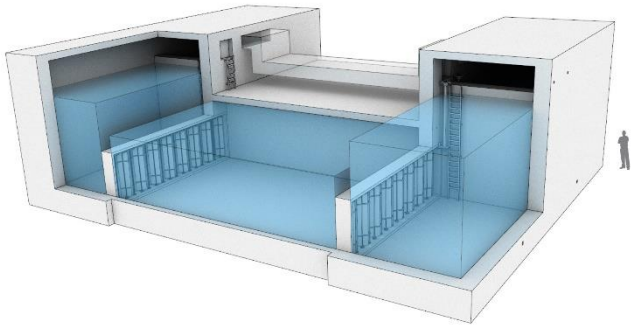

Figure 2.5: TLCD installed within Comcast Center (RWDI, 2016)

Throughout the years, TLCD has been installed in several known high-rise buildings around the world such as the Comcast Center in Philadelphia, PA (Avril. T., 2007), One Wall Centre in Vancouver (Glotmansimpson.com, 2016), Random House Tower in Manhattan (Tamboli et al., 2005) and others as well. Some researchers have too explored the possibility of utilizing TLCD in footbridge and long span cable-stayed bridge construction. The investigations have shown that the TLCD can provide effective damping for undesired pedestrian induced vibrations and significantly reduces the lateral and torsional displacement response of the cable-stayed bridge due to wind loading respectively (Reiterer et al., 2004) (Shum et al., 2007). Moreover, installation of TLCD that weighs 1.5% of the mass of wind turbine towers can reduces peak response due to wind loading by 53% and reduces their annual failing rate by 11%, thereby improves their long-term reliability and lower damage risk (Mensah et al., 2013).

2.7 Offshore TLCD Applications

In recent past, due to the growth in exploration and development of offshore structures of various kinds of applications, the applicability and effectiveness of integrating a TLCD with an offshore structure as a vibration mitigating device has been studied considerably as well. Vibration mitigation is necessary for offshore operations since out in the open sea, these offshore platforms are subjected to all kinds of loadings from its surrounding environment and the resultant vibrating motions exerted onto the platforms can be detrimental to not only the platform structural integrity but to the comfort of

the personnel on-board as well.

Back in 2006, Lee et al. have proposed the implementation of TLCD on a tension-leg platform (TLP) and through numerical analysis and conducted prototype experiments, it is concluded that the TLCD is effective in its vibration suppressing role with energy dissipation of more than 50% in general (Lee et al., 2006). The same researchers also studied and proposed the integration of a TLP with an underwater TLCD (UWTLCD) system that aside from capable of wave-induced vibration mitigation when accurately tuned, its columns can serve as floating barrels that provide buoyancy to the platform while not occupying any additional deck space since it is installed beneath the platform (Lee et al., 2012)

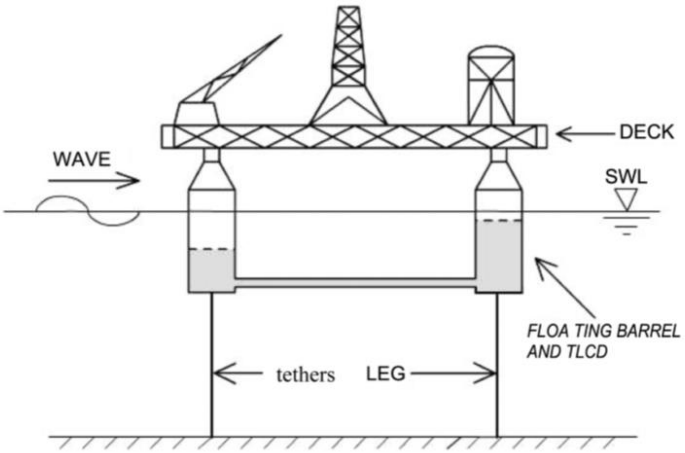

Figure 2.6: Illustration of underwater tuned liquid column damper (UWTLCD). (Lee et al., 2012)

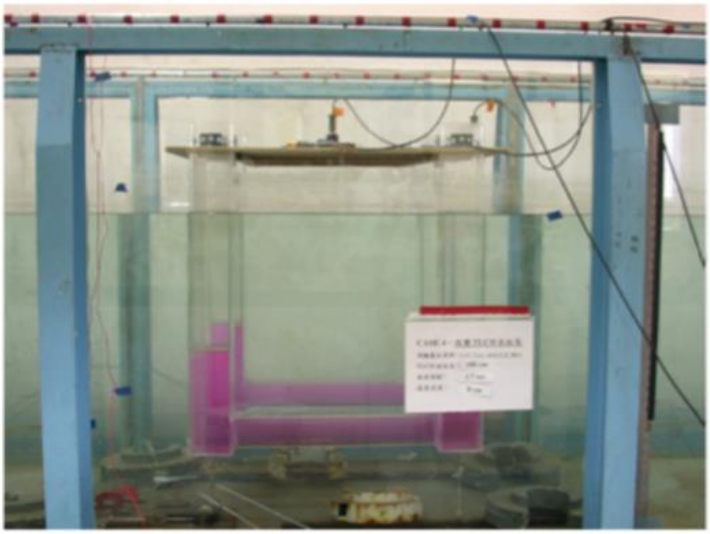

Figure 2.7: Experiment of platform with TLCD model. (Lee et al., 2012)

The application of TLCD in offshore wind turbines has also been explored by numerous researchers worldwide. It is found out that by equipping an offshore wind turbine with TLCD, it can greatly increases the fatigue life of the wind turbine through peak response reduction of up to 55% in comparison to those without TLCD, thus allowing a more efficient wind turbine design with lesser expenses (Colwell et al., 2008). In 2015, Jianbing et al. have experimented a 1:13 scaled wind turbine model installed with TLCD using shaking table and shown that TLCD system able to reduce the structural response of the offshore wind turbine system due to along-wind vibration, thereby improving its safety and serviceability (Jianbing et al., 2015). In general, these reviewed studies shown that the TLCD is certainly capable to be deployed in offshore environment through integration with offshore platform to provide suppression and mitigation of wind-wave induced vibrations.

2.8 Computational Fluid Dynamics Simulations

Computational Fluid Dynamics (CFD) is a numerical method in which the governing equations of fluid flows are solved numerically using powerful computational tools (Hanimann et al., 2018). It is one of the basic approaches to be employed to solve complex fluid dynamics and heat transfer problems for applied research and industrial applications. Nowadays, with the rapid advancement of current generation computers in terms of processing and computational powers, CFD presents the right opportunity to conduct detailed theoretical study on various terms in the related governing equations. By working in complement with experimental and analytical approaches, it also provides an alternative cost-effective means of simulating and solving real fluid flows, thereby reduces the lead times and costs of design and construction significantly (Tu et al., 2013).

There are multitudes of studies on the topic of structural control and designs of TLCD done worldwide, some researchers have employed CFD as part of their research methods. In one particular study, Chen et al. developed a tuned liquid wall damper (TLWD), a multi-column liquid damping system that can be constructed inside the walls of structures. In order to study the analytical model and the behavior of TLWD, Chen et al. employed CFD simulations using ANSYS Fluent 17.2 software to verify the analytical model with a CFD method that is validated against experimental test results from a typical conventional TLCD (Chen et al., 2017).

Similarly, CFD simulation is also applied in offshore floating structure researches to study the structural behavior of floating structure in response to sea currents and waves. In Romania, Ionuţ simulated a turbine carrier semisubmersibles with the CFD software CFX and Fluent using the rigid body solver and Volume of Fluid (VOF) method respectively as shown in Figure 2.8 and Figure 2.9. The study shown that both the software are capable of producing consistent and acceptable results for the hydrodynamic response of the semisubmersibles (Ionuţ, 2017).

Figure 2.8: Semisubmersible structure, WindFloat project by PowerPrinciple.

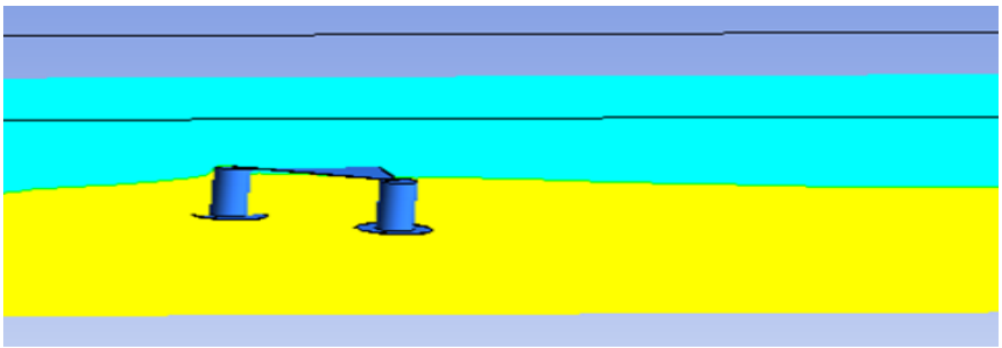

Figure 2.9: Fluent VOF results in CFD-Post. (Ionuţ, 2017)

In a recent review paper on wave energy conversion particularly on oscillating wave column (OWC), the CFD is employed to study the performance modeling and design optimization of well turbine which is commonly used by

OWC. It is found that the study of well turbine numerical model using CFD is capable of calculating the performance characteristic of the well turbine successfully (Shehata et al., 2016). Local researchers from Universiti Technologi Malaysia (UTM) have also performed CFD study on well turbine that is designed to generate electricity from Malaysian water using CFX software. The generated well turbine meshing is shown in Figure 2.10 with the turbine contained within a separated mesh volume. The study shown that a well turbine that uses airfoil NACA0020 design with turbine solidity of 0.64 is able to utilize the poor ocean wave characteristic of Malaysian water and converts the wave energy into usable electrical energy (Ahmed et al., 2014).

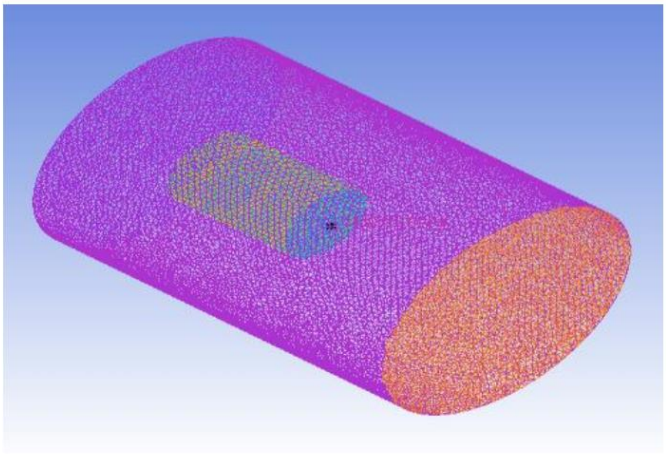

Figure 2.10: Meshes generated for the simulation model. (Ahmed et al., 2014).

CHAPTER 3

METHODOLOGY

3.1 Overview

In the methodology section, the author outlines and describes the procedures to achieve the previously established objectives in a progressive manner. As illustrated in the flowchart in the Figure 3.1, the procedures are segmented into interconnected steps and each step will be elaborated in detail in the following subsections.

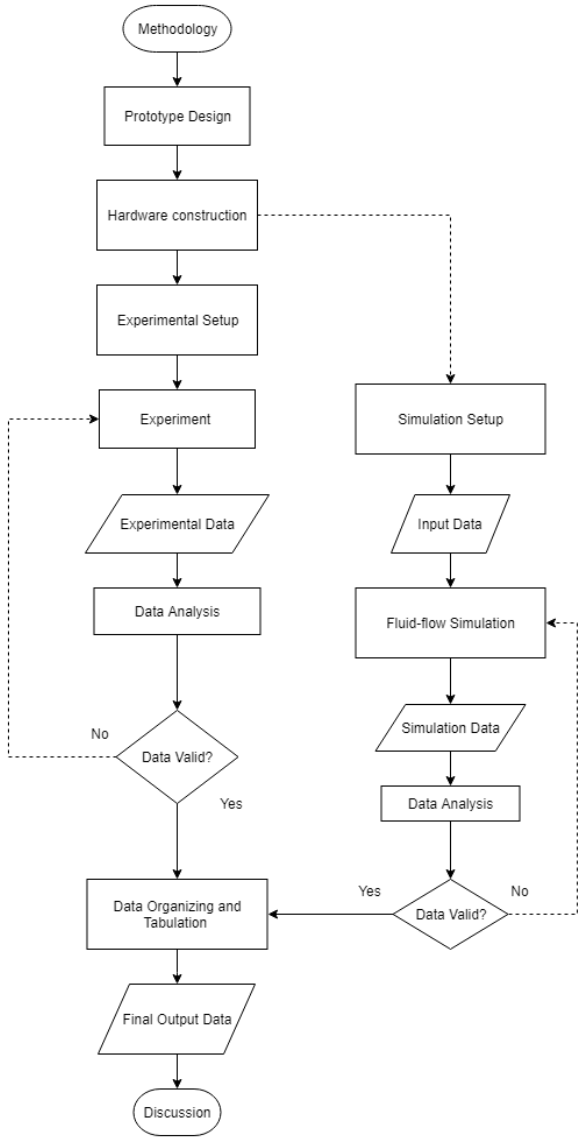

Figure 3.1: Overview flowchart of methodology.

3.2 Prototype Design and Construction

This section describes the details of concept design and construction for the project prototype.

3.2.1 Concept

The concept of the prototype emerged from the combination of both the operating mechanism of OWC and TLCD, through that the author developed a

new type of platform damping device that is capable of both structural vibration mitigation as well as harvesting ocean wave energy simultaneously. The concept fits well due to the nature of synergy between the two mechanisms in which: the liquid within the TLCD column oscillates up and down in response to the input excitation motion similar to that of an OWC and such motion can be utilized to generate electricity through the implementation of an air turbine, ultimately converting the absorbed external excitation force into usable electricity. This device is currently known as the damping wave energy converter (DWEC).

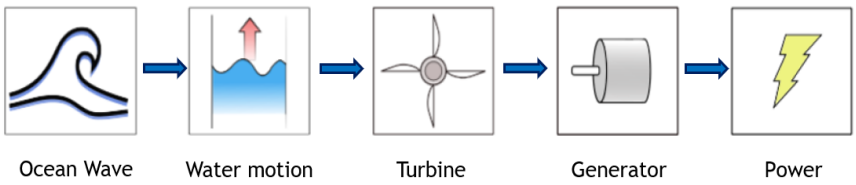

Figure 3.2: DWEC concept

As for the case of most existing WECs, these devices are designed to be deployed as standalone wave energy harvesting mechanism in their designated offshore environment. On the contrary, the DWEC is designed although can be deployed individually as well, but generally in mind to be implemented as an integrated part of an offshore floating platform. This provides opportunities for the floating platform to be utilized for other purposes such as solar and wind energy harvesting system, or even for large scale system such as floating oil/gas facility and TLP platform.

3.2.2 Design and Construction Process

Rather than having a semi-submerged chamber with open bottom as for the case of most OWCs, here the designed DWEC utilizes a closed-circuit flow where the chamber within is entirely isolated from atmospheric environment. Such design allows the DWEC to counteract the platform motion without any direct contact with ocean water. The internal chamber resembles the shape of a partially water-filled TLCD with its upper column sections inter-connected through an air turbine chamber while the bottom connecting duct enables the exchange of water level between the two columns. An energy harvesting mechanism is set to be installed to harness energy by converting the oscillating motion of water into usable electricity through the use of turbine generator.

In order for the DWEC prototype to perform as designed in response to the vibration similar to the designated sea condition, an operating frequency or natural frequency, f_n of 0.385Hz is chosen as it fits the ocean characteristic of Malaysia waters that has a wave peak period of 2-8s or in terms of frequency, 0.125-0.5Hz that carries 70% of the wave energy based on reviewed study by Muzathik et al.. The f_n is selected by not just computing the average of the said frequency range, but also slightly skewed to the higher end as lower frequency indicates larger weight and increasing difficulty to move or transport the structure in the future.

With the parameter natural frequency set, the size and shape of the DWEC can then be designed based around it using established equations:

$$f_n(Hz) = \frac{1}{2\pi}\left[\frac{g\left(1+\frac{A_2}{A_1}\right)}{h\left(1+\frac{A_2}{A_1}\right)+\frac{A_2}{A_3}L}\right]^{\frac{1}{2}} \quad (3.1)$$

Where g = acceleration of gravity, A_1 and A_2 = cross-sectional area of water column; A_3 = cross-sectional area of connector; h = height of liquid in tank; L = mean length of tube along centre line. By fixing the cross-sectional area of the water column and the dimension of the connecting tube according to the design requirement, the height of the water can be adjusted to change the effective length of liquid within the DWEC, shifting the natural frequency of the DWEC if necessary.

3.2.3 DWEC Design

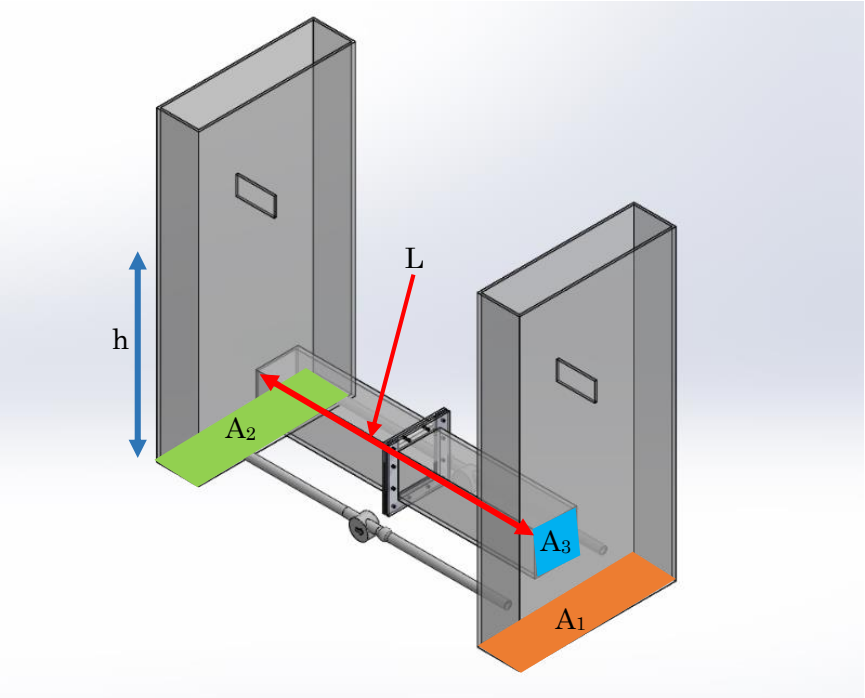

Figure 3.3: SolidWork drawing of initial DWEC design with variable labelled from equation 3.1 (no liquid shown as h represent liquid height).

The first design option of DWEC is modelled and drawn using SolidWork software as shown in Figure 3.3. The dimension of the DWEC is determined based on the pre-calculated operating frequency and the size of it is chosen in such a way that is feasible to build with available tools and limited personnel as well as can be fitted appropriately onto the shaking table for experiment later on, which has a dimension of (1.80 x 1.80)m^2. The selected height of the DWEC is set at 0.80m so that the water columns have sufficient height to hold the required water volume with ample distance from the opening at the top to prevent any sort of water spilling occur during the experiment phase. A piece of supporting strut is also inserted within the water column to provide additional structural protection by resisting horizontal compression acted upon the water column. The physical characteristic of the DWEC is (0.96 (Length) x 0.41 (Width) x 0.80 (Height))m^3 while the entirety of DWEC body is built using cast acrylic sheets.

Table 3. 1: Physical characteristic of the DWEC

Length (m)	0.96
Width (m)	0.41
Height (m)	0.80
Material	acrylic plates (5mm thickness)

In the first option of DWEC design, two sets of independent pipelines are attached on each lower sides of the bottom connecting duct, each comprised

of 1-inch PVC connecting pipe, one-way check valve and a DC 0-80V hydro turbine generator. These pipelines are designed initially to serve as the energy harvesting mechanism in which the flow of water from one column to another during oscillating motion would passes through the pipeline and drives the hydro turbine while the one-way check valve is installed to prevent backflow as the hydro turbine operates only in one-way direction. Each pipeline would operate in opposing direction thus energy would be harvested in both water flow direction.

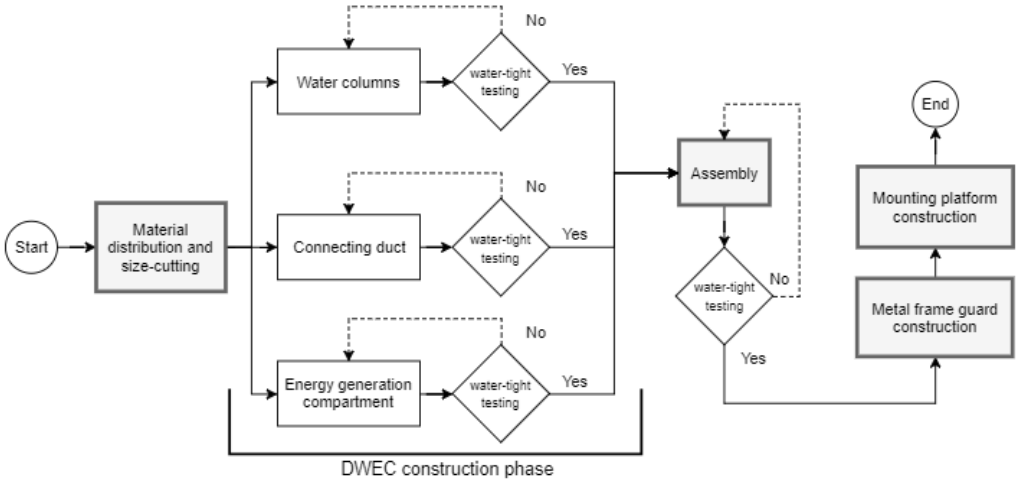

Figure 3.4: Prototype construction flowchart.

The construction of DWEC-structure is break down into comprehensive steps as shown in Figure 3.4. In the starting process, the acrylic sheets are cut into different parts and their respective sizes, each part are numbered accordingly based on their position to avoid mismatching between parts during construction phase. When the parts are ready, the construction phase is divided into 3 distinct units: water columns, the bottom connecting duct and the energy

generation compartment. Each unit are built separately but with accordance to the predetermined design dimension and are subjected to vigorous tests for water-tightness to prevent any presence of excessive leakage that will hamper the experiment outcome.

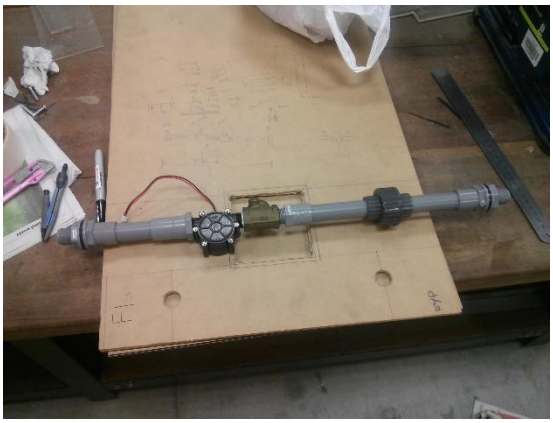

Figure 3.5: Pipeline design with hydro turbine connected through a one-way valve.

During the construction process, acrylic pieces are adhered into their respective place by applying even amount of chloroform along their connecting edges as it acts as a solvent-type bonding agent that joins acrylic pieces by melting and gluing them together. After the chloroform is applied, the connecting edges are then hold in place with weights or multiple F-clamps to allow the adhering sites to settle for at least 12 hours. When the adhering process is done, transparent silicone sealant is applied uniformly along the connecting edges from the inside to serve as an extra protection layer to ensure maximum water-tightness. The pipelines are built together from multiple components as previously mentions through pipe thread fittings and PVC glues, each end is fitted with a tank connector to attach to the water column and a set of pipe unions is inserted along the pipeline as well for ease of removal as shown in Figure 3.5. The centre of the main connecting tube is designed to be disjoint-able by

unfastening the screws around the opening to allow quicker water discharging without topping over the DWEC as well as any modifications such as orifice insertion and tube elongation if necessary in the future.

Once all the individual units are completed, the assembly takes place in steps as each unit are combined meticulously into one complete DWEC as designed. The assembly process is made simpler as the two identical sides of DWEC can be assembled separately and connected to each other afterwards. Once the assembly is finished, the DWEC is subjected to multiple iterations of integrity test by filling it with water of up to 0.50m height and inspected for any form of water leakage, any spots with leakage occurred are then marked for patching afterwards. The completed DWEC is displayed in Figure 3.6.

`

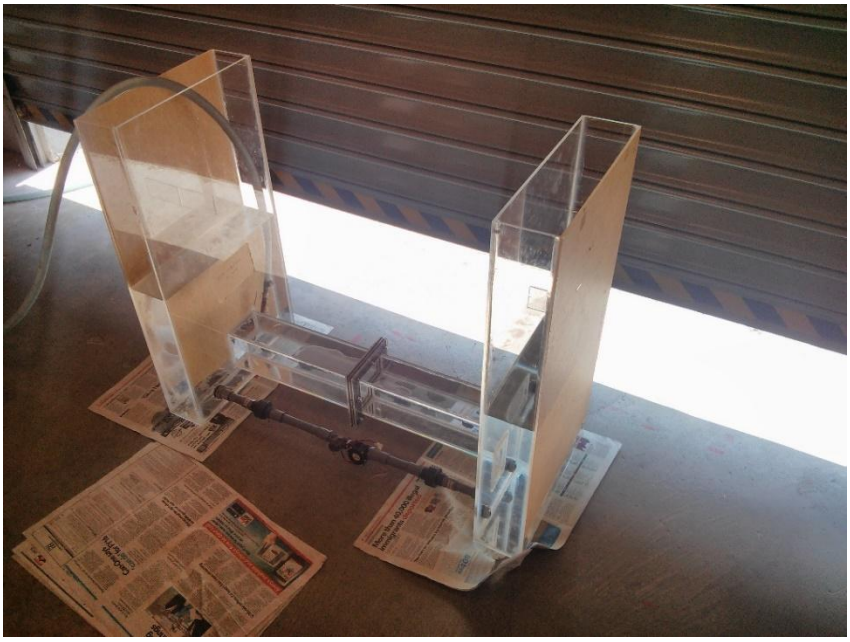

Figure 3.6: Water-tightness testing.

In the next step, a metal frame guard is built around the DWEC using slotted angle iron bars to keep the DWEC safe from all sorts of structural damage particularly during transportation and experiment. Additional steel brackets and corner bracers are installed at critical angles and corners of the frame guard to further reinforce it. Finally, a mounting platform that is capable of single-degree movement through two sets of wheel axle is manufactured to house the DWEC on it for upcoming experiment. The mounting platform comes with a storage section that allows author to store items beneath the structure as well as adjust the weight of the platform when needed. The combination of which the DWEC is mounted atop the platform is known as the DWEC-structure. The completed DWEC-structure is displayed in Figure 3.7.

Figure 3.7: Completed DWEC-structure with surrounding metal frame.

3.3 Experimental Setup

This section describes the experiments undergone to study the operating characteristic and motion response of the constructed DWEC prototype through vibration test.

3.3.1 Shaking Table

A shaking table that is available in the university campus is used to carry out the experiments as it is capable of generating single degree of vibrational motion, despite being used more often on ground-based models and soil structures.

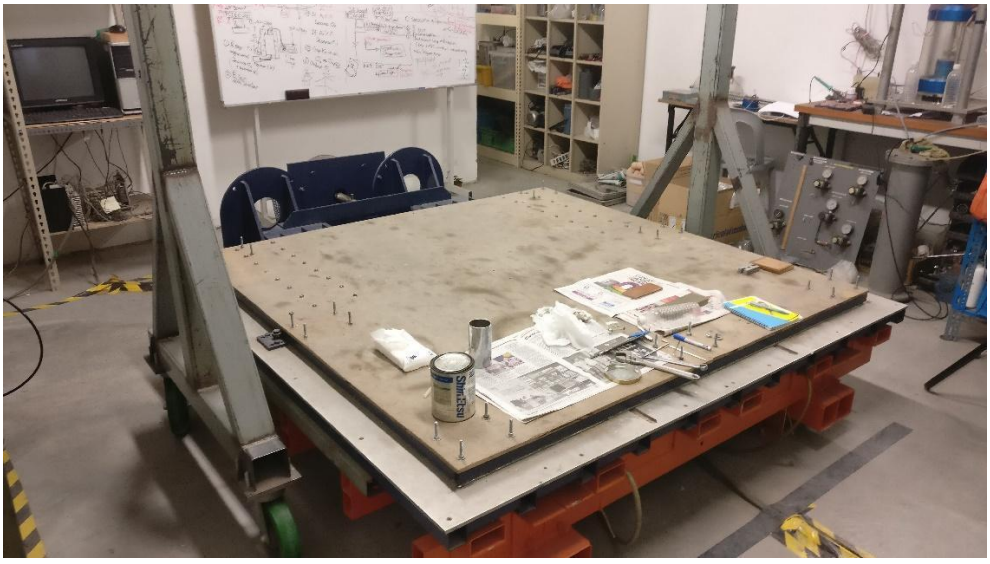

Figure 3.8: Shaking table

The shaking table and corresponding components of its control system are displayed in Figure 3.8. The Megatorque direct drive motor manufactured

by NSK Co. Ltd. that is connected to one end of the shaking table generates single degree-of-freedom oscillating motion by driving a threaded rod back and forth, a mechanism similar to that of a linear actuator, hence producing a vibrating motion to objects mounted on top of the table platform. The motor is controlled by its driver unit through a computer software named MotCtlProg that allows users to input required oscillation frequency and amplitude. The input signals from the computer is then sent to the driver unit through the control box that serves to stabilize the said input signals.

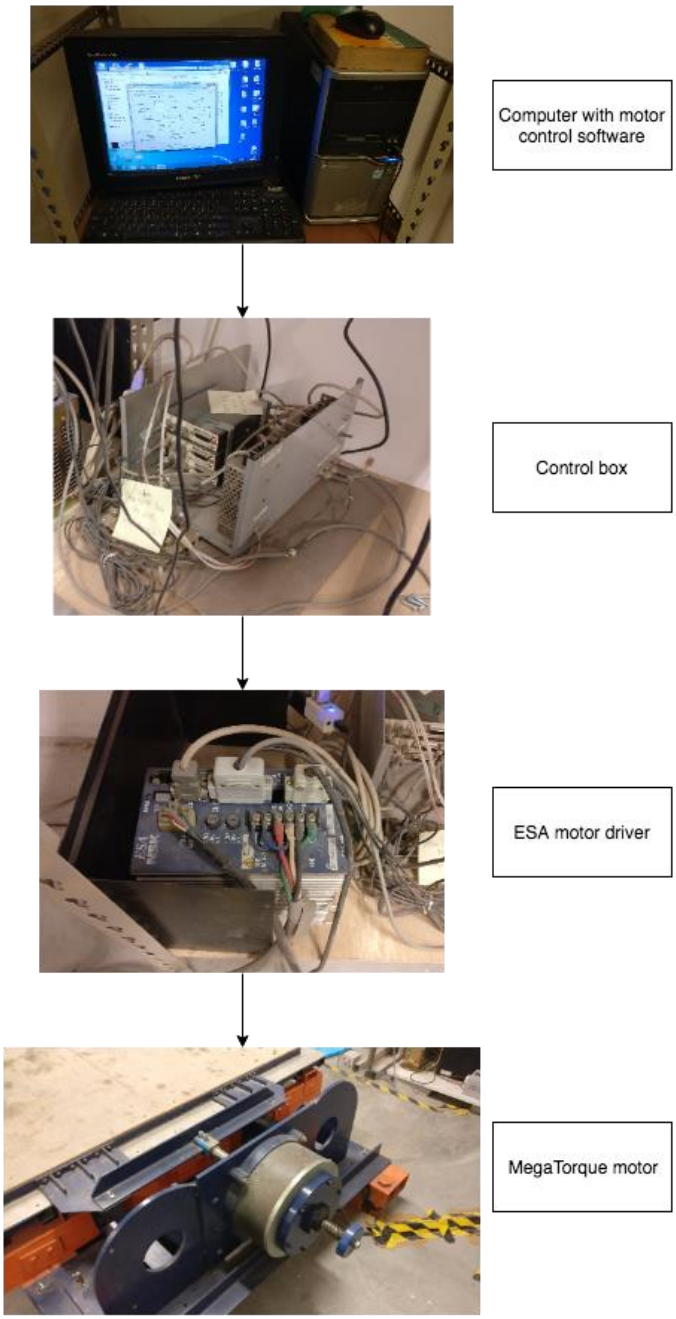

Figure 3.9: Shaking table control system components.

The motor is capable of generating triangular oscillating motion in the frequency range of 0.1-20Hz and displacement value from 0.1-50 unit with each unit represents approximately 4mm. The actual motor capacity is further tested for the experiment beforehand to determine the safe combination range of frequency and displacement. With an effective surface platform area of (1.8 x

1.8)m^2, the shaking table surface platform is lifted with pressurized air of 5 bar during operation and can sustain up to 3 tons of weight, which is more than suffice for the author's experiment.

Before conducting experiments, the author has performed tests on the shaking table under the guidance of a civil engineering student assigned by the Center of Disaster Risk Reduction. The shaking table is run for a range of frequency of 0.2-0.6Hz in combination of amplitude values to determine the input values that are within the operating boundaries of the shaking table to avoid overloading the platform driving mechanism with excessive motion. As the DWEC-structure is needed to be tested with different vibration frequencies, the displacement value of the shaking table is reduced accordingly as the frequency increases since oscillation with higher frequency at the same displacement induces larger loading onto the shaking table system. As shown in Table 3.2, the boxes with ticks represent the acceptable combination of frequency and displacement value or otherwise unsafe as indicated by red crosses. The green ticks represent the selected combinations to be applied during the vibration experiments later.

Table 3. 2: Shaking table safety working range testing results.

Displacement (mm/unit) \ Frequency (Hz)	0.2-0.39	0.40	0.41	0.42	0.44	0.46	0.48	0.50	0.55	0.6
48 (6)	✓	✓	✓	✓	✓	✓	✓	✓	✓	✓
56 (7)	✓	✓	✓	✓	✓	✓	✓	✓	✗	✗
60 (8)	✓	✓	✓	✓	✓	✓	✗	✗	✗	✗
72 (9)	✓	✓	✓	✗	✗	✗	✗	✗	✗	✗
80 (10*)	✓	✓	✗	✗	✗	✗	✗	✗	✗	✗

* indicates input values for the shaking table control program.

3.3.2 Setup Procedure

The first vibration experiment is setup according to the equivalent free-body diagram as shown in Figure 3.10. As illustrated, the DWEC-structure is represented as a single degree-of-freedom (DOF) damped spring-mass system comprised of moving structure of mass M with a DWEC and is subjected to external periodic vibration force, F which is exerted by the shaking table. The displacement amplitude denoted by X represents the responding motion of the DWEC-structure due to the input vibrating motion while K and C represents spring constant and damping constant respectively. Therefore, by inducing an input periodic vibrating motion of F, the structural response of the DWEC-structure can be studied by measuring the output X.

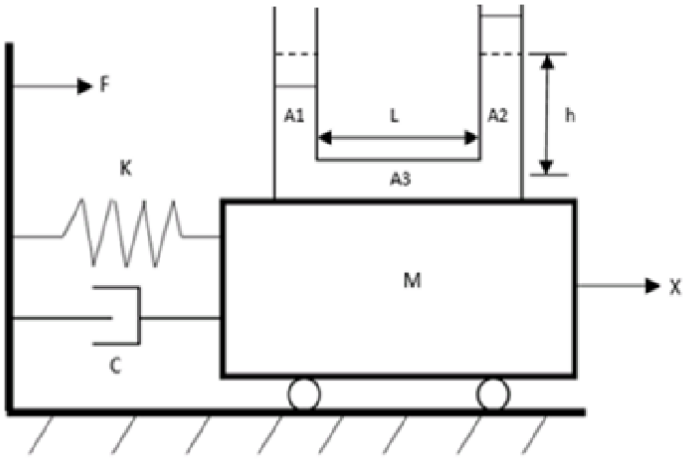

Figure 3.10: Free body diagram of the DWC-structure experiment setup.

The planned setup for the first vibration experiment is illustrated in Figure 3.11. The DWEC-structure is secured onto the moving platform with tension springs on both ends on the shaking table. The springs are attached to the G-clamps and are pre-tensioned at an equal length of 0.275m on both ends in their respective equilibrium positions. The G-clamps are tightened onto steel bars that are secured to the moving platform at the protruded bolts as seen in the image taken. The properties of the springs are as stated in Table 3.3.

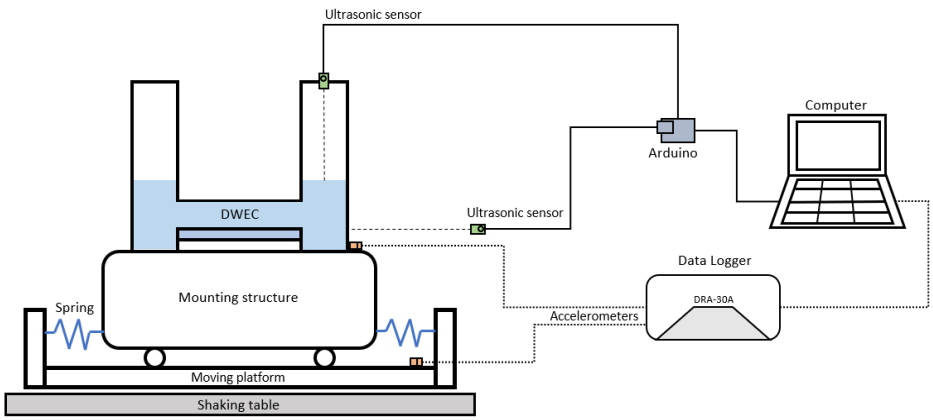

Figure 3.11: Experiment complete setup illustration.

As one of the main objectives to study the structural response of the DWEC-structure, sensors are required to measure and collect essential experimental data as follow:

I. Two sets of ultrasonic sensor:
    a. measure the change in water level within the DWEC column and the displacement of the DWEC-structure respectively,
    b. first one is attached at the opening of the water column and point directly inwards onto the water surface,
    c. second one is placed at a fixed elevated position pointing towards the foreside of the DWEC-structure to measure it's absolute displacement with respect to the ground**.**

II. Two sets of accelerometers:
    a. provide accurate acceleration monitoring of the shaking table and the DWEC-structure as well.

The first ultrasonic sensor is slightly modified by wrapping the transmitter and receiver port with hollowed cylindrical tube to prevent erroneous reading in which the signal bounces off from nearby obstacle instead of from the water surface. The HR-04 sensors are capable of measuring object within the distance range of 0.02-4m with high resolution of 3mm. These ultrasonic sensors are controlled using an Arduino Uno microcontroller board that is connected to the PC, the collected sensory data are then logged from the serial port and stored as csv file using Processing 3 software.

Table 3.4 provides further information of the deployed accelerometers. The coefficient of each accelerometer is obtained from previous calibration work and is required for data processing to compute the actual acceleration data. These accelerometers are connected to the computer through a multi-channel data logger DRA-30A with its supplied data recording software DRA-730AD. The software is required to be installed in PC for displaying and monitoring the accelerometer data as well as converting the data collected from the accelerometer into csv format that is readable by other analytic software such as Microsoft Excel and Matlab.

In addition, one of the hydro turbines installed along the pipeline is modified with a see-through acrylic casing and a visible white line is drawn on the turbine surface for better observation of the turbine motion during experiments.

Table 3. 3: Spring properties.

Type	Tension spring
Spring Constant (N/m)	~120.7
Original Length (m)	0.15
Maximum Length (m)	0.40

Table 3. 4: Accelerometer data.

Accelerometer Label	Model	On-Body Code	Coefficient
Tml1	TML ARH-20A	52145	0.0227
Tml2	TML ARH-20A	52144	0.0212
Tml3	TML ARH-20A	04062	0.0233

In order to accurately study the vibration mitigating effect induced by the DWEC upon the DWEC-structure, the natural frequency, ω_n of the DWEC-structure is needed to be determined beforehand using the equation $\omega_n = \sqrt{\frac{k}{m}}$ where k and m represent the spring constant/spring stiffness and weight of the system respectively. To that end, the weight of the DWEC-structure is computed by measuring the weight of each individuals components and summed up in a tabulated manner as shown in Table 3.5, and with a total of four tension springs used for the setup, the spring constant is measured at ~483 N/m. With that, the calculated natural frequency of the DWEC-structure based on the previous equation yields 0.48Hz. However, for the purpose of maximum mitigation effect to occur, the DWEC-structure should be designed to have a similar or equal natural frequency as the DWEC itself, hence additional dead weight is added to the storage compartment in the mounting platform to further reduces the natural frequency of the structure as observed in Figure 3.12 where the full experimental setup is shown. By adding on an additional dead weight of

25.16kg, the natural frequency of the DWEC-structure is at 0.402Hz which is sufficiently close to that of the DWEC for experimental usage.

Table 3. 5: Overall weight calculation.

Item	Weight per length (m) /area (kg/m2)	Quantity/ Length(m)/ Area(m2)	Unit weight (kg)	Weight (kg)
Wheel + shaft + pillow block	-	2	3.400	6.800
Thick metal hollow bar	2.168850073	1.8	-	3.904
Thin metal hollow bar	1.485319516	4.652	-	6.910
Small angle slotted bar	0.596721311	14.795	-	8.828
Large angle slotted bar	0.737142857	3.435	-	2.532
Acrylic sheet	5.546536797	2.0508	-	11.375
Wooden plank (base level)	-	1	3.320	3.320
Wooden plank (2nd level)	7.453042825	0.63056	-	4.700
M8 (bolt, nuts & 2 washers) (3cm)	-	100	0.021	2.100
Pipeline	-	2	0.441	0.882
Slotted angle iron bracer	-	16	0.022	0.352
Right angle steel bracket	-	4	0.087	0.348
M8 (5cm)	-	14	0.029	0.406
Locking cable	-	1	0.418	0.418
			Total weight (kg)	52.875

Figure 3.12: The completed experimental setup (red square indicates the added dead weight)

The DWEC functions in a similar way in terms of mechanism as a typical TLCD, that is vibration absorption through the back and forth sloshing motion of liquid within the columns over a connecting tube, albeit with add-on tools to extract energy from the water motion. Therefore, as previously stated in the design section, the same method that is applied to calculate the natural frequency of a TLCD based on its structural design can be used here as well. The natural frequency of the DWEC can be adjusted to a certain extend by manipulating the water height within the column, hence based on the calculation, the DWEC is filled with water up to a height of 0.24m measured from the base to attain a natural frequency of 0.38Hz. After the process of water filling, the DWEC is rocked back and forth lightly to eliminate the air bubbles that are trapped at the connecting tube section and within the pipeline which may interfere with the experimental result. As seen in Figure 3.13, a small

amount of dye is also added to the water for better observation of the water oscillating motion during experiment.

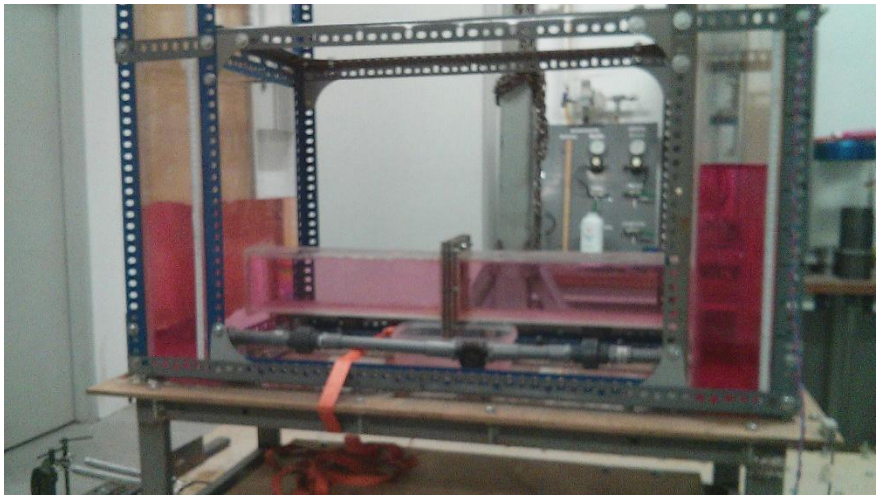

Figure 3.13: Water column with added red dye for ease of observation.

The following precaution steps were also taken to ensure the safety of the DWEC and surrounding equipment within the shaking table room. A sets of L-shaped metal blocks are added on both ends of the moving platform in perpendicular to the wheels of the DWEC-structure to prevent it from launching off from the shaking table in the case of mechanical failure in the spring sections. Furthermore, an industrial ratchet tie is used to secure the DWEC firmly onto the mounting platform to eliminate any possibility of unwanted DWEC movement on the mounting platform during experiments.

3.4 Experiment Set 1 (Hydro Turbine Pipeline)

The experiments are conducted using two different configurations and in such order: without operating DWEC and with operating DWEC, for the validation of model design and DWEC performance evaluation respectively. Figure 3.14 shows the configurations and the motions that are monitored throughout the vibration tests. The DWEC-structure is first tested to study its structural frequency response and in turn validates the model design through the occurrence of resonance event. A resonance is a phenomenon in which the frequency of the external vibration induced matches or resonates with the natural frequency of the system causing the system vibrational motion to amplify to a certain degree based on its damping characteristic and hence, the natural frequency of a system can be determined through this event.

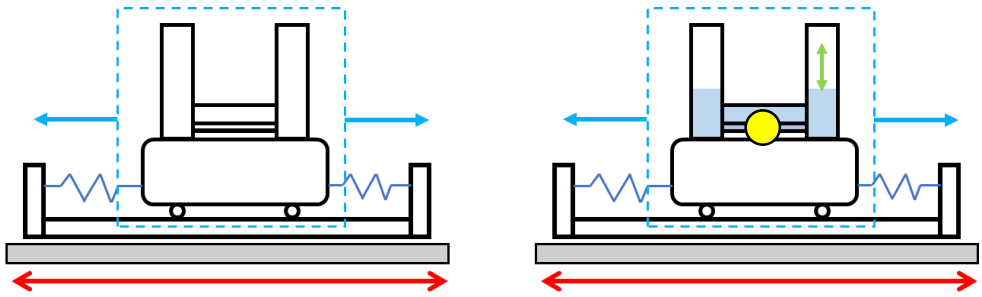

Figure 3.14: Configuration (a) without operating DWEC and configuration (b) with operating DWEC with the respective monitored motions: Shaking table (red), DWEC-structure (blue), water level changes (green) and hydro turbine (yellow).

In the first configuration, the DWEC is mounted on the structure albeit not filled with water, rendering it non-operational. The dead weights are loaded into the storage section of the DWEC-structure to adjust its natural frequency

as previously mentioned and the sensors are setup accordingly. For first DWEC design option, the experiment is ran for a set of frequency points: 0.20, 0.25, 0.30, 0.35, 0.40, 0.45, and 0.50Hz. For each frequency point, the shaking table is set to run for a minimum of 30s to ensure the full range of the DWEC-structure's motion from transient to steady-state is captured unless the structure is oscillating to an excessive degree of movement especially during resonance.

In the second configuration, the performance of the DWEC in terms of vibration mitigation of the DWEC-structure in comparison to the previous configuration, and the air turbine motion are studied. With the DWEC partially-filled with water as indicated in the configuration illustrated in Figure 3.14, an additional set of data is collected from the measuring water height within the DWEC column and the movement of hydro turbine is solely observed from the side to see if the water flow induced from the oscillation is able to drive the turbine. All the collected data are then compiled and organized using Microsoft Excel for tabulation and further analysis.

3.5 Experiment Set 2 (Air Turbine Chamber)

In this section, the energy harvesting mechanism is shifted up and covers on top of the DWEC as shown in Figure 3.15. By enclosing the upper portion of the DWEC columns that are previously open to surrounding environment and connecting them through a narrow air chamber, a bi-directional air turbine is installed within the said connecting chamber to extract energy from air flow

generated by the relative motion of water within the DWEC with respect to the movement of the structure.

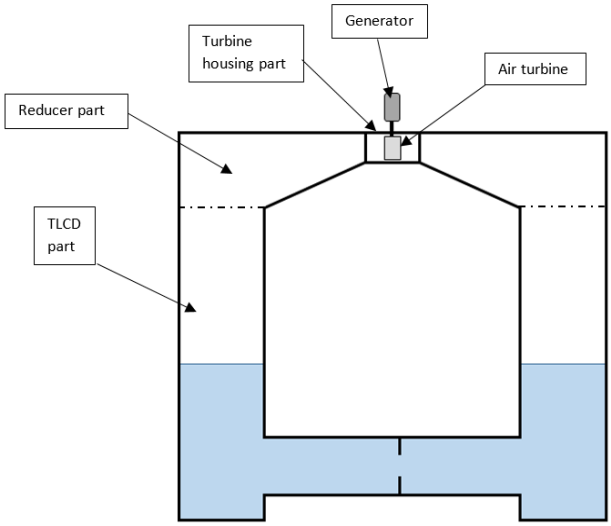

Figure 3.15: 2D illustration of DWEC model with labelled parts.

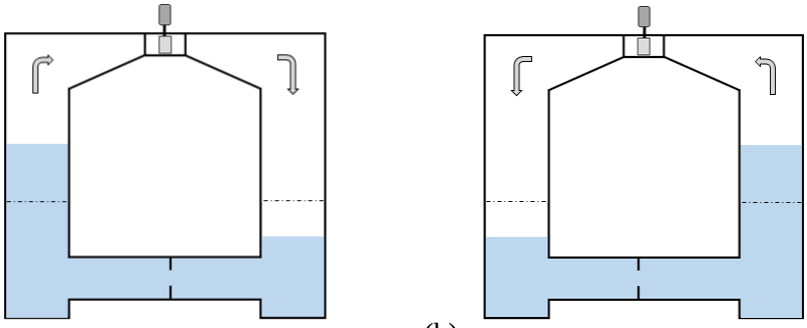

Figure 3.16: The air flow across the turbine alters direction between (a) and (b) as the water column oscillates.

As seen in the 2D conceptual drawing of the DWEC and its operating concept in Figure 3.15 and Figure 3.16, since the internal volume is isolated from the external environment, the air confined within the water column are forces through the air chamber by the rising water level and into the opposite

chamber where the water level simultaneously drops, hence the air flow alters between two directions over the air chamber as the water level changes, driving the turbine coupled with generator for every oscillating cycles. The eccentric reducers are pipeline components that are installed to reduce the duct size in a gradual manner to minimize energy loss in air flow due to fitting configurations such as elbows and sudden contraptions. The 3D drawing of the retrofitted DWEC is as shown in Figure 3.17, with the pipelines taken out and an upper section is added.

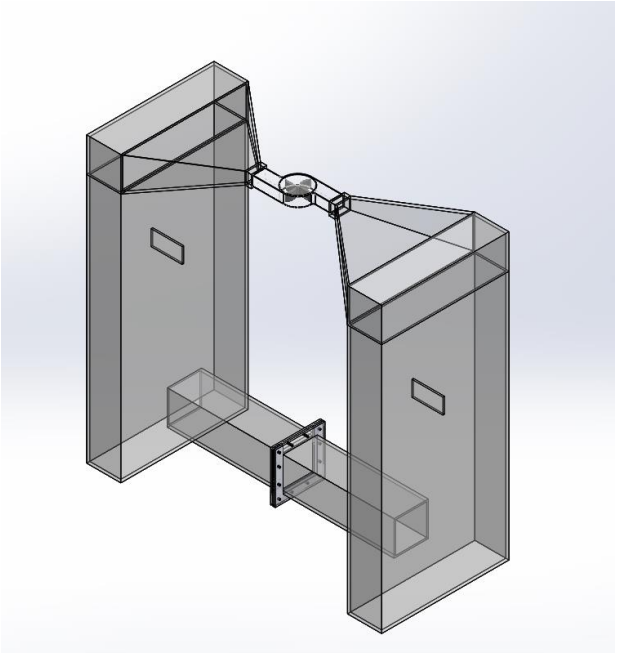

Figure 3.17: SolidWord 3D model of set 2 DWEC design.

Within the air chamber, a 3D-printed vertical-axis drag-type four-blades turbine is installed perpendicularly to the air flow direction to extract energy from the drag force exerted by air flow across the blades. Despite commonly known to have a lower efficiency in comparison to a lift-type turbine, the drag-type turbine is opted here due to simplicity of turbine design and fabrication, its capability to operate regardless of wind direction and non-

flow-interrupting rotor shaft. The chamber itself is also shaped in a way to accommodate the integration of a drag-type turbine by directing the air flow towards the concave face of the blades to maximize energy output. As illustrated in Figure 3.18(a) and (b), the turbine would rotate in the counter clockwise direction regardless of the incoming direction of airflow.

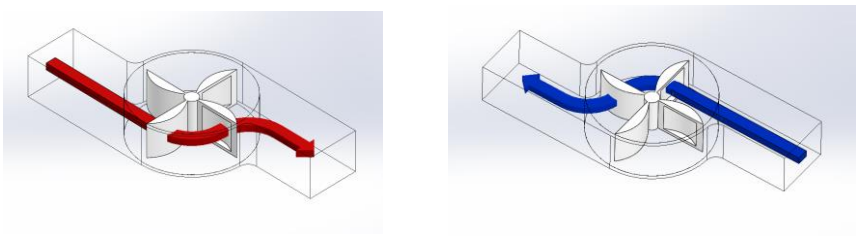

(a) *(b)*

Figure 3.18: The air flow as indicated by red (a) and blue (b) line passes through the turbine blades on different sides so it rotates only in a single direction.

As observed in the second DWEC design illustrated in Figure 3.17, an hourglass shaped upper section comprised of two reducer sections and the air chamber, which are all fabricated using acrylic sheet as well is mounted atop of the current DWEC. For experimental purpose, the upper section is built to be removable to accommodate for water filling process before conducting vibration test. Each reducer is seated on the opening of the DWEC column and lock in placed with protruded slots on both sides and a bolt that screws into the metal frame guard. One of the reducer is fabricated with a set of holes for the transmitter and receiver port of the ultrasonic sensor to fit inside and measure the water height without adverse effect on the air-tightness of the structure.

As the DWEC design changes, some modifications have been made in the second vibration experiment setup as well. For one, an additional IR sensor

is installed at the air chamber section and pointed directly towards the turbine blades to measure the turbine rotational speed by sending a pulse whenever the turbine blade passes through and reflects the transmitted signal back to the sensor. Furthermore, a rotary encoder model TR1-U2R6 that is connected to its corresponding data logger CRONOS-PL2 is attached to the bottom of the DWEC-structure with the rotary wheel landed on the surface of the shaking platform to measure the relative displacement between the DWEC-structure and shaking table. The updated experiment free-body diagram and the complete setup illustration are shown in Figure 3.19 and Figure 3.20.

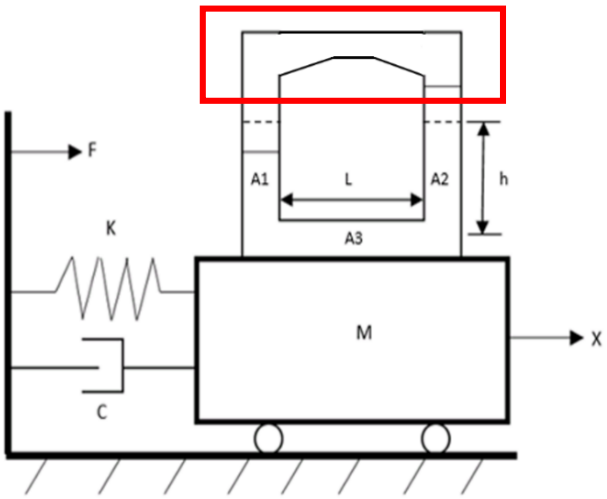

Figure 3.19: Free body diagram of the experiment setup with added top section highlighted in red square.

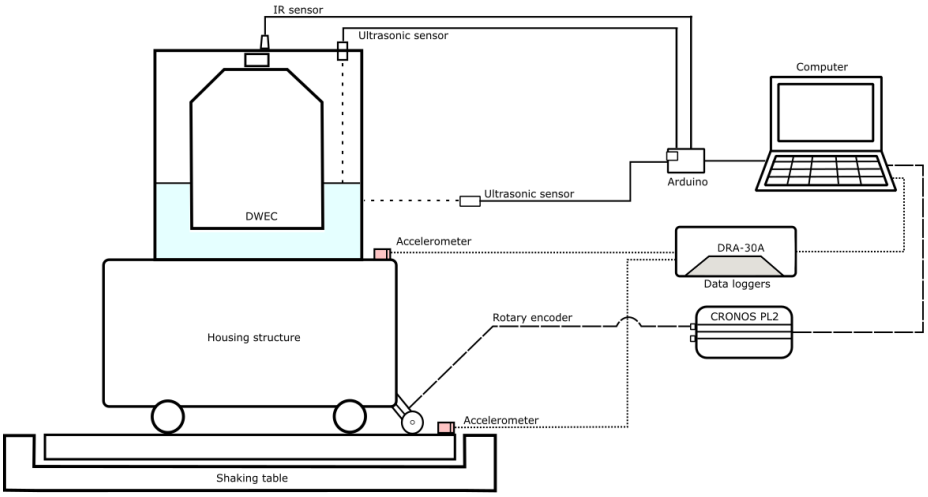

Figure 3.20: Experiment setup diagram.

The experiment is conducted in the similar procedure as the previous one but with more dataset to collect, thus an extra computer was needed later on to distribute the data collection process. In comparison to the Set 1 experiment, the applied frequency range is extended to 0.60Hz with a smaller interval used specifically around the 0.40Hz point so that the operating range of the DWEC can be better observed. The air-tightness of the DWEC is also emphasized due to air leakage from the DWEC inner atmosphere during the experiment may contribute to significant energy loss as the airflow generated from the water column motion escaped into external atmosphere before the air reaching the turbine chamber. Therefore, oil-based modelling clay and tapes are applied along the contact surface between the upper-section and the water column opening during the setup to ensure maximum air-tightness and minimize energy loss from it.

3.6 CFD Simulation

After conducting the hardware experiment, the author proceeds to perform study primarily focusing on the energy generation mechanism using CFD simulation. In this case, the CFD analysis software ANSYS Fluent under Workbench v17.0 (& later on upgraded to v18.2) is opted to be used for simulation purpose due to its multitude of physical modelling capabilities required to simulate industrial-oriented applications such as air flow, multiphase fluid flow and fluid-structure interaction (FSI) as well as its compatibility with CAD software specifically SolidWork as object parts and assemblies can be directly imported as simulation geometry in Ansys Fluent. The simulation goal is to analyse the performance of a well turbine in terms of energy generation with the same DWEC design and how much energy can be extracted from the air flow generated by the water height changes within the DWEC column during oscillation.

In the third experiment, the air turbine chamber design in the set 2 experiment has been replaced with a well turbine that is situated at the center of a cylindrical duct as shown in Figure 3.21. The well turbine is a type of axial flow air turbine that is commonly deployed in typical OWC as it is self-rectifying and capable of operating in bi-directional air flow which converted into mechanical energy through a unidirectional shaft. The designed turbine has 6 rotor blades and each has a symmetrical profile that is with respect to the plane perpendicular to the rotor axis and are set at a stagger angle of 90° as well as with a solidity of 0.6. These rotor blades are designed with aerofoil section profile NACA 0021 indicates that the blade has maximum thickness of 21% at

1/3rd of the chord length measured from the leading edge. The suitable rotor design is selected based from previous studies in which an air turbine blade with thicker profile (e.g. NACA0021) is less prone to stalling and has larger operating range, and similarly the symmetrical aerofoil NACA 4 digits design is commonly used as rotor profile by well turbine designers (Falcao et al., 2012). A higher solidity, σ which denotes the total rotor blade area divided by the air turbine sweep area, of 0.60 can improve the self-starting capability of the turbine as well (Tummala et al., 2016).

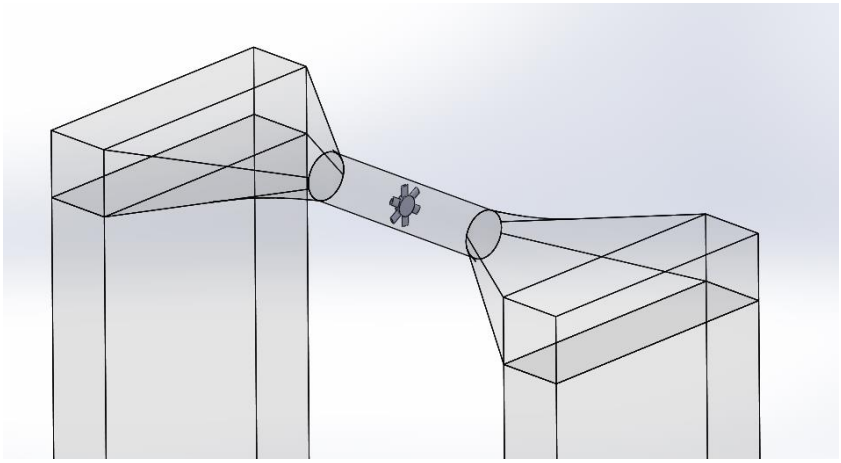

Figure 3.21: 3D model of the DWEC with an air turbine installed at the centre of the upper connecting duct.

3.6.1 Simulation Setup

The simulation workflow is divided into two parts, first the DWEC without the air turbine section and secondly, the air turbine section without the DWEC. This helps to reduce unnecessary complexity for the CFD software by providing a more simplified simulation work as computational resources are limited and less complicated simulation model allows faster trial-and-error process and settings adjustment. Therefore, part 1 simulates the water motion within the DWEC and

air flow across the upper duct when a periodic oscillating motion is applied while part 2 simulates the turbine motion when it is subjected to a bi-directional air flow.

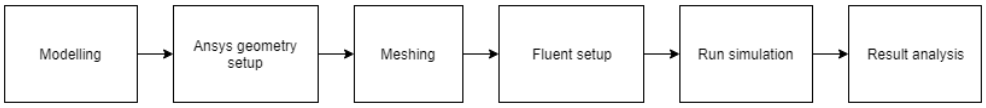

Figure 3.22: The simulation setup process.

The simulation setup process goes as shown in Figure 3.22. The simulation setup for part 1 will be covered first and followed by part 2. First the 3D model is drawn using SolidWork and imported to the fluid-flow geometry component, DesignModeler in which the computational domain for the CFD analysis is defined as shown in Figure 3.23.

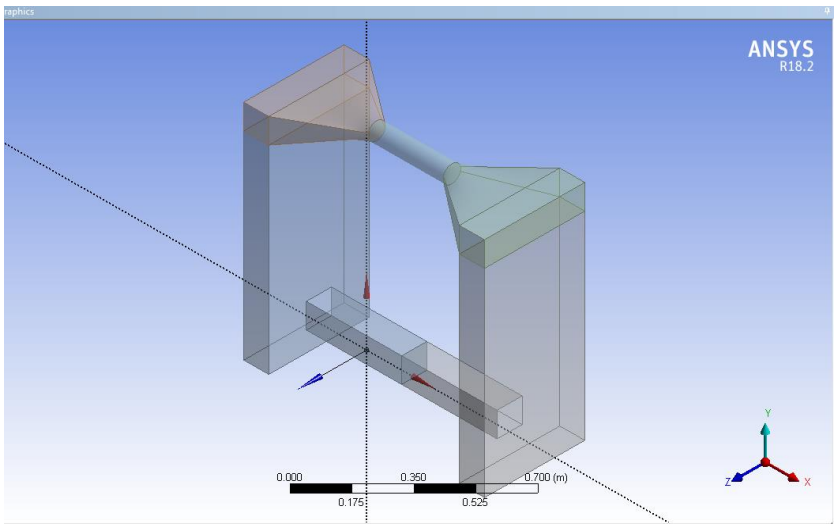

Figure 3.23: Geometry setup of the DWEC model.

In the next component, a mesh is generated for the given model and important surfaces are named based on their roles such as walls, inlet, outlet, turbine faces and etc. A meshing is an integrated part of CFD process where the model of a continuous body is discretized into finite number of elements so that the associated governing equations of fluid dynamics can be solved numerically, hence the meshing process plays a crucial role in determining the speed and accuracy of the solution depending on how the meshing is done.

In general, for the case of which the author intended to simulate, the number of total mesh elements is kept within 100-200k for the best compromise to achieve acceptable simulation time needed and without sacrificing the overall model accuracy as higher mesh elements indicates higher resolution or cell count and thus takes longer time to iterate. It is also essential to keep the model mesh quality in check as it plays a significant role in determining the accuracy, rate of convergence and stability of the simulation computation. As a rule of thumb provided in the Ansys documentations, it is recommended to keep the following cell properties above a minimum/maximum value:

- *Orthogonal quality*: > 0.01 for all types of cell, and significantly higher average value.
- *Skewness*: < 0.95 for triangle/tetrahedral cells, and significantly lower average value.
- *Aspect ratio*: < 35:1 for energy solution stability, no limitation for flow solution.

Figure 3.24 shows the mesh generated for the DWEC in simulation part 1. As seen in the named selection on the left, each body part is named after their

respective side (left and right) to avoid confusion. The mesh qualities and element number are as listed below:

- *Orthogonal quality*: Min: 0.20288, Average: 0.78358.
- *Skewness*: Max: 0.79712, Average: 0.22341.
- *Aspect ratio*: 8.9343:1
- *Elements/cells count*: 127,079

The proximity and curvature size function is selected to provide greater control over the mesh distribution on faces or within the body. For one, the number of cells across gap is increased from the default number to five to obtain an adequate resolution within the DWEC columns and the ducts due to the nature of the DWEC structural design in which the cross-sectional area for most sections are narrow with respect to the volume occupied by the DWEC body.

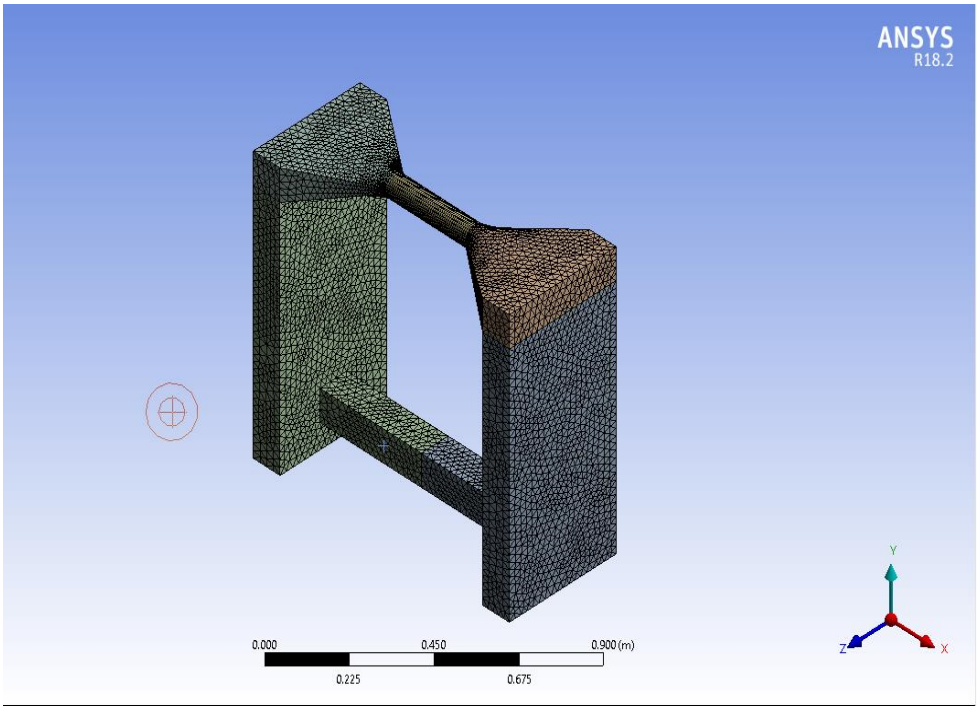

Figure 3.24: Generated mesh of the DWEC for simulation.

In the next section, the fluent simulation is setup based on the type of solution required. For part 1 of which incompressible flow is assumed, the pressure-based solver is applied for transient flow simulation with gravity enabled. The SST k-ω (Shear Stress Transport K-omega), a commonly used turbulence model for most industrial applications is opted for the simulation. Multiphase volume of fluid (VOF) model is enabled as well for the purpose of simulating two immiscible phases: water and air flow within the DWEC. In this case, the water-liquid (or H_2O) which added from the material database represents phase 2 while the air is represented by phase 1. Once the solution is initialized afterward, the phase 2 is then patched into the computational domain by defining its occupied volume with x, y and z axes value while the rest would be occupied by air.

In order to create a periodic oscillatory motion for the DWEC, a specific user-defined function (UDF) is assigned to the cell zones in the DWEC body in the dynamic mesh setting section. A UDF is a function file that is written in C programming language by the user to modify the behaviour of the Ansys Fluent to attain certain needs required for the simulation. The UDF is then hooked to the solver after being compiled or interpreted and allows the user to use the UDF for desired function from within the solver settings. In this case, the UDF defines a sinusoidal motion with specified frequency and amplitude value and is assigned to the cell zones as a rigid body motion.

Once the motion setting is done, the solution is to be initialized where the flow field within the simulation domain is given some initial variable values for the calculations. For the calculation setting, the time-step size is set initially as 0.05s but gradually reduced to 0.002s due to divergence issue. A default max iterations per time-step of 20 is set as it is suffice for the calculation to reach convergence as previously tested. Additionally, a copy of Fluent solution file is saved automatically at every 25 time-steps as a backup contingency plan in case the simulation shuts down unexpectedly due to multiple possible reasons so that the simulation can be restarted without losing too much progress. When the simulation is completed, the DWEC motion and relevant data can be analysed in the CFD post-processing component.

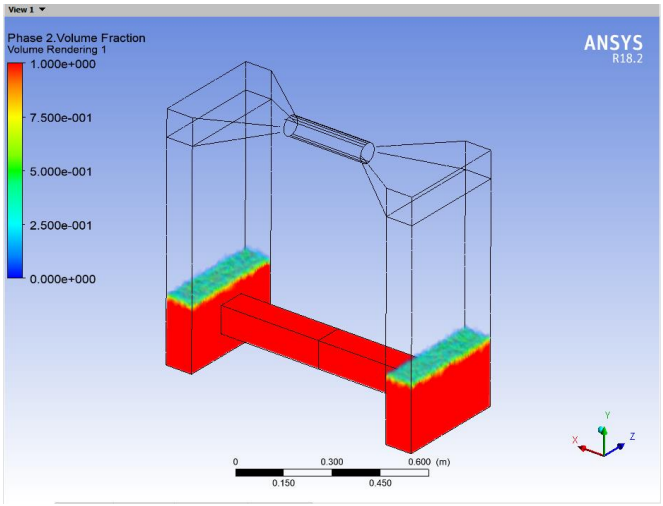

Figure 3.25: The DWEC model with the water volume fraction (red) in the CFD post-processing component.

Prior to the beginning of part 1 simulation, the author also first simulated an operating 1:1 scale 3D DWEC model as shown in Figure 3.25 and study the water height changes within the column for different frequency in comparison

to that of the real DWEC prototype to validate the DWEC design is performing as intended for the following simulations. The DWEC model is subjected to single-degree triangular oscillating motions similar to that of the shaking table experiment for a frequency range of 0.20-0.60Hz and the result is analysed using the Post-processing component.

After part 1 simulation is completed, the cylindrical duct with the well turbine is ported as the simulation model for part 2 according to the setting process. As seen in the Ansys geometry view in Figure 3.26, the well turbine is retrofitted with a round-tip hub on both ends to guide the air flow to the turbine blades and in the meantime reduces the stagnant area where the air flow comes in contact directly with the turbine.

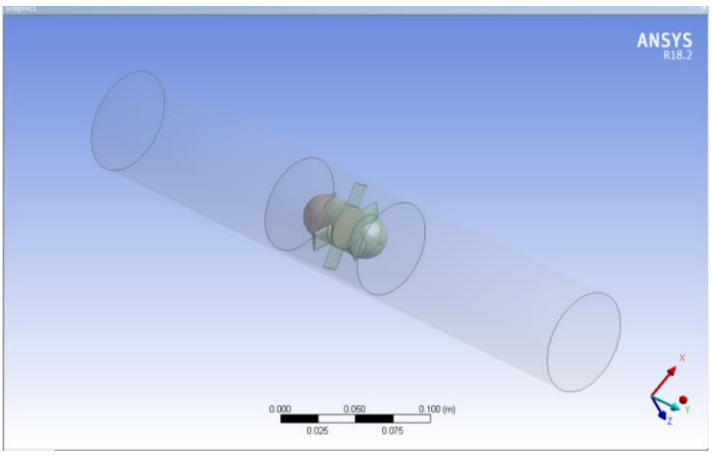

Figure 3.26: The air turbine model in the ANSYS DesignModeler.

In the mesh generating process, the size function curvature is applied and several adjustments were made to attain the best possible meshing outcome that befits the minimum qualities and element count requirements after some

trials and errors. As such, the maximum face size and tetrahedral size are manually adjusted and the minimum element size is increased to eliminate overly small element size specifically around the turbine blade area. In general, a finer mesh is created around the turbine area so that the key features of the turbine blades can be properly resolved by the CFD solver. An inflation layer is also created from the faces of the turbine blades to provide a boundary layer with higher resolution to capture the flow field better. Due to the sharp end of the turbine blades at their trailing edges, the maximum degree of the curvature normal angle is manually increased so that mesh can be properly generated around the edges. Figure 3.27 and 3.28 shown the cut section and cross section of the generated mesh respectively. The quality metrics and element count of the final mesh are as follow:

- *Orthogonal quality*: Min: 0.08024, Average: 0.73022.
- *Skewness*: Max: 0.91976, Average: 0.26838.
- *Aspect ratio*: 25.552:1
- *Elements/cells count*: 202,714

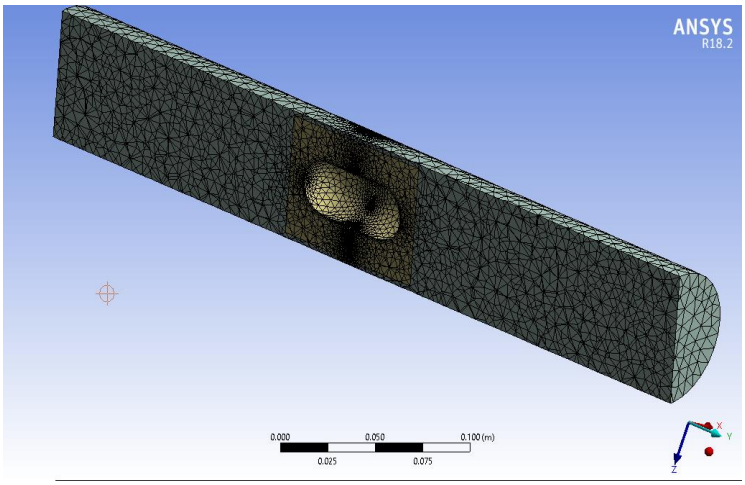

Figure 3.27: Cut section plane of the generated mesh for the air turbine simulation.

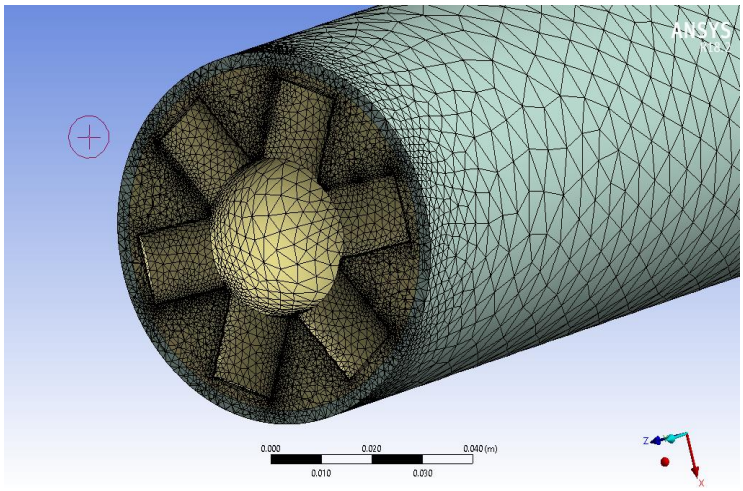

Figure 3.28: Cross-section of the air turbine.

In the Fluent general setting, the same pressure-based solver on transient fluid-flow with gravity enabled is applied. In order to simulate the turbine motion within the DWEC upper connecting duct during oscillation, the air flow changes across the DWEC upper duct from part 1 simulation results are compiled and loaded into Fluent as individual profiles that each carries the parameter of that defines the inlet settings for part 2 simulation. In details, these profiles are segregated by the oscillation cycle of the air flow across the upper duct such that each profile defines the air flow velocity over time before it changes direction as the next cycle starts. As seen in the plotted graph of air flow over time in Figure 3.29, the red section highlights a single air flow profile and the next profile would began right after it as the air flow velocity changes from positive to negative which indicates change in direction. These profiles are read in the boundary conditions task page in the Fluent setup.

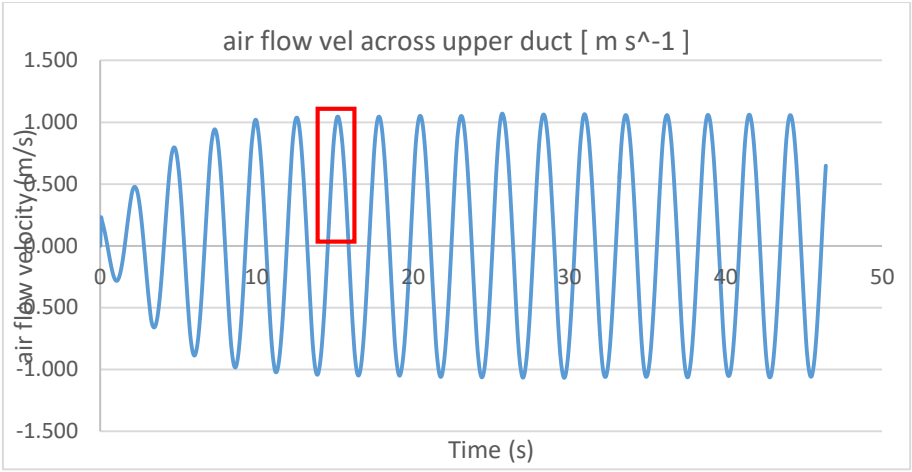

Figure 3.29: Air flow velocity across the upper duct data obtained from the simulation.

After all the profile files are loaded, a user customized program is needed to automatically assign the profiles to the inlet and outlet as the correct inflow openings in which the air flow direction is altered. Therefore, a scheme file is written using LISP programming language is set to run when a command is executed every time step. The executed command loads the scheme file and run the program which checks the current time step and switches the inlet and outlet settings in the solver and assigns the air flow profile accordingly, with this the bi-directional air flow across the upper connecting duct with well turbine can be correctly simulated in isolation from the rest of the DWEC body.

In the dynamic mesh settings, the 6-DOF (Six Degree of Freedom) solver provided by Fluent is enabled to resolve the force and momentum acted on the turbine and computes its angular motion with respect to its centre of gravity. The reason why 6-DOF is used is because it is capable of computing translational and angular motion of the center of gravity of an object using the object's forces and moments. To do so, a .C source file that defines the mass

properties, moment of inertia and its unrestrained DOF of the turbine is written and attached to the turbine in the 6-DOF settings. After that, a motion history file will be written every time step to record the turbine motion in terms of its DOF. As seen in the snapshot of Fluent dynamic mesh settings below, all smoothing, layering and remeshing methods are enabled as for the case of part 2 simulation, the mesh within the computational domain will undergo changes due to the rotating turbine. Thus, these mesh update methods will determine how the mesh changes will be dealt with by the solver during the simulation.

Once all the settings are done, the simulation is initialized and the calculation is set to run with a starting time-step of 0.001s and gradually reduced over time to 0.00025s with a max iteration of 40 per time step. The time step used here is noticably smaller in comparison to the part 1 due to dynamic mesh changes and a much complex simulation model. Figure 3.30 shows the visualized the simulated air flow (in arrows) across the air turbine.

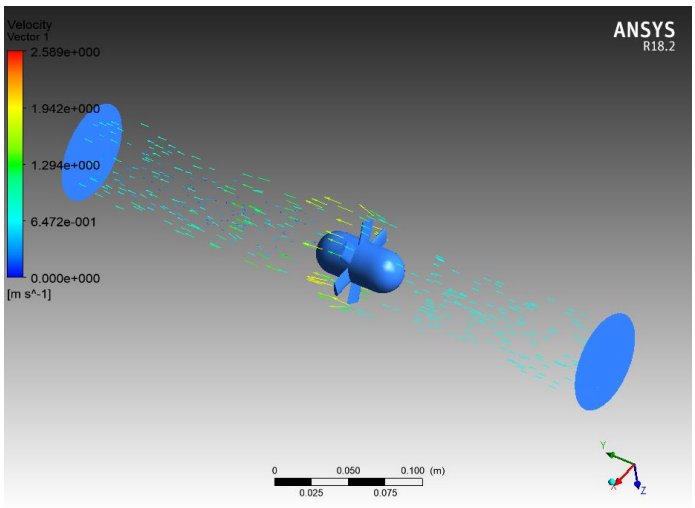

Figure 3.30: The visualized air flow across the air turbine using vector display.

CHAPTER 4

RESULTS AND DISCUSSIONS

4.1 Overview

In this section, the author tabulates, and analyses results from the experiments and simulations, follows up with in-depth discussion on the findings and their relations to the objectives to be achieved throughout the project. As organized in the methodology section, data results from three different sets of experiment: DWEC experiment set 1, set 2 and CFD simulation are analysed and discussed in that order. The flowchart in Figure 4.1 recaps the data collection as well as the data processing which are carried out in this section along with their associated components on the side.

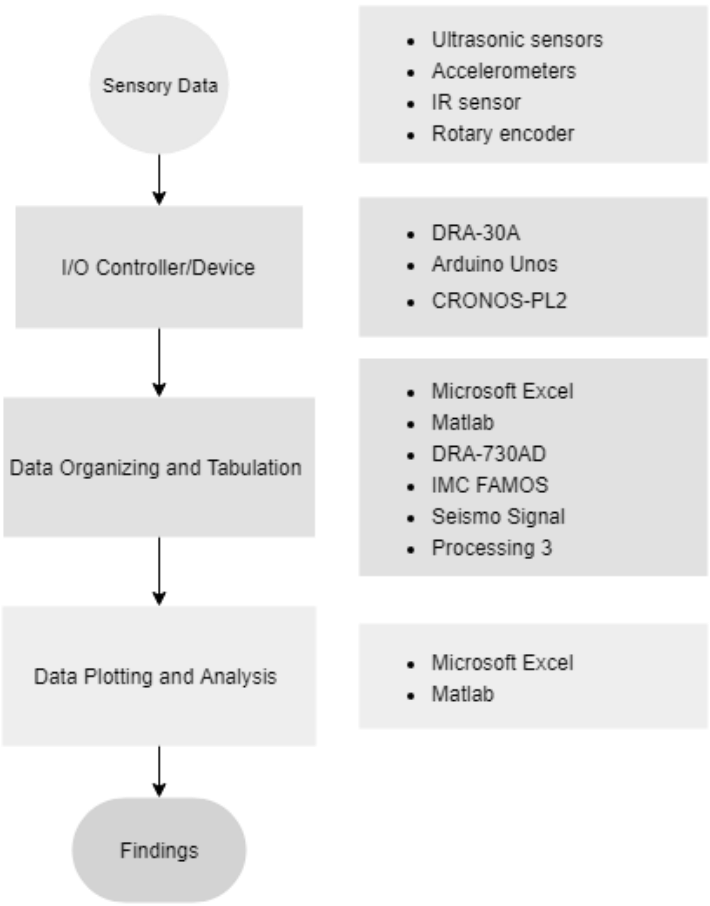

Figure 4. 1: Data collection and processing flowchart.

4.2 Experiment Set 1 (Hydro Turbine Pipeline)

Experiment Set 1 explores the first designed DWEC prototype whereby the DWEC model design is tested for its validity and its effectiveness as a vibration mitigating device on a platform when subjected to external periodic vibration by means of vibration test using shaking table. The feasibility of embedding an energy generating mechanism on the DWEC prototype in the form of pipelines and hydro turbines is also monitored for its potential in accordance to the design.

4.2.1 DWEC Performance Set 1

For the first configuration experiment, the oscillating motions of the DWEC-structure without presence of operating DWEC in response to a range of vibration frequency by the shaking table are recorded using ultrasonic sensor and accelerometer. The data obtained from the sensors are then processed and interpreted using different software and the significances of the result are discussed afterwards.

The ultrasonic sensor data are transferred from the Arduino controller to the PC through the connected serial port and are stored in PC using Processing 3 software in which a user written program that reads the outputs from the serial port and write them to a user named csv files. The first set of ultrasonic sensor data measures the displacement of the DWEC-structure on the shaking table from a fixed position over a range of frequency of 0.20-0.50Hz and ran for a time period of at least 20s. In the next section, three sets of selected raw readings for the frequency of 0.30, 0.40 and 0.50Hz respectively are plotted here in Figure 4.2.

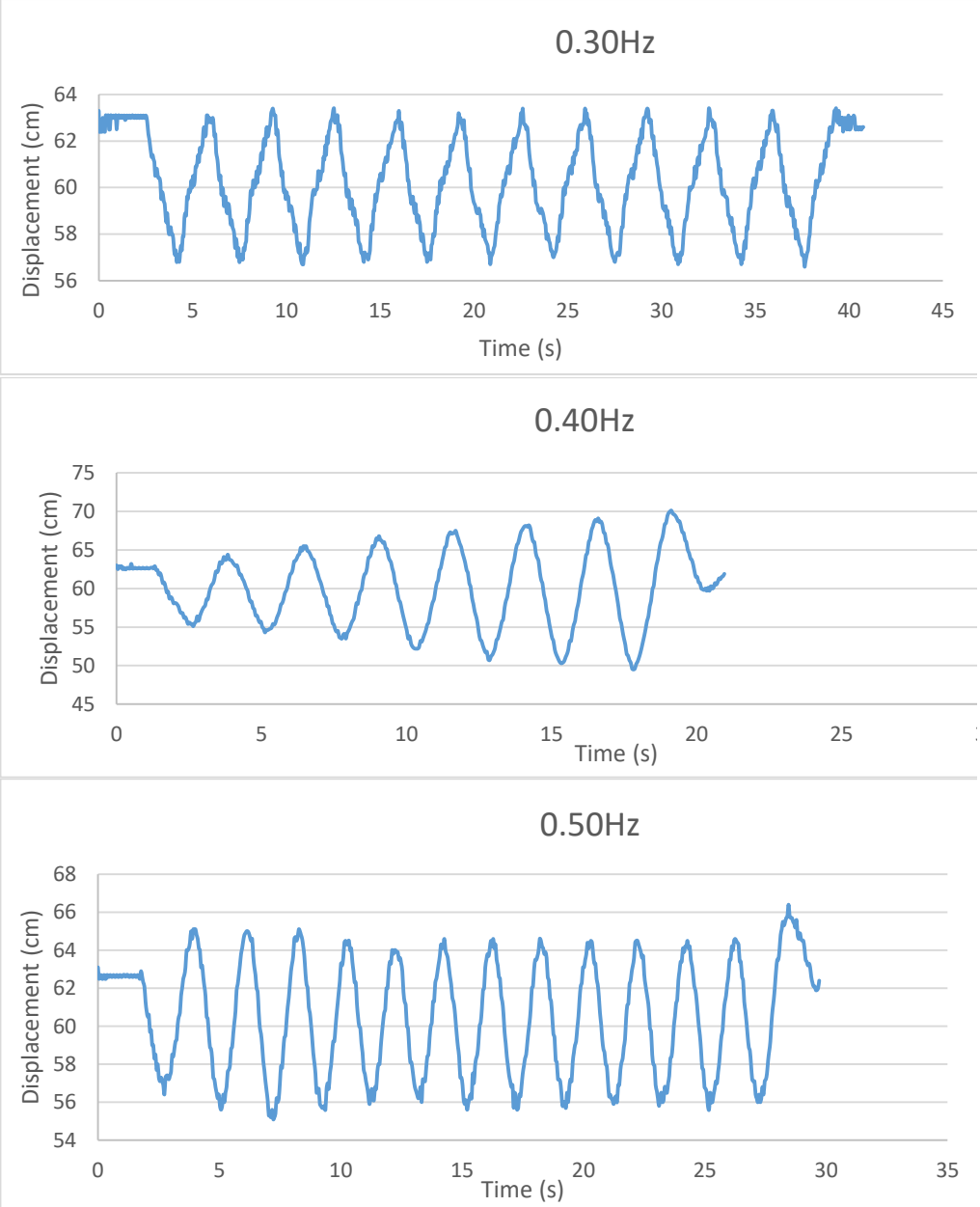

Figure 4. 2: Set 1 ultrasonic sensor readings of DWEC-structure displacement over time for the frequency point of 0.30, 0.40 and 0.50Hz without operating DWEC.

As observed from the raw ultrasonic sensor readings, the higher the input frequency the more the oscillating cycles occur within the same timeframe since higher frequency indicates shorter oscillation period ($f = \frac{1}{T}$). Some data noise from the sensor can be discerned from the charted outputs as well in the form of rapid fluctuation of data points during the oscillating motion. The

vibrating motion of the DWEC-structure are measured using the unit of centimetre (cm) during the time of experiment at which the starting point is approximately 63cm which is the distance of the sensor from the DWEC-structure.

To produce a clearer presentation of the data output, a series of data processing methods are applied as a prerequisite steps for the purpose of better data analysis. First off, zero offset is applied to the data to provide a clearer comparison outlook of the plotted graphs by shifting the all the data starting points to a fixed value of 0. Meanwhile, the measurement unit of the DWEC-structure's displacement is changed to metre (m) by reason of consistency throughout the thesis. Next, a low-pass filter with a cut-off frequency of 1Hz is designed and applied on the data with the use of Matlab software to eliminate unwanted noise data while preserving essential data information. The processed data for the previous three sets of raw data are presented in Figure 4.3. Similarly, the displacement data for the second configuration of the prototype in which the DWEC is operational undergoes the same processing methods and the results are shown as in Figure 4.4.

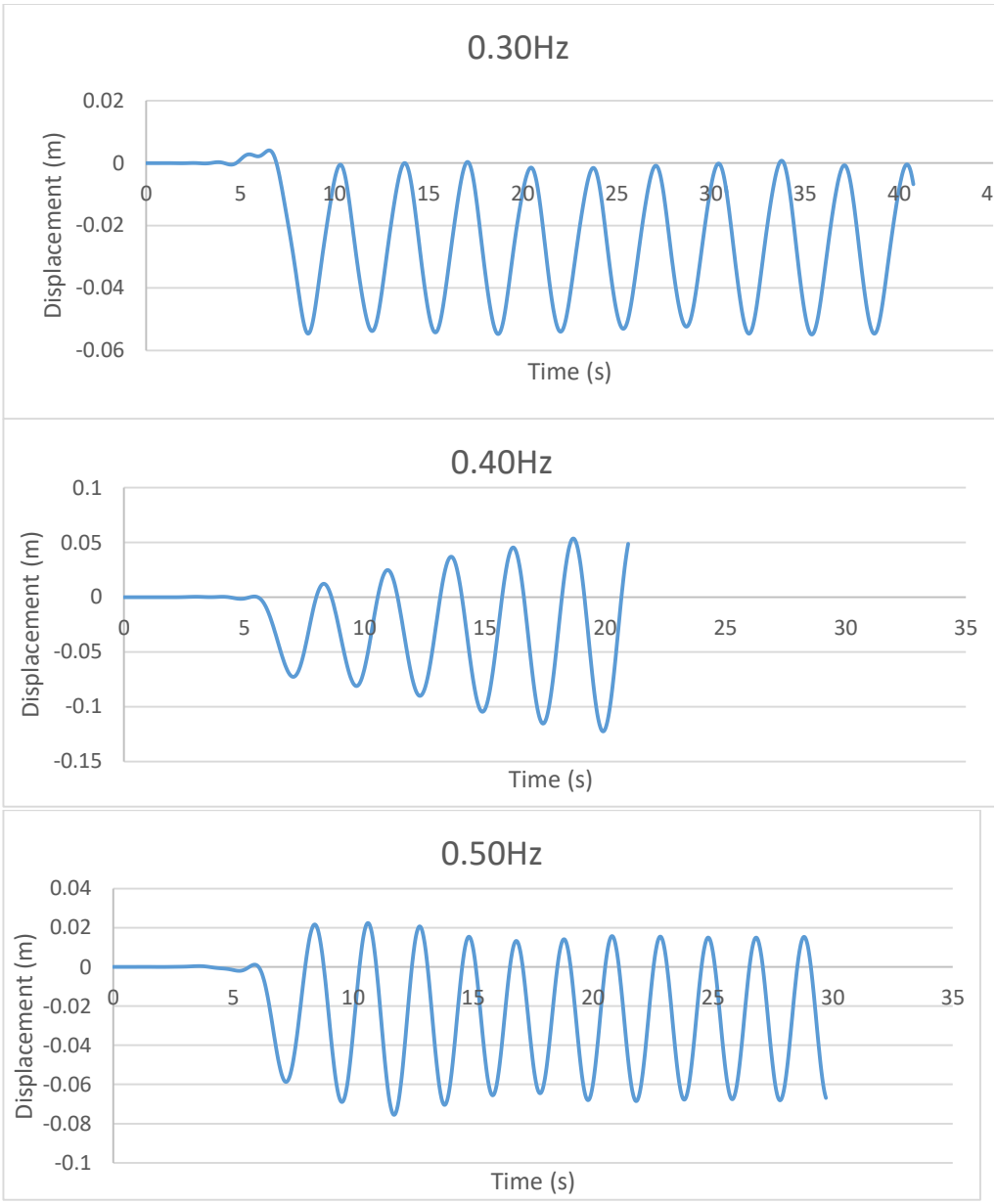

Figure 4. 3: Processed Set 1 ultrasonic sensor readings of DWEC-structure displacement over time for the frequency point of 0.30, 0.40 and 0.50Hz without operating DWEC.

At the 0.40Hz frequency point, the DWEC-structure's motion displacement is amplified as it increases by about 15% on each cycle due to the resonance phenomena in which the externally induced vibration frequency matches that of the system itself. For safety reason, the experiment was paused after the 20s mark to prevent further damage to the shaking table setup due to

excessive motion of the structure. In this case, the absolute peak-to-peak displacement value is obtained by measuring the sum of last two successive peaks before stopping.

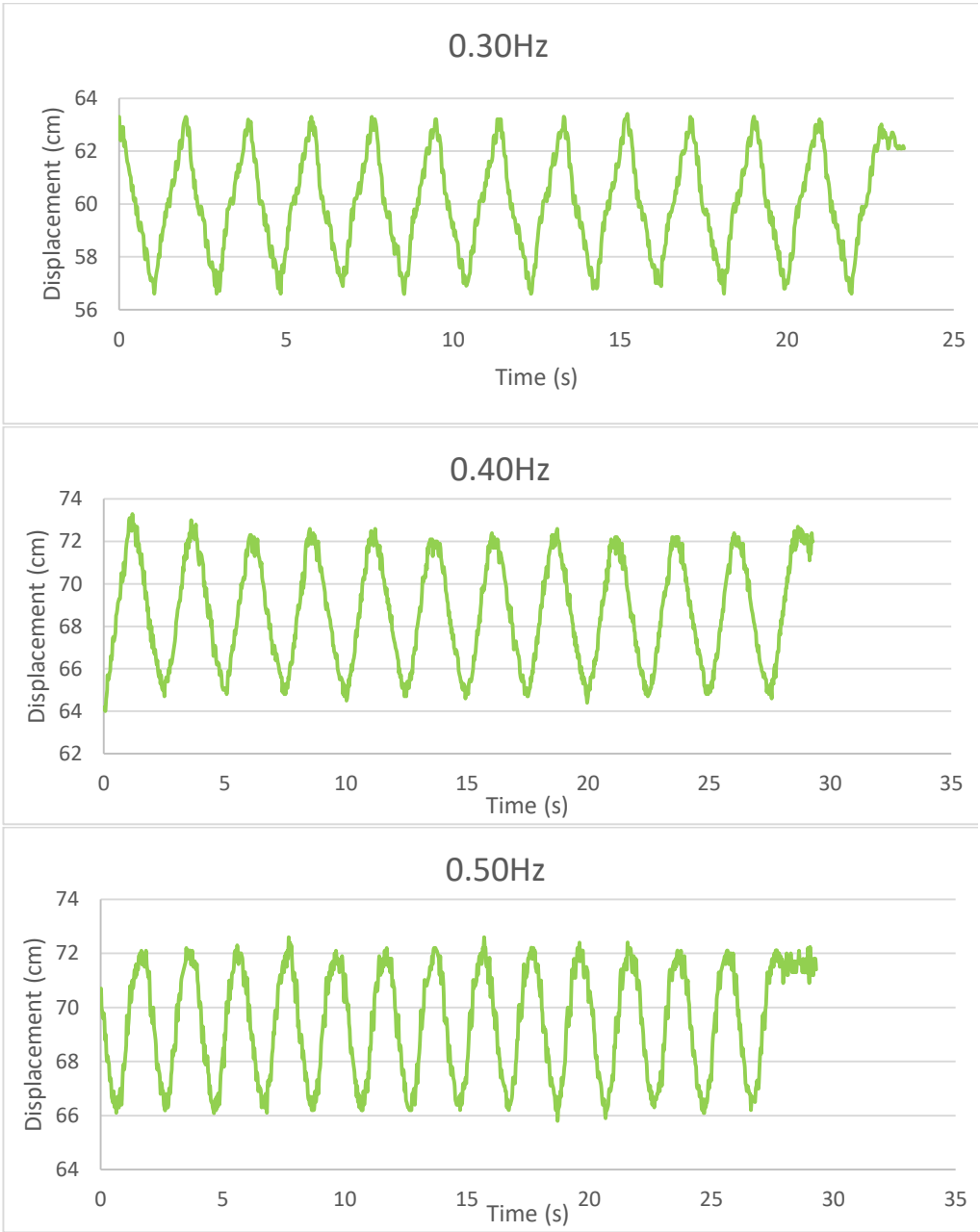

Figure 4. 4: Set 1 ultrasonic sensor readings of DWEC-structure displacement over time for the frequency point of 0.30, 0.40 and 0.50Hz with operating DWEC.

From the DWEC-structure displacement data as indicated by graphs in Figure 4.4, one particular issue is discovered here in which the data recorded

section was started too late as the shaking table vibration begins, resulting in a few seconds loss of vibration data at the beginning of the experiment, although the data result would not be affected, the initial starting position is deviated from the centre equilibrium point as observed in the first configuration graphs.

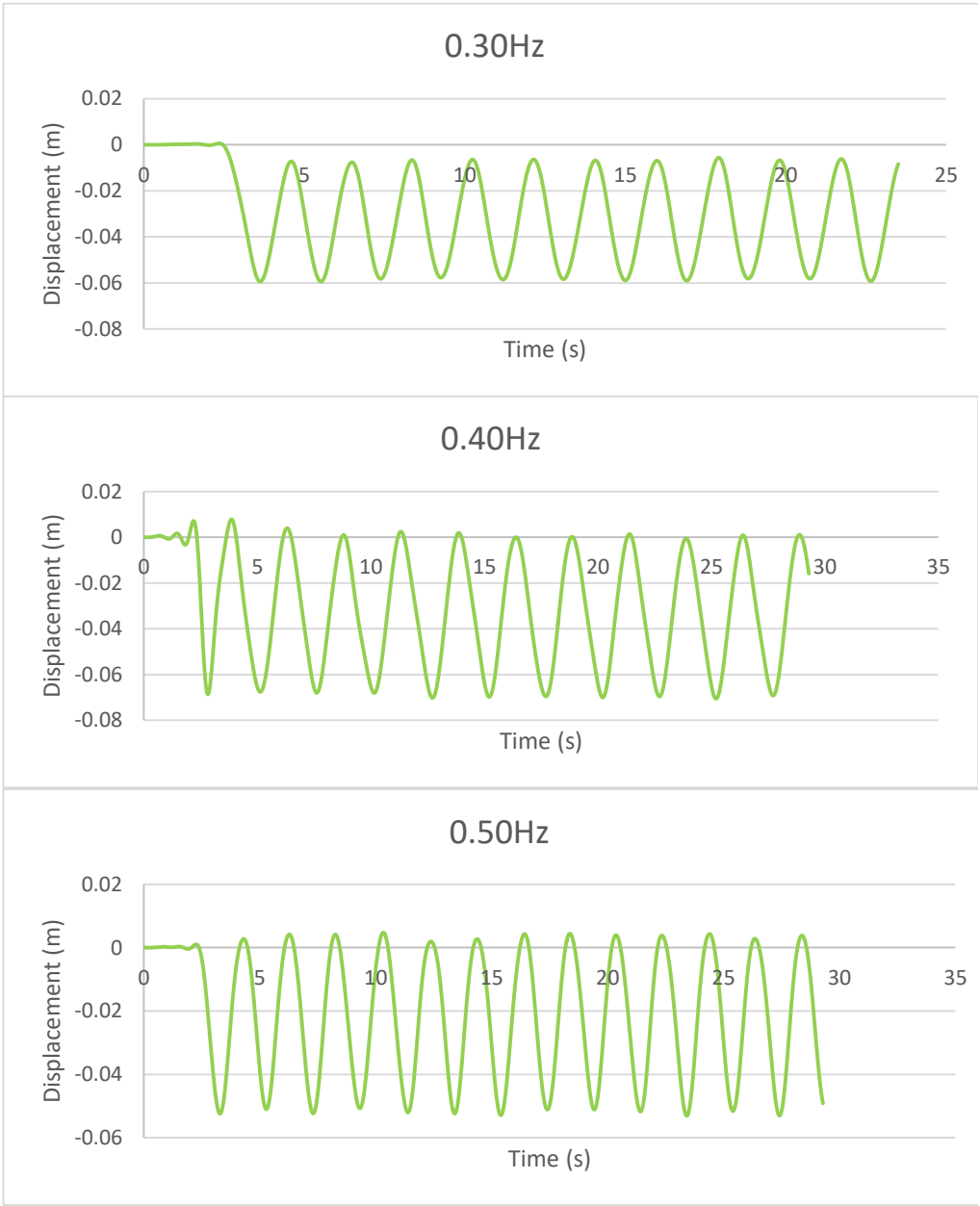

Figure 4. 5: Processed Set 1 ultrasonic sensor readings of DWEC-structure displacement over time for the frequency point of 0.30, 0.40 and 0.50Hz with operating DWEC.

With the processed displacement data, the average peak-to-peak displacement values for each frequency points and for both configurations are then computed by using Matlab. At first, the local maxima for each displacement data are first determined using the provided Findpeaks function and by inverting the data points (*-1), the local minima can then be determined using the same function as well. Due to the fact that the DWEC-structure's vibrating motion takes a brief moment to start-up and reach its steady-state motion, only the peak values past a given time period (15s in this case) are selected for further calculations. And by averaging the selected said peak values for both configurations, the comparison graph between the DWEC-structure's oscillating motion with and without an operating DWEC is plotted as displayed Figure 4.6.

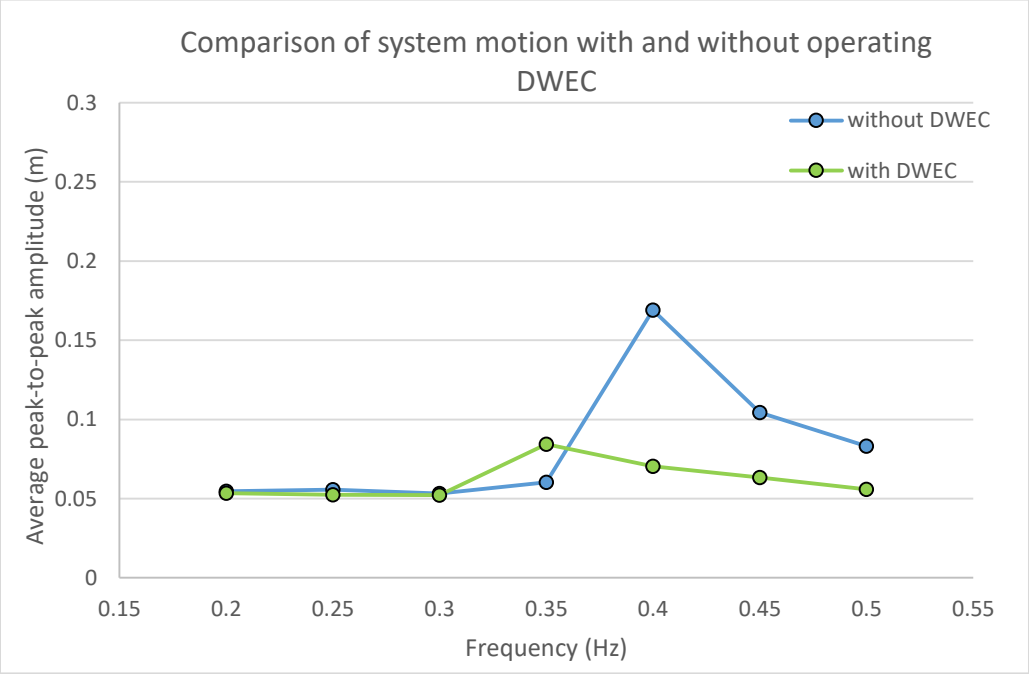

Figure 4. 6: Comparison graph of system motion with and without operating DWEC.

The comparison graph depicts the absolute motion of the DWEC-structure measured from a fixed point when oscillating motion of frequency from 0.20-0.50Hz is induced by the shaking table. Upon initial observation, the system of first configuration without the operating DWEC as indicated by blue line oscillates at a steady displacement of 0.05m at lower frequency range of 0.20-0.35Hz, then shows an abrupt increase in absolute displacement value of 0.168m at the frequency point of 0.40Hz and proceeds to fall off as the frequency increases. It is deduced that the DWEC-structure has a natural frequency at 0.40Hz as designed due to the occurrence of a resonance event in which the frequency of the induced vibrating motion matches natural frequency of the mechanical system, causing it to vibrate at an even greater amplitude. With that, the DWEC-structure prototype design is validated as it is operating as intended by the author's design.

The second configuration with the presence of an operating DWEC as indicated by the green line shows a different pattern in which the displacement value of the system gradually decreases as the frequency increases in comparison to that of the system without DWEC. As observed, the oscillating motion of the system with second configuration reduced as it passes over the frequency point of 0.40Hz. However, at 0.35Hz point the system experienced a larger oscillating motion with an operating DWEC, this indicates that the DWEC having an opposite effect on the system as the induced vibration frequency is not within its designed working range.

Therefore, similar to the mechanism of a typical TLCD, the DWEC is proven to be capable of mitigating externally induced vibration by the shaking table upon the DWEC-structure up to 58% of motion reduction albeit only within a frequency range that is pre-determined by the DWEC design. As the induced vibration frequency goes below or beyond the operating range of the DWEC, it may not able to provide an effective vibration reduction effect and may even worsen the vibration issue of the said system as indicated by the previous results.

4.2.2 Energy Generation Set 1

In this section, another sets of data of which the water height changes within the DWEC column which are collected simultaneously with the displacement data and are tabulated for further analysis. During the experiment for second configuration, the DWEC provides vibration mitigation on its mounted system through the sloshing water within its columns that oscillates out of phase with the incoming externally induced vibration and thus counteracts the movement of the system. Therefore, the measurement of water height changes for different induced frequency is important for studying the potential of harvesting energy from the oscillating motion of the water, specifically through the installation of hydro turbines.

In the following figure, three sets of raw ultrasonic sensor data for frequency points of 0.30, 0.40 and 0.50Hz are displayed in such order. As observed, the data are riddled with high frequency noises and some erratic readings that are easily distinguishable from the plotted graphs. Therefore, as per procedure, the data are processed with similar methods as previously applied to provide a clarified and standardized version of ultrasonic data for further analysis.

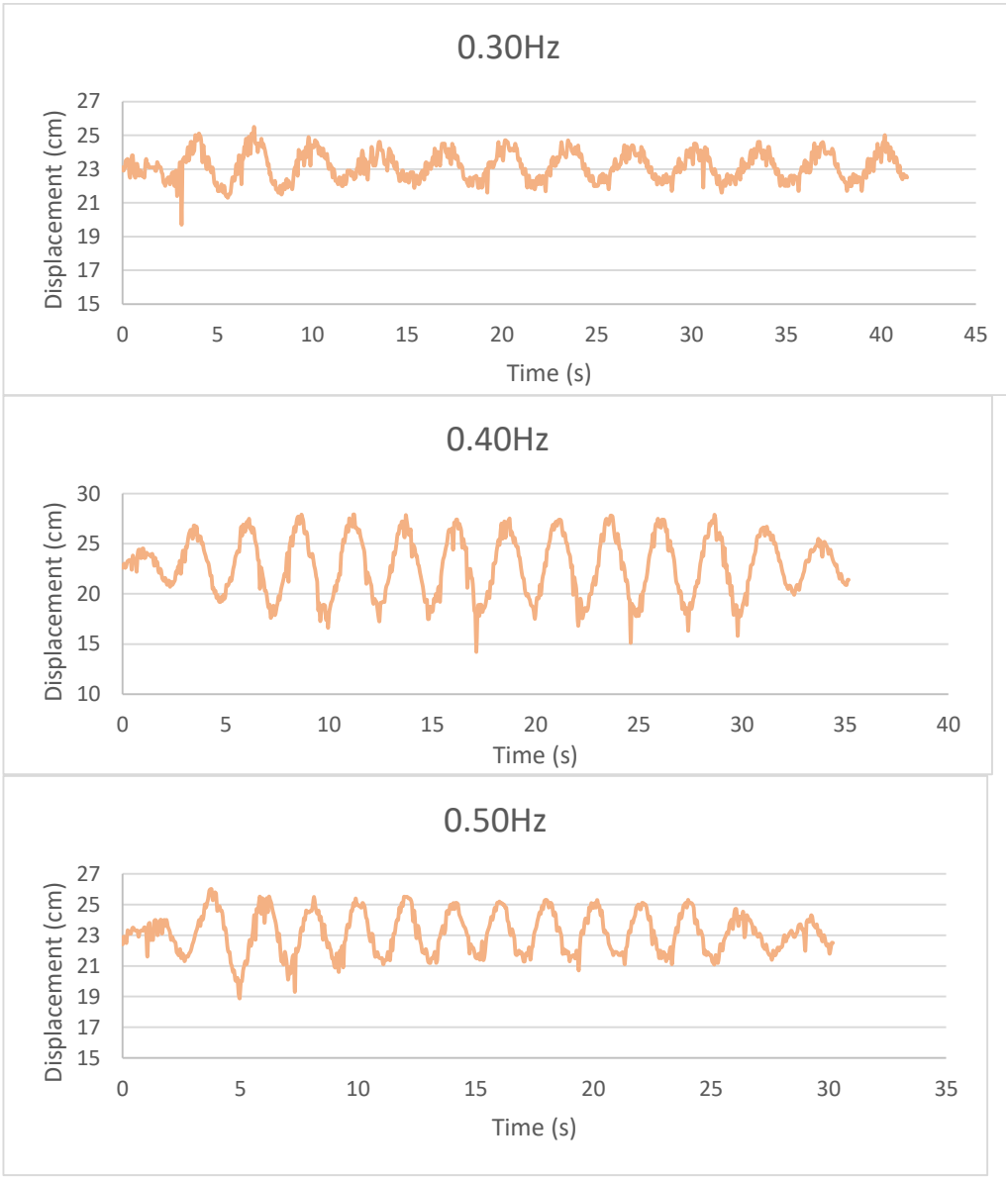

Figure 4. 7: Set 1 ultrasonic sensor data for water height changes within DWEC column for frequency point of 0.30, 0.40 and 0.50Hz.

The three sets of processed data are as displayed in Figure 4.8. As observed, the data readings are visibly cleaner and easier to quantify the difference between the data for each frequency points. With all the data processed, the average peak-to-peak water height changes for all frequency points can be compiled and plotted in the following graph.

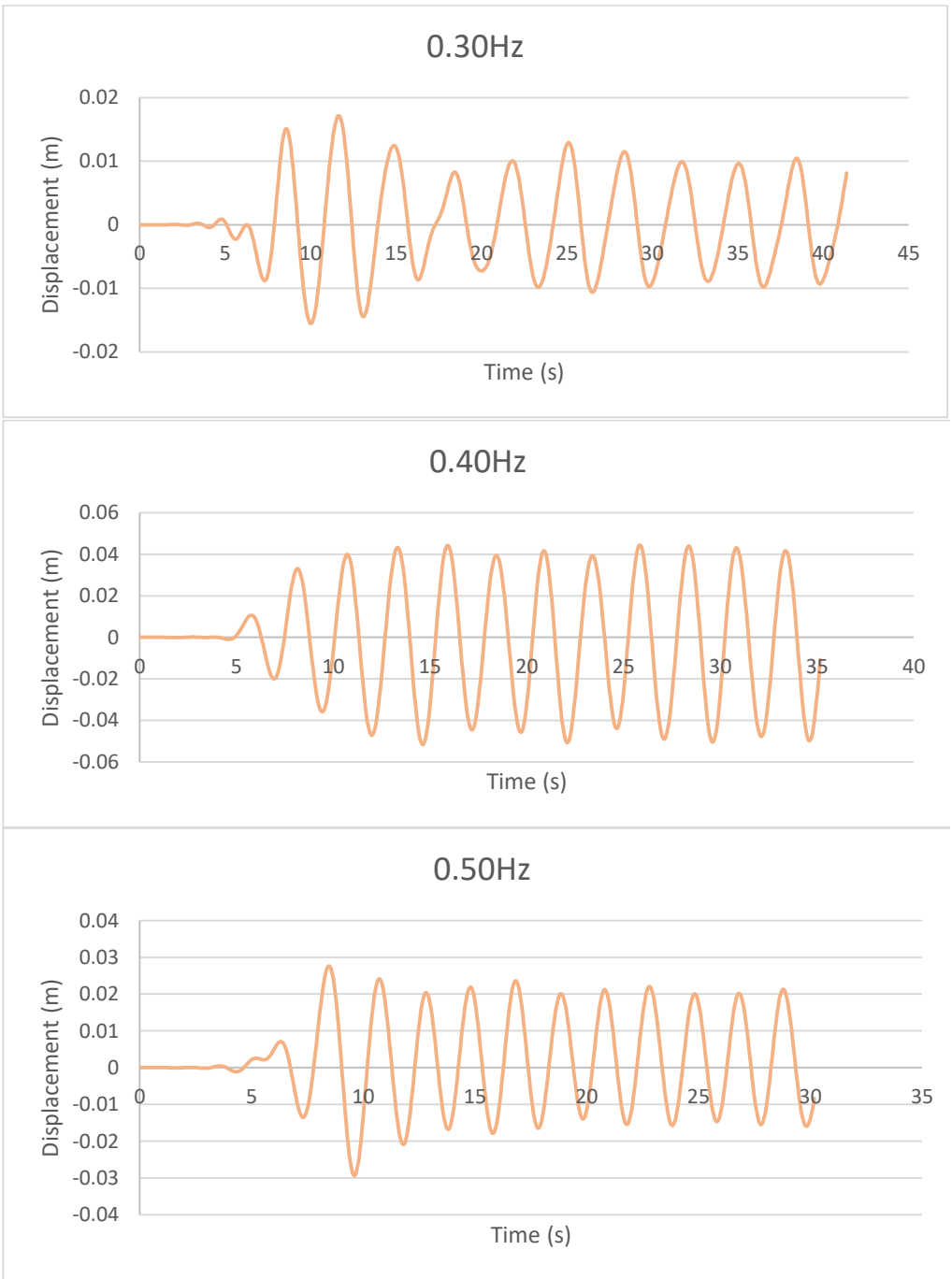

Figure 4. 8: Processed Set 1 ultrasonic sensor data for water height changes within DWEC column for frequency point of 0.30, 0.40 and 0.50Hz.

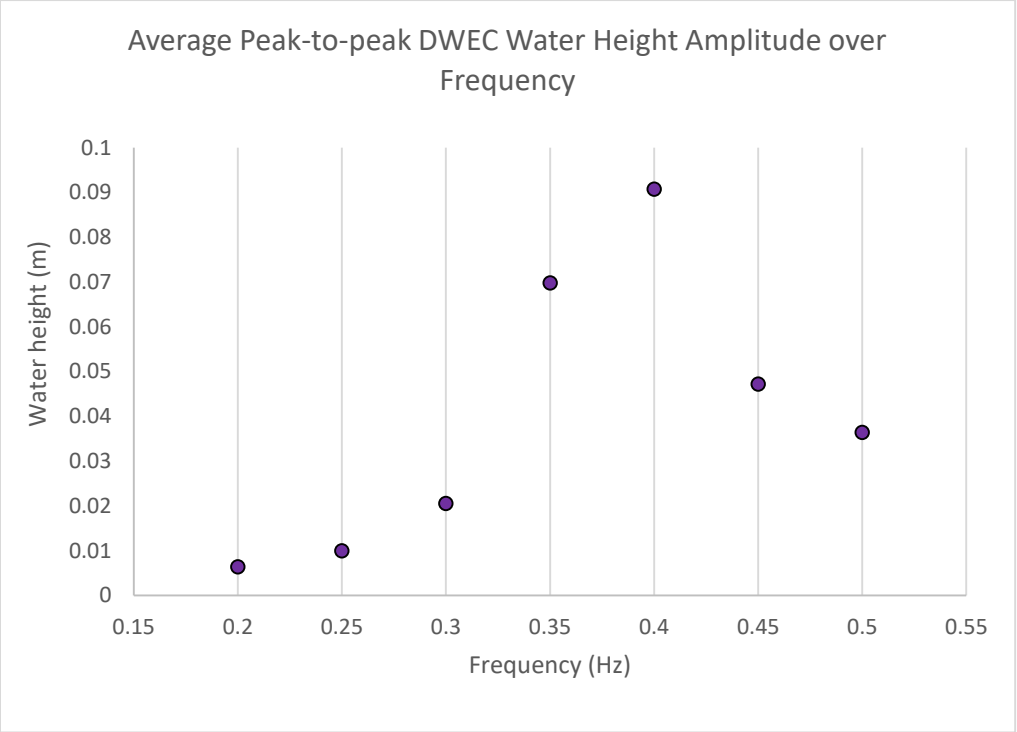

Figure 4. 9: Graph of peak water height changes within DWEC column over frequency range.

From the plotted graph of results in Figure 4.9 compiled from the water height data, the largest absolute height change of 0.09m is located at the 0.40Hz, followed by 0.07m at frequency point of 0.35Hz, while the data curve falls off on both ends. As the induced vibration frequency approaches the natural frequency of the DWEC-structure, the DWEC-structure's dynamic response becomes greater, the more the energy is absorbed by the sloshing water within the DWEC column as indicated by the larger change in water height, thus the vibrating motion of the system is effectively suppressed by the DWEC.

On the other hand, throughout the vibration experiment, the installed micro hydro turbines shown no sign of notable rotational movement through observing the indicator regardless of any induced vibration frequencies and the water height changes within the DWEC column. According to the specifications of the hydro turbine provided by the supplier, the turbine requires a minimum water flow rate of 4L/min (or 0.068 kg/s) to begin generate electricity.

At the largest water height changes of 0.09m at 0.40Hz frequency point, the average water flow rate from one column to another can be determined by calculating the mass of water transferred during each half of the oscillating cycle as following:

$$water\ flow\ rate\ \left(\frac{kg}{s}\right) = \frac{mass\ of\ water}{time\ taken} = \frac{1000\ (\ 0.09\ x\ 0.4\ x\ 0.1\ )}{1.25} = 2.88\frac{kg}{s}$$

From the calculation above, the maximum water flow rate across the pipeline through the hydro turbine can then be computed by relating the cross sectional area of the turbine pipeline and the bottom connecting duct with the following method:

$$cross\ sectional\ area\ of\ bottom\ connecting\ duct = (0.1\ x\ 0.1)m$$

$$= 0.01m^2$$

$$cross\ sectional\ area\ of\ pipeline = \pi\ (0.0075m)^2 = 1.767\ x\ 10^{-4}m^2$$

$$Maximum\ flow\ rate\ across\ pipeline = 2.88\ x\ \left(\frac{1.767\ x\ 10^{-4}}{0.01 +\ 1.767\ x\ 10^{-4}}\right)$$

$$= 0.05\,\frac{kg}{s}$$

Based on the calculations, the maximum flow rate from the experiment at the 0.40Hz frequency point in which the water height change is the highest did not exceeds the minimum required to drive the turbine. With an added-on one-way swing check valve along the pipeline that further impedes the water flow across the pipeline, the installed micro hydro turbine for the DWEC was not capable to extract energy from the water flow during the oscillatory motion of the structure.

4.3 Experiment Set 2 (Air Turbine Chamber)

In this section, the results data obtained from the experiment Set 2 for the second DWEC design option are tabulated and analysed accordingly.

Prior to the beginning of experiment, a sanity test on the vibrating motion of the shaking table is also conducted to ensure that the vibration frequency generated is the same as input by the user through the controller. The shaking table is ran for the same set of frequencies as applied in the experiment Set 2 with the DWEC-structure mounted on the platform and the acceleration data obtained from the attached accelerometer are analysed. An Excel macro is written to speed up the data conversion process in which the raw accelerometer

data are zero-offset, multiplied with coefficient value in accordance to the accelerometer used and saved in an individual csv file. Using the FFT method, the frequency components for each vibration test are studied and their respective dominant frequencies are extracted and compared with the intended input frequency values in Table 4.1.

From the processed shaking table acceleration data, the average discrepancy of the generated vibration frequency is about 1.16% from the input frequency value which is suffice for the experimental purpose onwards.

Table 4. 1: Comparison of user input frequency and measured shaking table vibration frequency.

Input frequency (Hz)	Shaking table vibration frequency (Hz)	Discrepancy (%)
0.2	0.2004	0.200
0.25	0.2425	3.000
0.3	0.2974	0.867
0.32	0.3094	3.313
0.34	0.3503	3.029
0.36	0.3618	0.500
0.37	0.365	1.351
0.38	0.382	0.526
0.39	0.3944	1.128
0.4	0.4007	0.175
0.41	0.4065	0.854
0.42	0.4169	0.738
0.44	0.4357	0.977
0.46	0.454	1.304
0.48	0.4805	0.104
0.5	0.4984	0.320
0.55	0.5457	0.782
0.6	0.5897	1.717
	Average:	1.160%

4.3.1 DWEC Performance Set 2

Likewise, the ultrasonic sensor data for both first and second configuration are collected from the experiments are organized and tabulated with three sets of raw data selected for illustration purpose as shown in plotted graphs in Figure 4.10 and the consequential processed data with the aforementioned methods respectively.

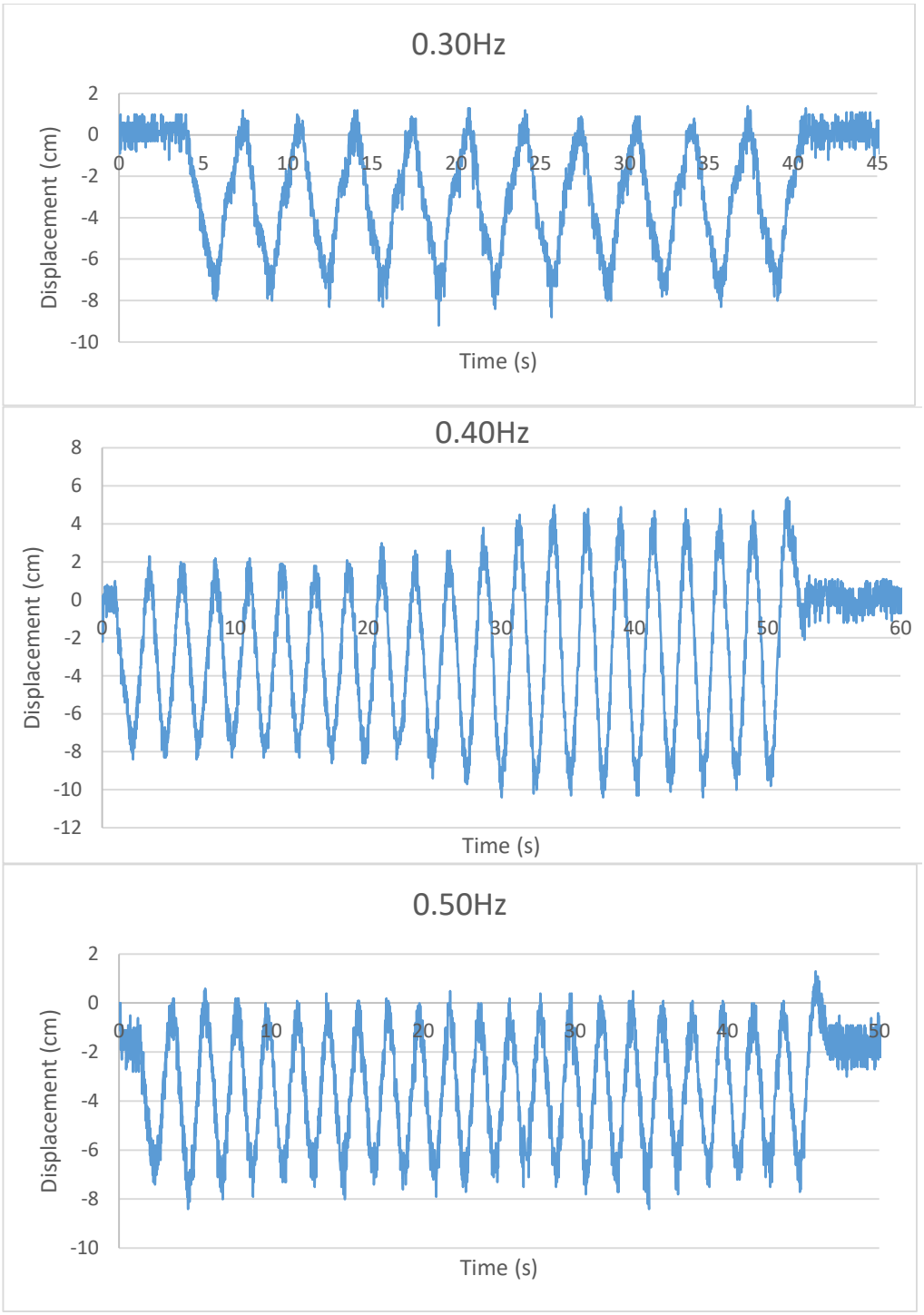

Figure 4.10: Set 2 ultrasonic sensor readings of DWEC-structure displacement over time for the frequency point of 0.30, 0.40 and 0.50Hz without operating DWEC.

In comparison to the Set 1 results, the amount of data noises present in the plotted line is higher due to the doubled in sampling rate from 0.05s per data point (20Hz) to 0.025s per data point in the case of Set 2 experiment. Upon

observation, the resonance phenomena that took place in the Set 1 experiment at the frequency point of 0.40Hz is also observed in the Set 2 result albeit to a lesser extent as the absolute displacement of the DWEC-structure rapidly increased by 33%.

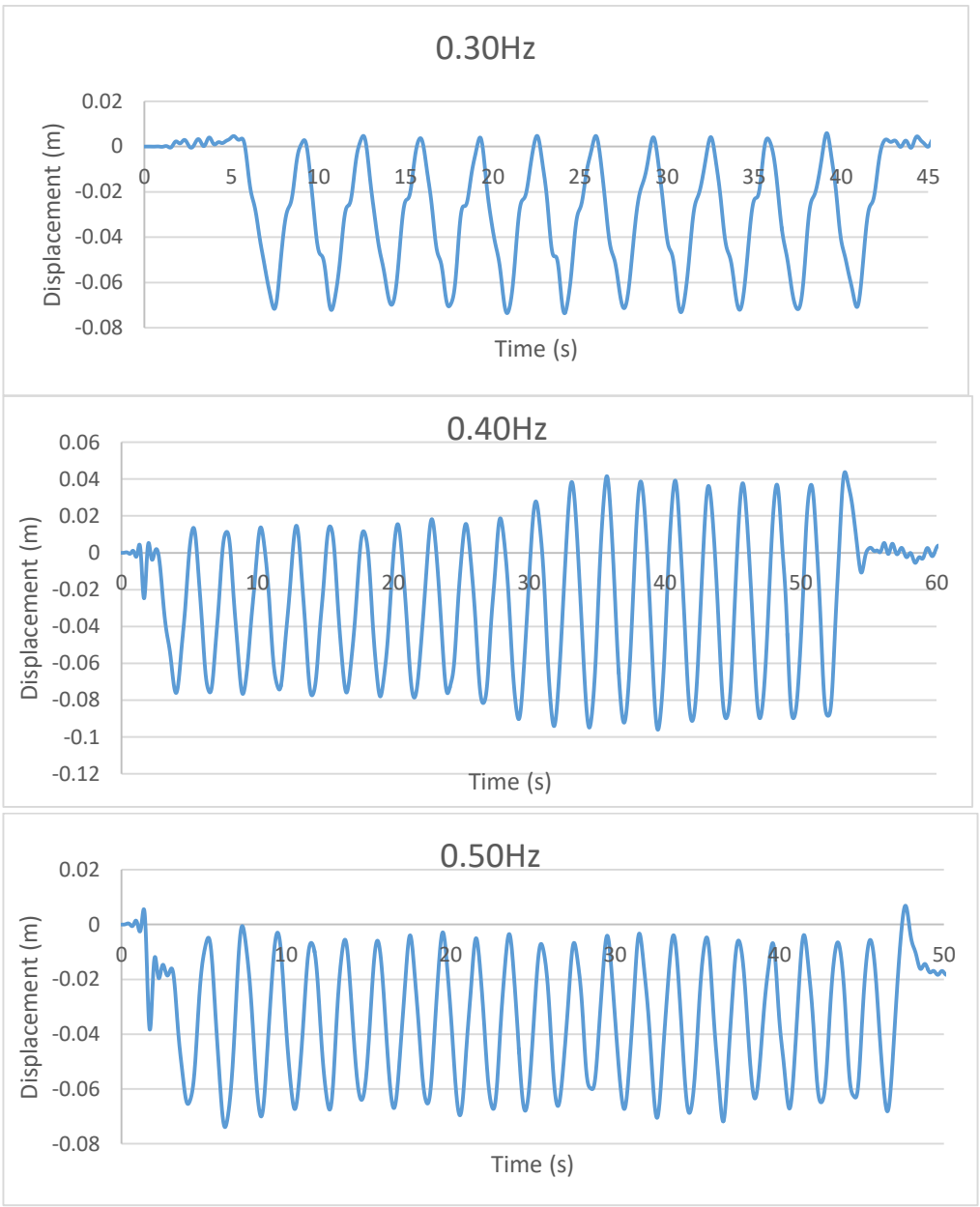

Figure 4.11: Processed Set 2 ultrasonic sensor readings of DWEC-structure displacement over time for the frequency point of 0.30, 0.40 and 0.50Hz without operating DWEC.

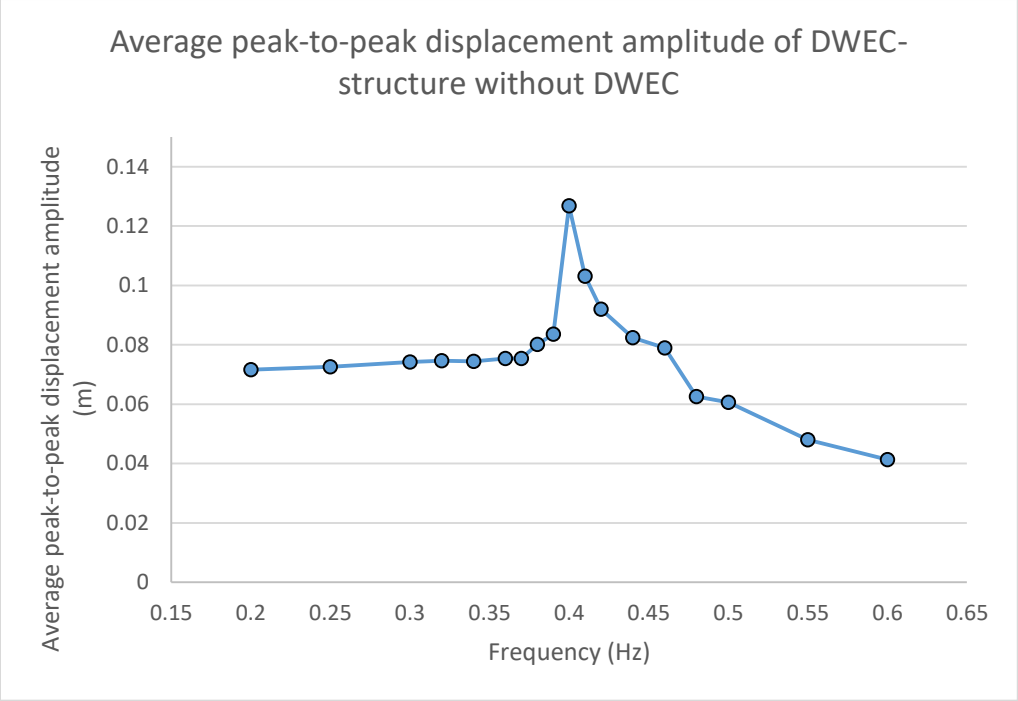

Figure 4.12: Graph of Average peak-to-peak displacement amplitude of DWEC-structure without DWEC over frequency range.

The average peak-to-peak displacement for each frequency point for first configuration is compiled and plotted in the Figure 4.12. With a higher resolution data that is obtained in the experiment Set 2, the experimental result is made comparison with that of the theoretical values for the motion response of the DWEC-structure under harmonic motion of the base that is calculated using the derived equation of motion:

$$X = Y\left[\frac{1+(2\zeta r)^2}{(1-r^2)^2+(2\zeta r)^2}\right]^{1/2} \quad (4.1)$$

Where X is the motion response of DWEC-structure, Y is the displacement of the base which in this case, represents the shaking table moving platform, ζ denotes the damping ratio while r denotes the frequency ratio of the induced vibrating motion with respect to the structure's natural frequency. The damping ratio is calculated from the equation:

$$\zeta = \frac{c_{equivalent}}{c_{critical}} = \frac{\frac{4F_f}{\omega \pi x}}{2m\omega} \quad (4.2)$$

Where:

$c_{equivalent}$ = equivalent damping coefficient,

$c_{critical}$ = critical damping coefficient,

m = mass of the DWEC-structure,

ω = natural frequency of DWEC-structure,

F_f = friction force,

x = maximum displacement from initial position.

The values of the latter two variables are obtained from the natural decaying of the free vibration motion of the DWEC-structure in which the structure is pulled and released from a point away from its equilibrium position without interference from any external force. With that, the calculated damping ratio of the DWEC-structure is 0.19045.

Since the motion response equation is derived with the assumption that Y is a sinusoidal motion or $Y = \sin \omega t$ while the vibration generated by the shaking table is in triangular wave form with the given inputs of frequency and amplitude, an approximation of the system theoretical response, X is obtained by applying a 0.21 coefficient on Y based on theoretical kinetic energy difference between sinusoidal and triangular wave as since with the same given amplitude and frequency, the sinusoidal wave has 21% higher kinetic energy in comparison to that of triangular wave, as shown in Figure 4.13. The resultant

theoretical values for sine wave approximation is as plotted in Figure 4.15(red-triangle line).

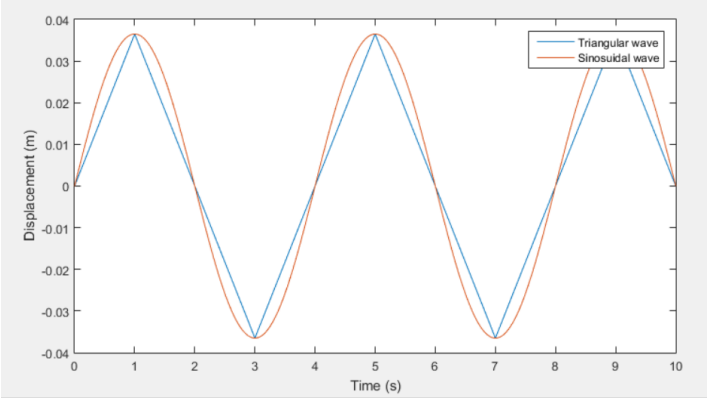

Figure 4.13: Plotted curves of triangular and sinusoidal wave with same frequency and amplitude.

A better approximation of the theoretical system response is further done by improving the base motion accuracy through signal reconstruction. As shown in Figure 4.14, the frequency components for each triangular wave input motions are analysed through FFT method in MATLAB and the frequencies points with significant amplitudes are extracted, then a replicated base input motion is reconstructed with the extracted information using sinusoidal wave form and the resultant average peak-to-peak displacement values are used to compute the system theoretical response with the same equation, as plotted in Figure 4.15(brown-diamond line).

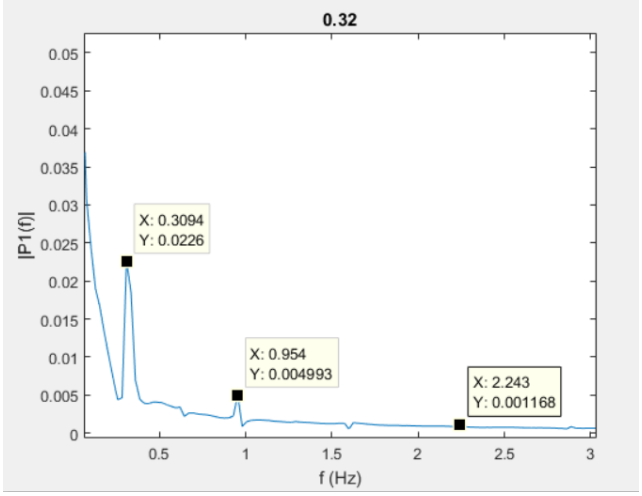

Figure 4.14: Graph of magnitude over frequency domain for frequency point of 0.38Hz.

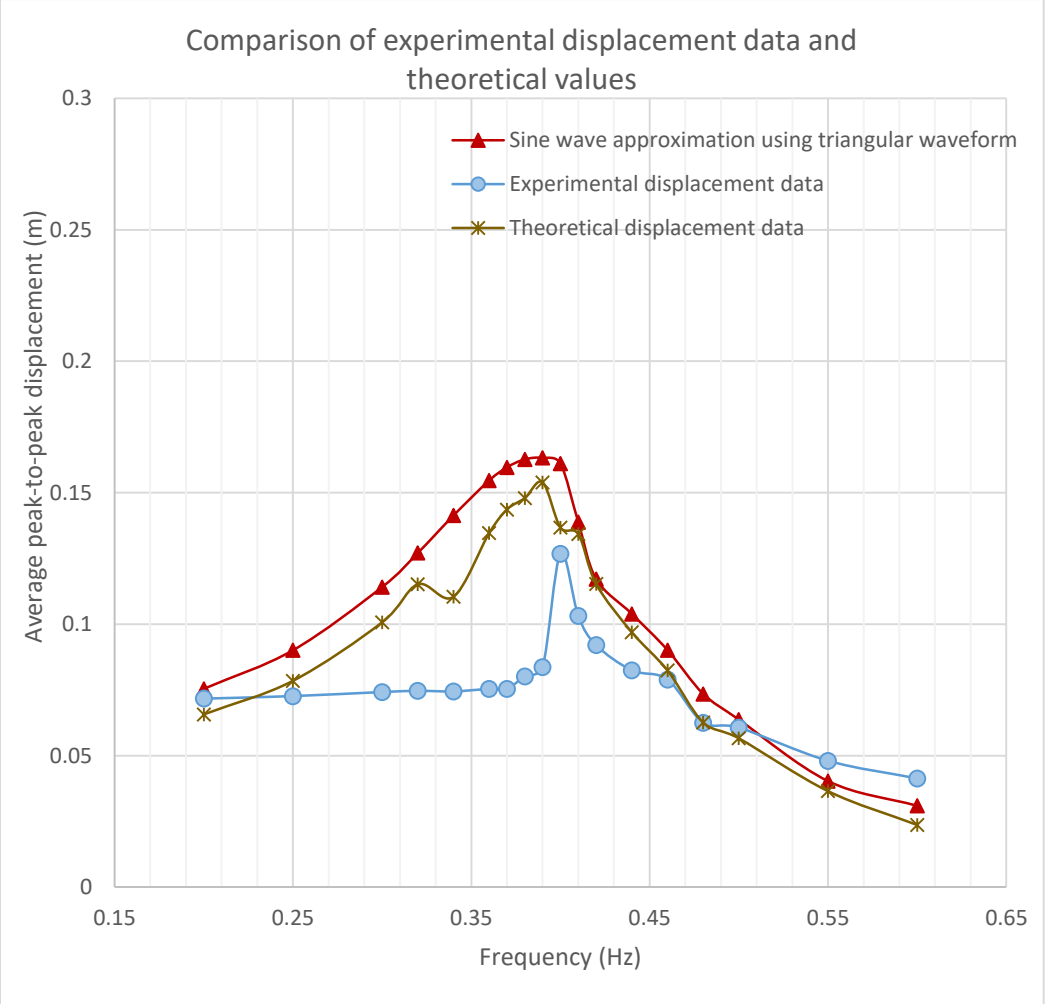

Figure 4.15: Graph of plotted theoretical values in comparison with experimental data.

As observed in Figure 4.15, the charted experimental data (blue-circle line) did not exhibit the similar ascending displacement value in the opening slope as the frequency ratio increases as indicated by the expected theoretical data curve (brown-diamond line), but instead remains at around 0.07m mark until frequency point of closing to 0.38Hz. Such phenomena is explained in the next paragraph where the displacement profiles of the DWEC-structure with respect to the shaking table are obtained from rotary encoder for three selected different input vibration frequency: 0.32Hz (a), 0.40Hz (b) and 0.44Hz (c) are shown in Figure 4.16-4.18.

In the case of 0.32Hz (a), the vibrating motion of the DWEC-structure is not completed as it slows down and came close to a halt before completing a full oscillation cycle, at which the next cycle begins as indicated by the stuttering movement observed at the equilibrium position. Reaching over the 0.40Hz point (b) and beyond, the oscillating motion of the DWEC-structure seen to be completed and fully developed as shown in the 0.44Hz case (c). Despite such phenomena may be resolved by increasing the input displacement of the shaking table, allowing the DWEC-structure to complete its oscillation due to an indirect increase in oscillating velocity, the maximum allowable input displacement of the shaking table has already been applied for these frequency points during the experiment.

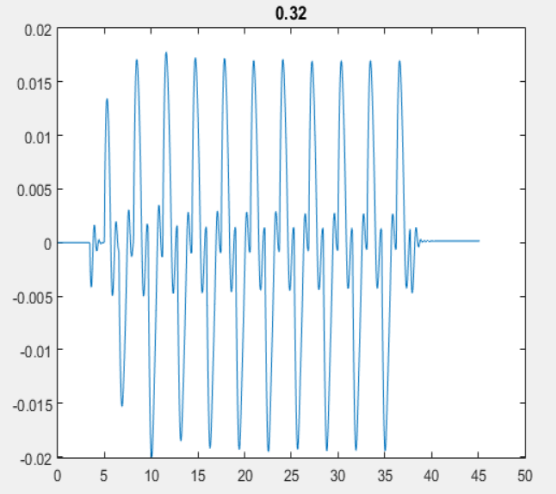

Figure 4.16: 0.32Hz (a)

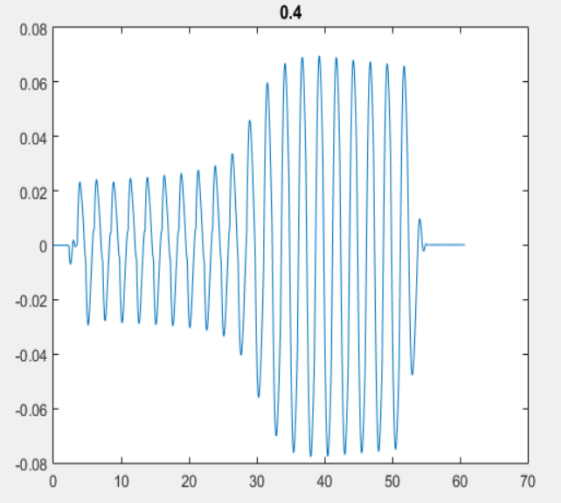

Figure 4.17: 0.40Hz (b)

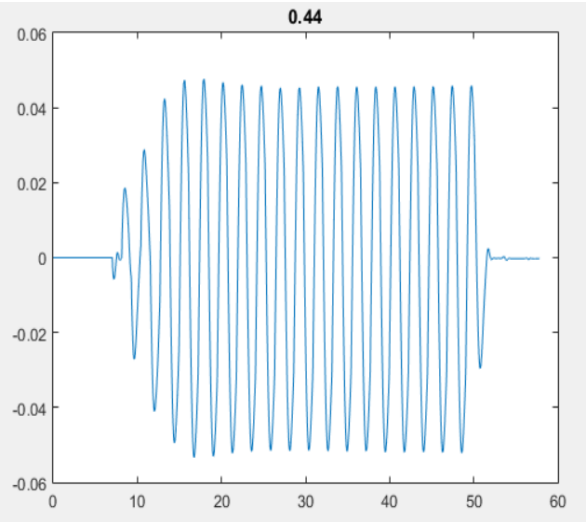

Figure 4.18: 0.44Hz (c)

Therefore, the obtained experimental average peak-to-peak displacement amplitude data displayed a similar trend as the theoretical one except the preceding part of the data due to experimental limitations, since the vibration characteristic of the DWEC-structure is behaving as initially designed. As seen from the theoretical data curve, a higher peak-to-peak displacement value of 0.14m is expected to be located at frequency point of 0.39Hz due to the natural of a damped system as illustrated in Figure 4.19 where the greater the damping ratio of the system, the lower the frequency point at which the resonance occurred as it gets reduces.

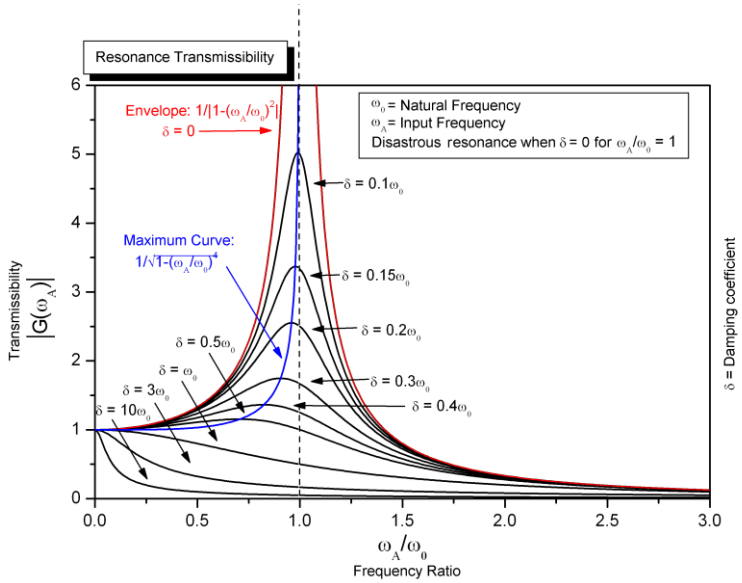

Figure 4.19: Displacement transmissibility over frequency ratio (Katsuhiko, 2005).

Similarly, three sets of raw and processed data for the second configuration experiment where the DWEC is operational are plotted in Figure 4.20 and 4.21 respectively. In comparison to the Set 1 results, the off-the-mark

data recording issue is solved by starting the recording sessions before the shaking table starts to vibrate.

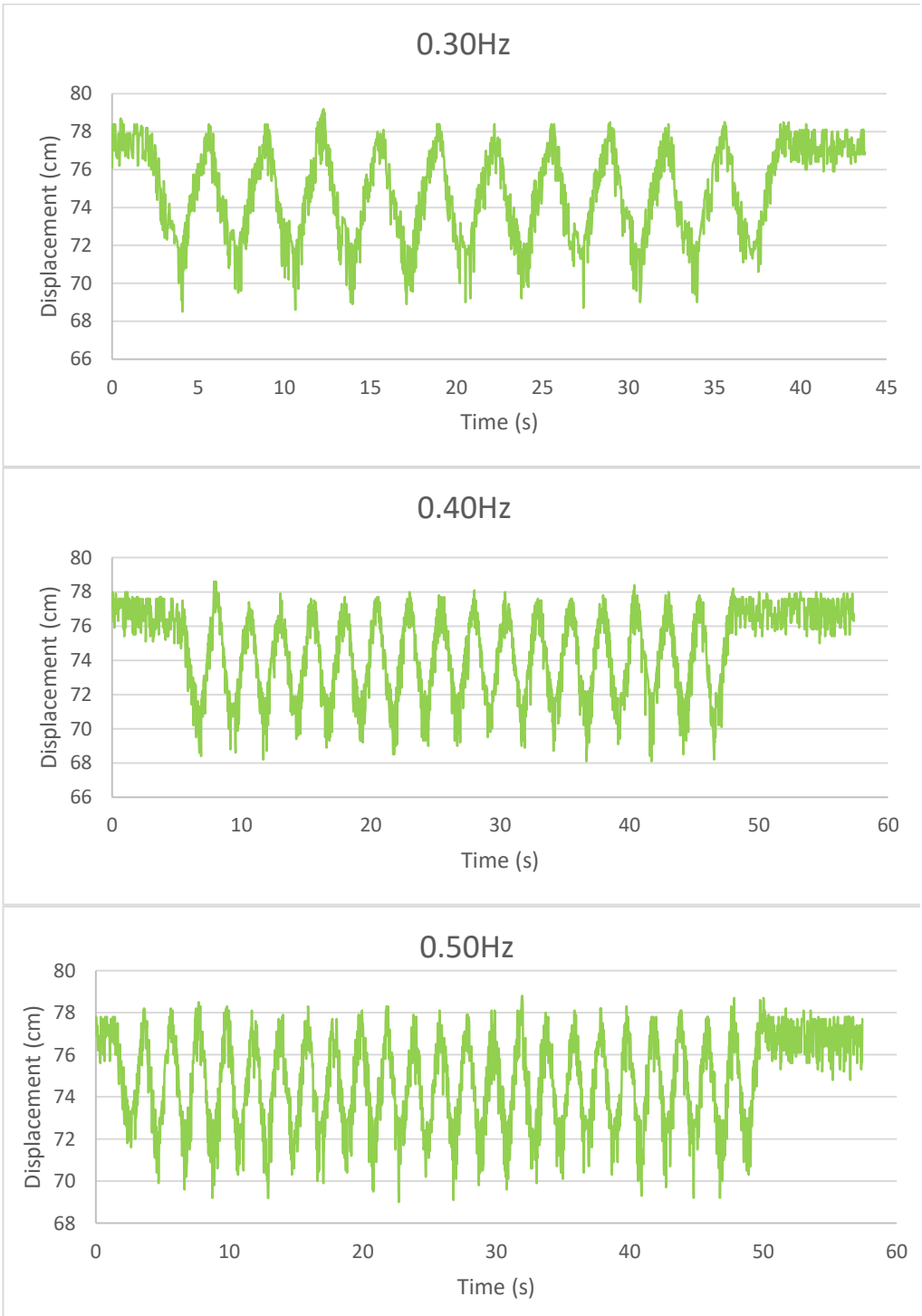

Figure 4.20: Set 2 ultrasonic sensor readings of DWEC-structure displacement over time for the frequency point of 0.30, 0.40 and 0.50Hz with operating DWEC.

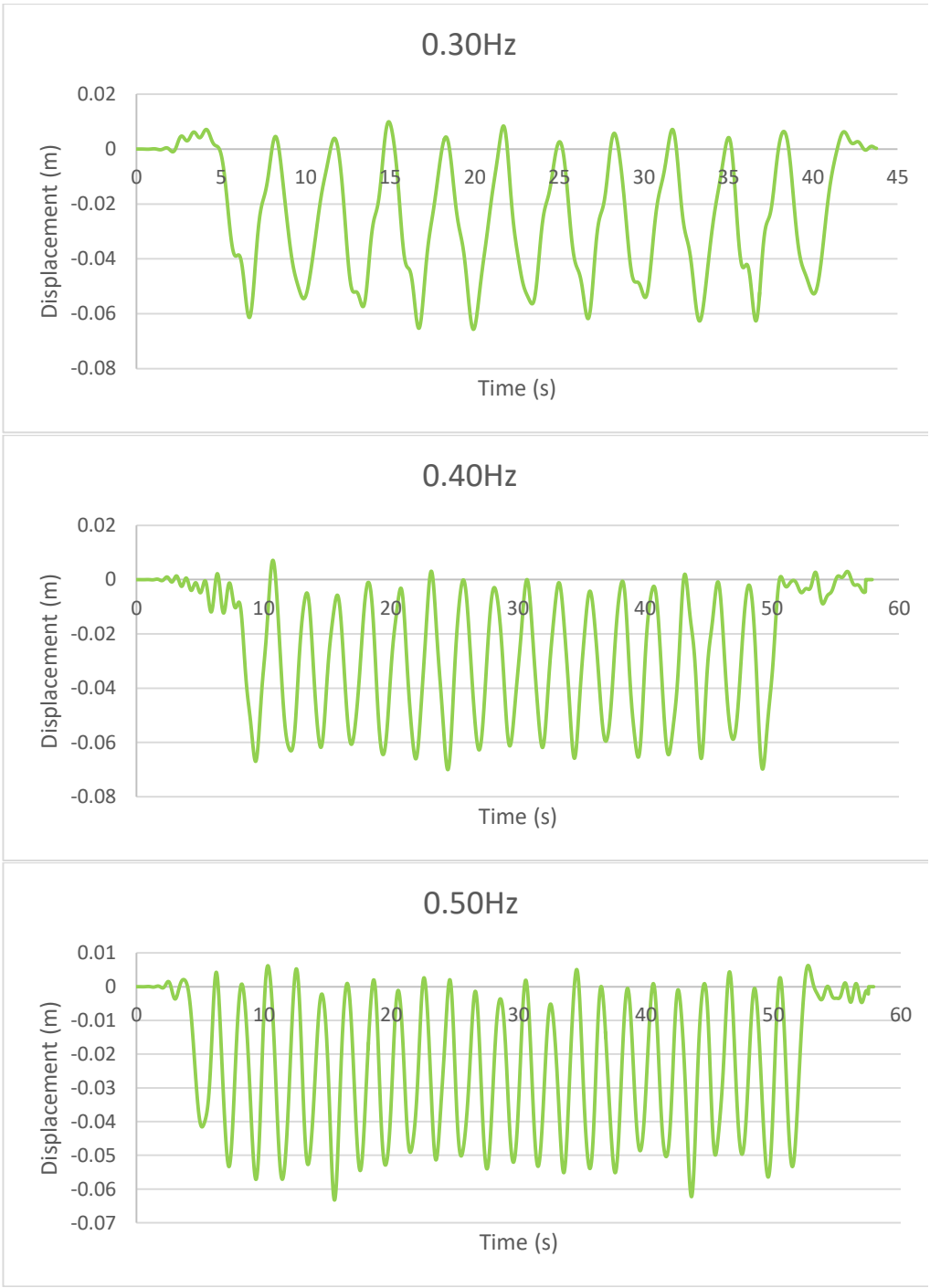

Figure 4.21: Processed Set 2 ultrasonic sensor readings of DWEC-structure displacement over time for the frequency point of 0.30, 0.40 and 0.50Hz with operating DWEC.

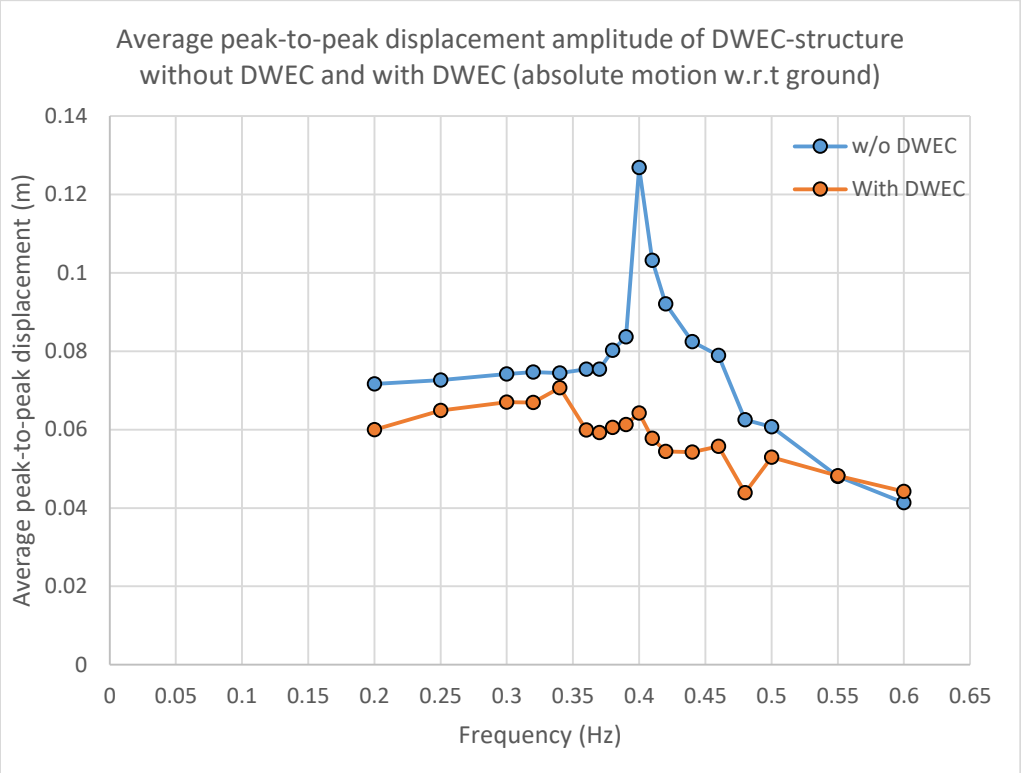

Figure 4.22: Graph of comparison between average peak DWEC-structure displacement with DWEC and without DWEC over frequency range.

Figure 4.22 shows the comparison of average peak-to-peak displacement of the DWEC-structure with and without operating DWEC. To better explicate the effect of the DWEC on the system motion, a graph of displacement reduction with the DWEC is plotted by computing the percentage difference in terms of the average peak-to-peak displacement using the formula $R(\%) = \left(\frac{disp_{without\ DWEC} - disp_{with\ DWEC}}{disp_{without\ DWEC}}\right) x\ 100\%$ for each frequency points. As seen from the plotted graph in Figure 4.23, the DWEC is capable of reducing the oscillating motion of the system within the frequency range of 0.36-0.46Hz by at least 20% and achieved a maximum displacement reduction of 49% at the resonance frequency of the DWEC-structure. However, as the plot goes further the reduction percentage drops rapidly as frequency increases over the 0.48Hz

mark, and eventually reaches an increase in displacement value of 7% at 0.60Hz. Therefore, the DWEC in experiment Set 2 performs as intended as it is capable of suppressing externally induced vibration at its operating frequency as designed. In comparison to the result obtained in Set 1, the maximum displacement reduction at frequency 0.40Hz is slightly lower than the 58% obtained in Set 1. This is due to the slightly larger weight of the DWEC-structure caused by added air chamber section, and also the theoretical resonant frequency for Set 2 prototype is around 0.39Hz which is slightly lower than that of 0.40Hz in Set 1.

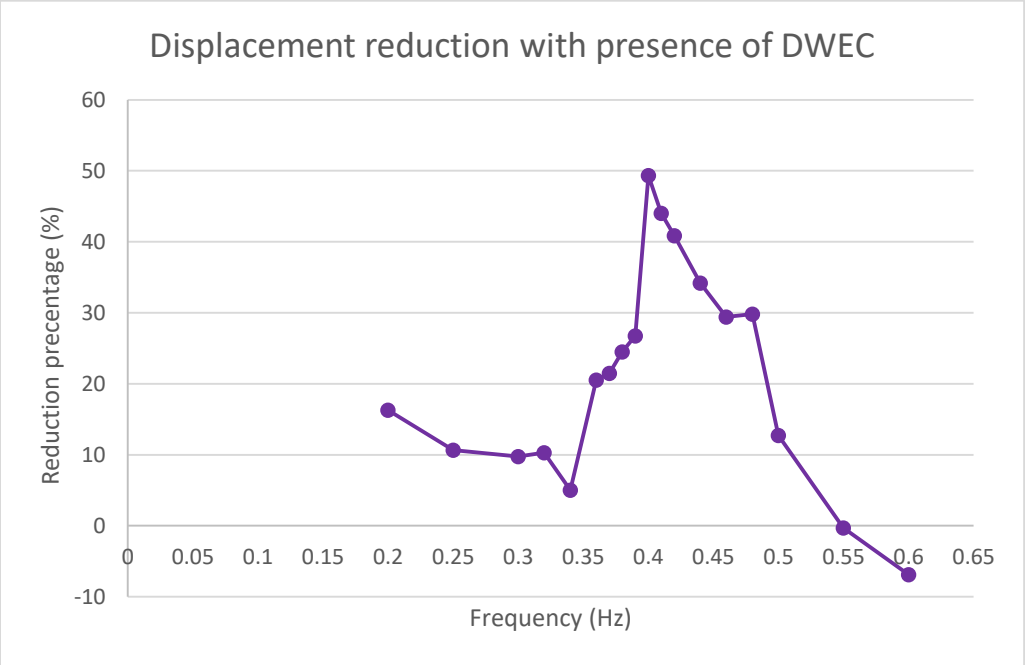

Figure 4.23: Graph of DWEC-structure displacement reduction with operating DWEC.

4.3.2 Energy Generation Set 2

In this section, the results from collected data on water height changes within the DWEC column and the air turbine are tabulated and analysed.

In Figure 4.24, three sets of raw ultrasonic sensor data for frequency points of 0.30, 0.38 and 0.50Hz are displayed in such order. As observed, the data are riddled with high frequency noises as well as some erratic readings that are easily distinguishable from the plotted graphs. As per procedure, the data are processed with correct methods as previously applied to provide a clarified and standardized version of ultrasonic data for further analysis.

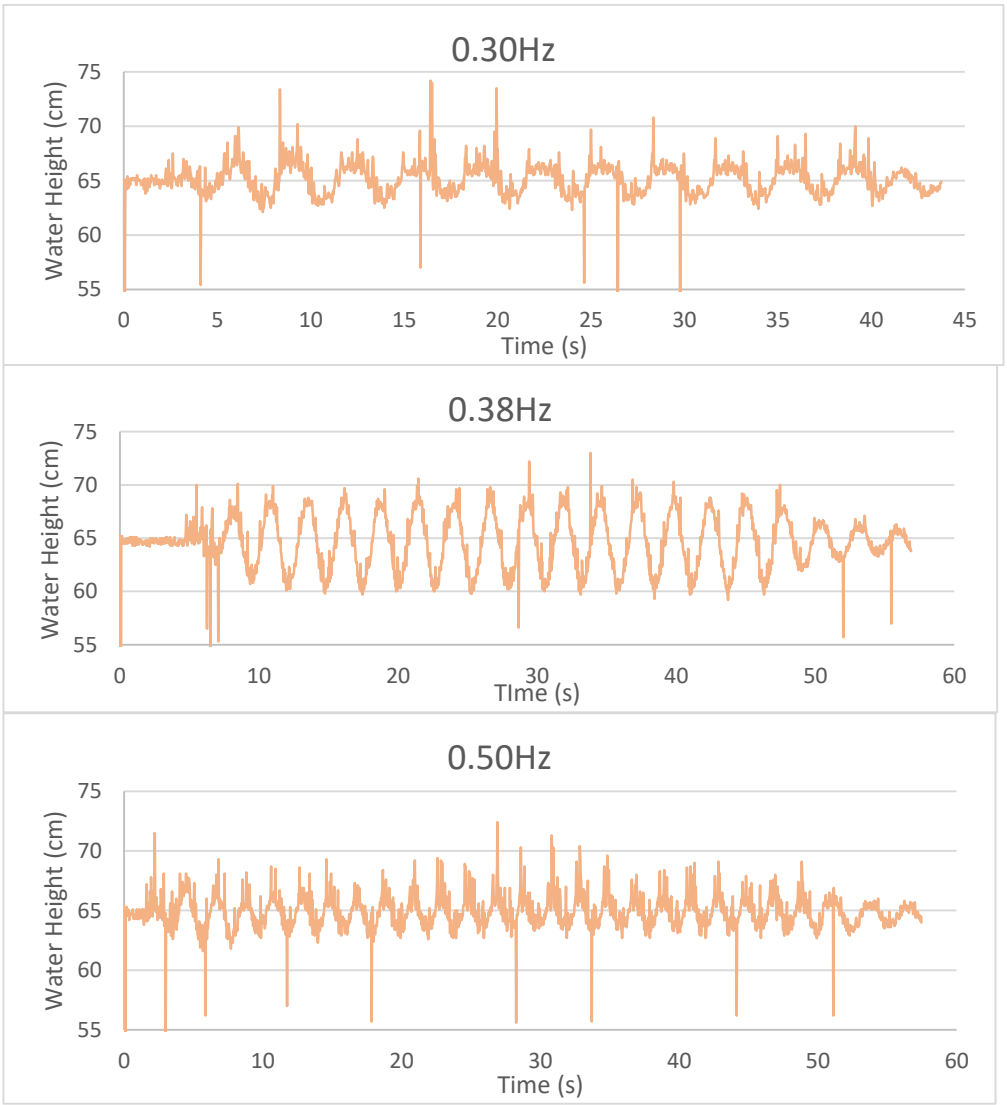

Figure 4.24: Set 2 ultrasonic sensor data for water height changes within DWEC column for frequency point of 0.30, 0.40 and 0.50Hz.

The three sets of processed data are as displayed in Figure 4.25. The data readings are visibly cleaner and easier to quantify the difference between the data for each frequency points. With all the data processed, the average peak-to-peak water height changes for all frequency points are then compiled and plotted in Figure 4.26.

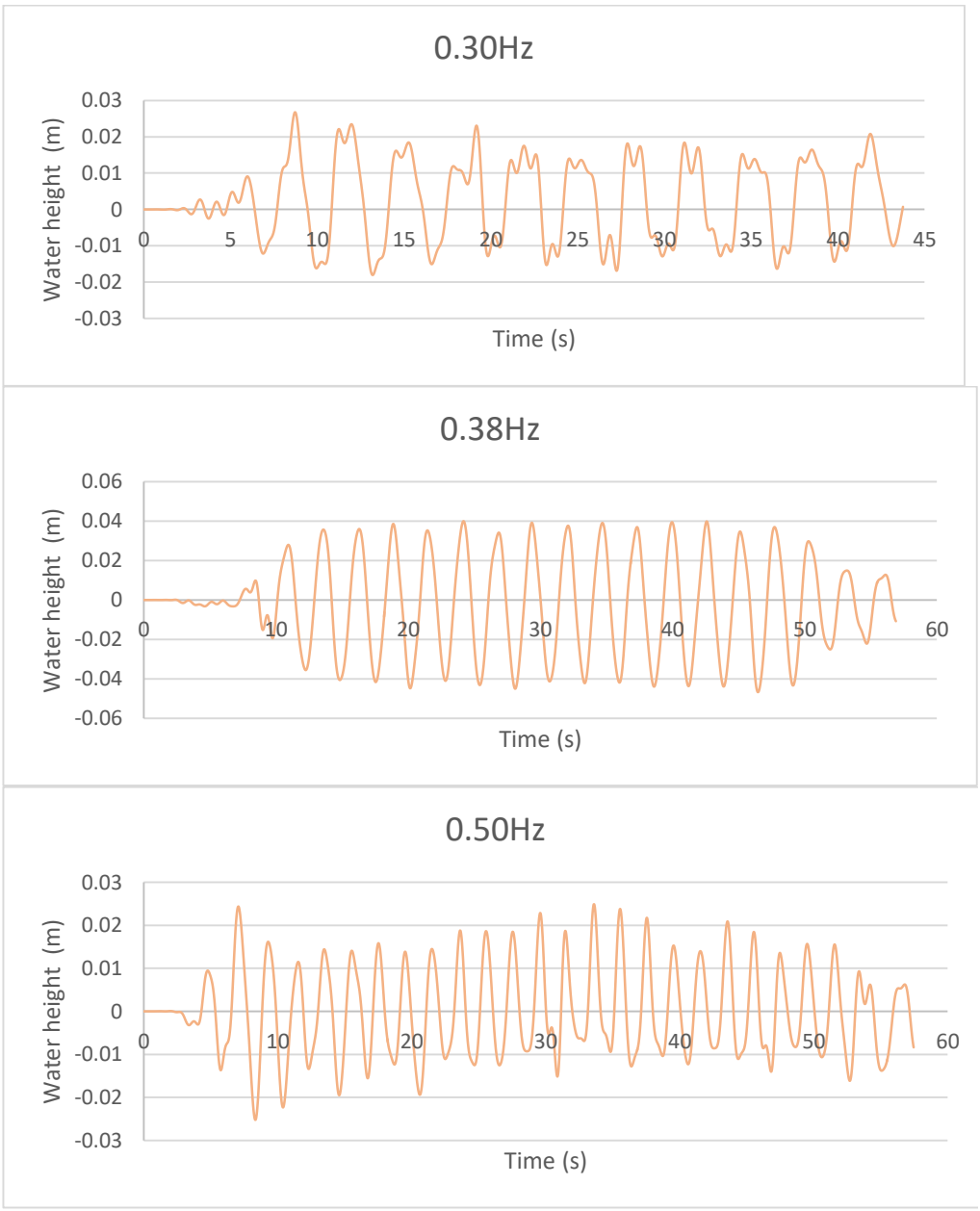

Figure 4.25: Processed Set 2 ultrasonic sensor data for water height changes within DWEC column for frequency point of 0.30, 0.40 and 0.50Hz.

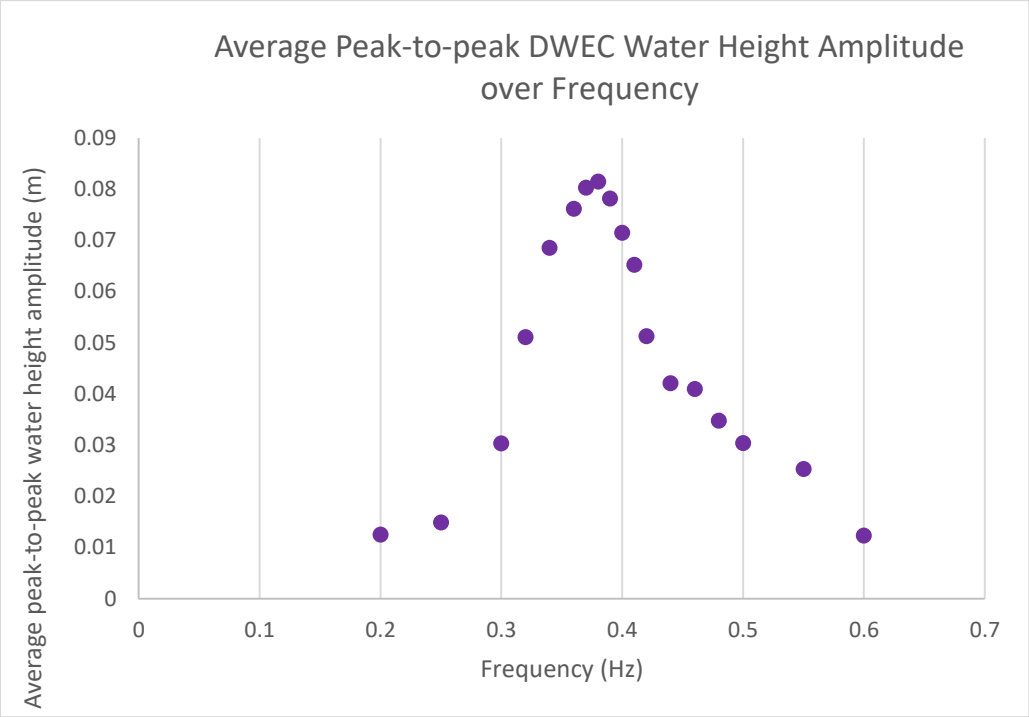

Figure 4.26: Graph of peak water height changes within the DWEC column over frequency range.

As observed in Figure 4.26, the average amplitude of the oscillating water level within the DWEC column increases exponentially as the input frequency increases and reaches the highest measured amplitude value of 0.0815m at the frequency point of 0.38Hz, and finally falls off towards the end. As the frequency of the induced vibration increases, the motion force exerted upon the DWEC-structure increases as well, especially around the natural frequency of the DWEC-structure at 0.40Hz. Thus, with the presence of an effectively tuned DWEC that matches closely with the natural frequency of the DWEC-structure, the more the motion energy is absorbed by the sloshing water within, hence the larger the change in water height. Up next, the air turbine data are collected and the average turbine rotational velocity as recorded by the IR sensor are tabulated and plotted in Figure 4.27.

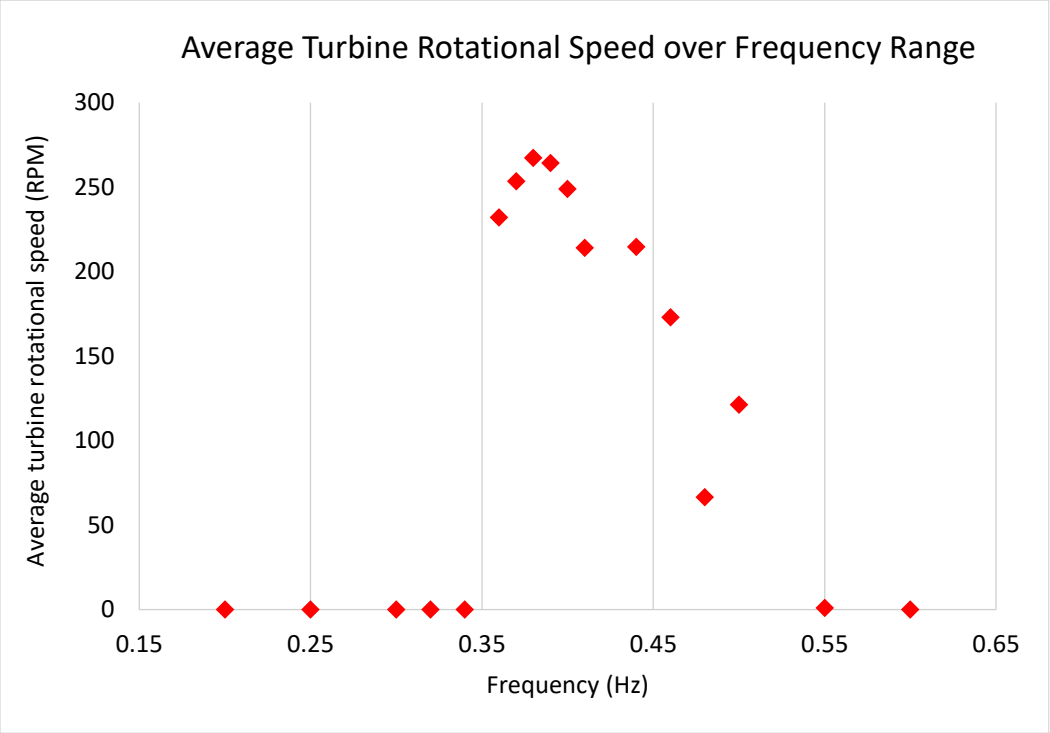

Figure 4.27: Graph of average turbine rotational speed over frequency range.

As shown from the graph in Figure 4.27, 0 rotation per minute (rpm) of the air turbine is measured from the frequency 0.20-0.34Hz and after that, an abrupt leap from 0 to 231 rpm is seen at the frequency point of 0.36Hz and continually increases to the peak at 0.40Hz where the maximum rotational speed of 267 rpm is obtained before steadily declined thereafter until 0.55Hz where no rotational speed is recorded again.

Therefore, it is apparent that the rotational speed of the mounted air turbine is directly impacted by the change in water height within the water column, since the higher the change of water height within an oscillation cycle, the greater the compression effect that pushes the confined air within the water

column through the air turbine chamber. Case in point, the maximum rotational speed of 267rpm (or 28 rad/s) is recorded at the frequency point of 0.38Hz, the point where the maximum water height change is measured. It is also deduced that at the frequency range below 0.36Hz and above 0.50Hz, the drag force generated by the relatively low speed air flow through the air turbine chamber due to the smaller change in water height is insufficient to drive the turbine to overcome its inertia to rotate.

With the collected air turbine rotational speed data, the amount of generated turbine power can be computed. The calculation method is organized and explained in details in the following section. The turbine power is calculated using the equation:

$$P = \tau\omega \tag{4.3}$$

Where τ denotes the torque (Nm) exerted onto the turbine about its center of gravity and ω denotes the angular velocity (rad/s) of the turbine. The data for angular velocity, ω of the air turbine are collected from the conducted experiment. To calculate the torque, τ the following equation is used:

$$\tau = f_{airflow} r_{turbine} \tag{4.4}$$

Where the r denotes the turbine radius and the f denotes the force exerted by air flow upon the turbine blade surfaces and is computed using the equation:

$$f = \frac{1}{2}\rho V^2 A \tag{4.5}$$

Where V is the air flow velocity and A represents the area of impact or in this case, the surface area of the turbine blades. The air flow velocity enters the air

chamber can be calculated using the continuity equation $V_1A_1 = V_2A_2$ by relating the velocity of air flow within the air column that is equal to the change in water level during the oscillation cycle to the air flow that enters the chamber. The average turbine power for each frequency point during the experiment are computed and plotted. As the air turbine operates similarly to that of a wind turbine, the maximum extractable power from the air turbine, or known as the Betz limit, can be calculated using the equation:

$$P_{max} = 0.593(\frac{1}{2})\rho AV^3 \quad (4.6)$$

With that, the average turbine power and the maximum theoretical power are plotted together in Figure 4.28. From the experimental result, a peak turbine power of 2.87mW is measured at the frequency point of 0.38Hz with about 48% efficiency in comparison to the theoretical peak power available at the frequency point. This shown that the air flow that is generated during the sloshing motion of the water within the DWEC column at its operating frequency can be utilized to harness energy using an air turbine.

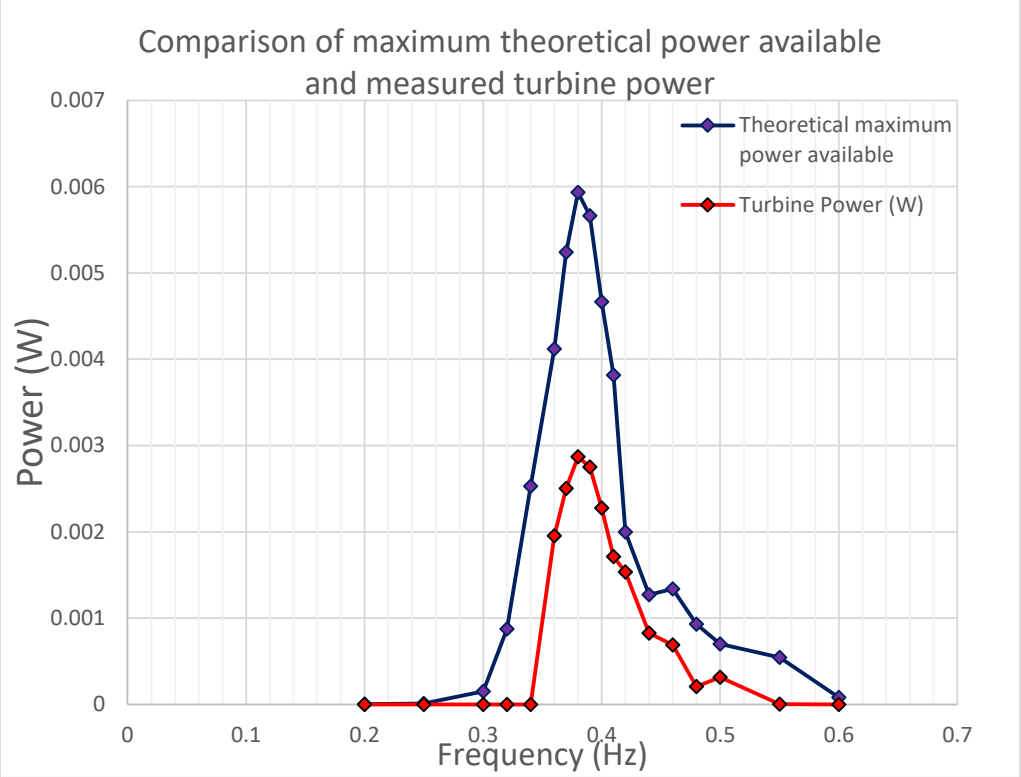

Figure 4.28: Graph of measured turbine power compared with theoretical maximum power available.

4.4 CFD Simulation

In this section, the CFD simulation results are compiled and analysed in accordance to the procedure that is laid out during the methodology section.

4.4.1 DWEC Design Validation

To first validate the DWEC design and its operating frequency with a more scientific approach, a set of transient fluid-flow simulations are completed using the selected CFD software Ansys Fluent to study the vibrational motion of the 1:1 scale 3D DWEC model. The simulated DWEC model is as shown in Figure 4.29. After the simulation data are collected, the peak-to-peak change in water

height amplitude obtained from simulation for each frequency point is charted against the experimental data in Figure 4.30.

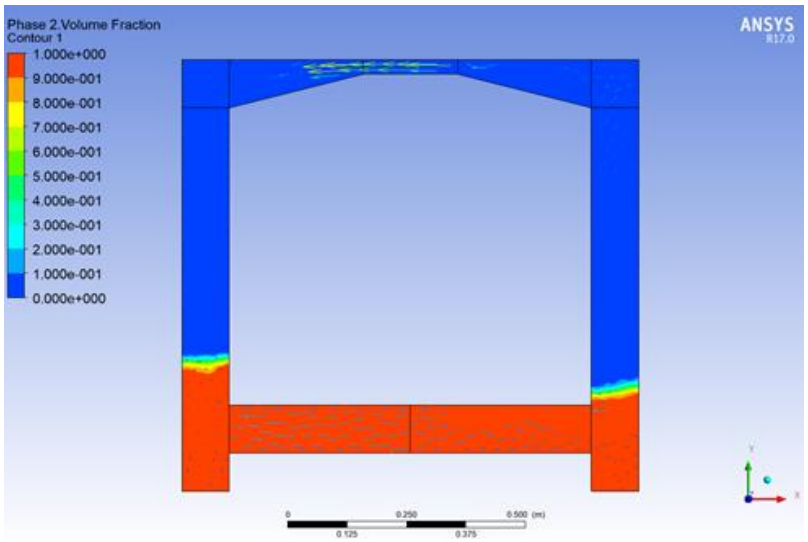

Figure 4.29: Side view of the simulated DWEC model in CFD post-processing.

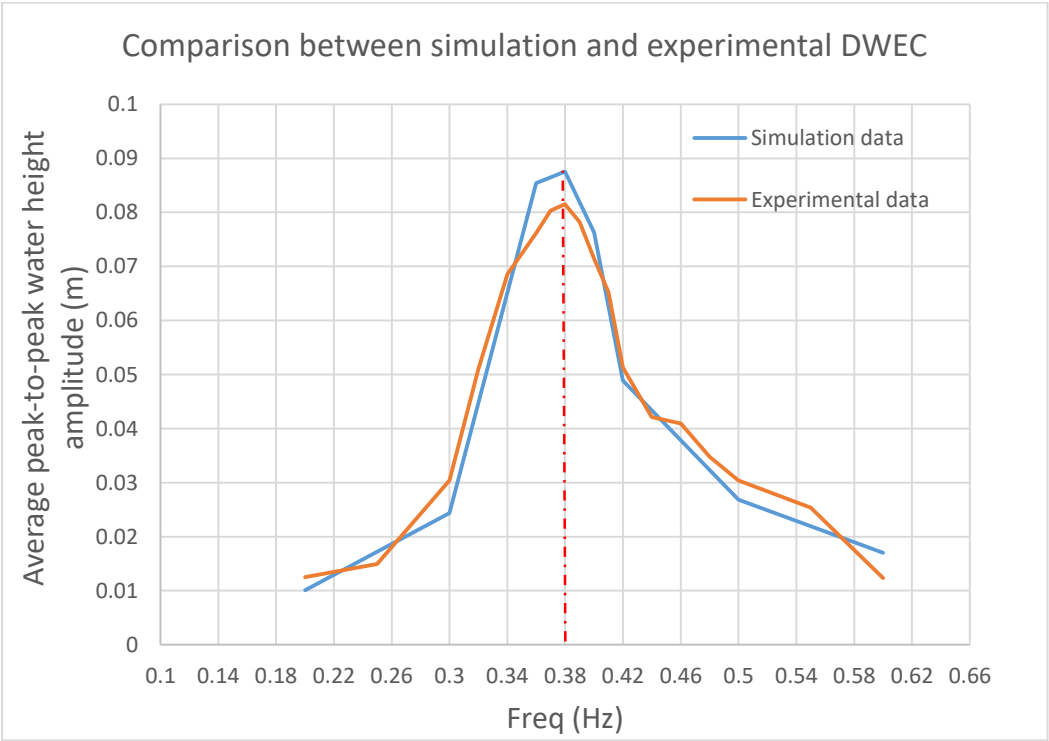

Figure 4.30: Graph of plotted simulation and experimental data of average peak water height changes over frequency range.

As observed from the water displacement result, the simulated DWEC model displays identical vibrational behaviour as the constructed DWEC prototype in which both resonant frequencies occurred at 0.38Hz as designed. Despite a slight 6% higher peak amplitude of 0.087m can be observed for the ideal simulation data in comparison to the experimental data, both data curves fit relatively well with each other. Hence the DWEC model design here is validated and operating as intended.

4.4.2 Energy Generation CFD

In this section, the performance of the simulated well turbine in the DWEC model in terms of energy generation is tabulated and studied. As previously established in the experiment set 2, the frequency point 0.38Hz is opted for the setup of CFD simulation since it is the point where the largest water height changes occurred and hence the point of interest for the study to obtain the largest extractable energy from the current DWEC design.

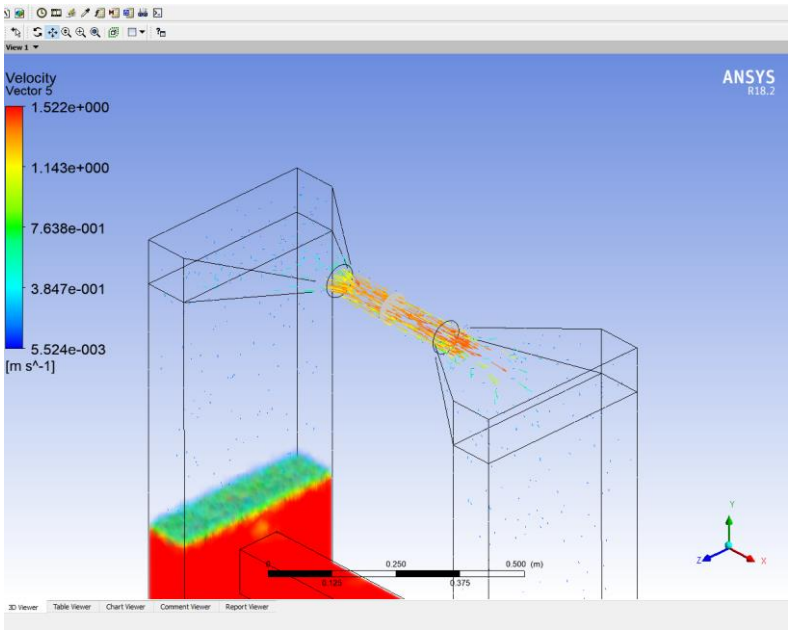

Figure 4.31: Illustrated air flow across the upper duct during the simulation.

In the first part of the simulation, the data of velocity of air flow across the upper duct where the turbine is installed are collected. Using the CFD post-processing, the air flow through the upper cylindrical duct is visualized with vector plotting is displayed here, where the average air flow velocity across the middle cross-section as defined by user is recorded during every time steps. The air flow data is then plotted along with the water height changes in the DWEC column in Figure 4.32.

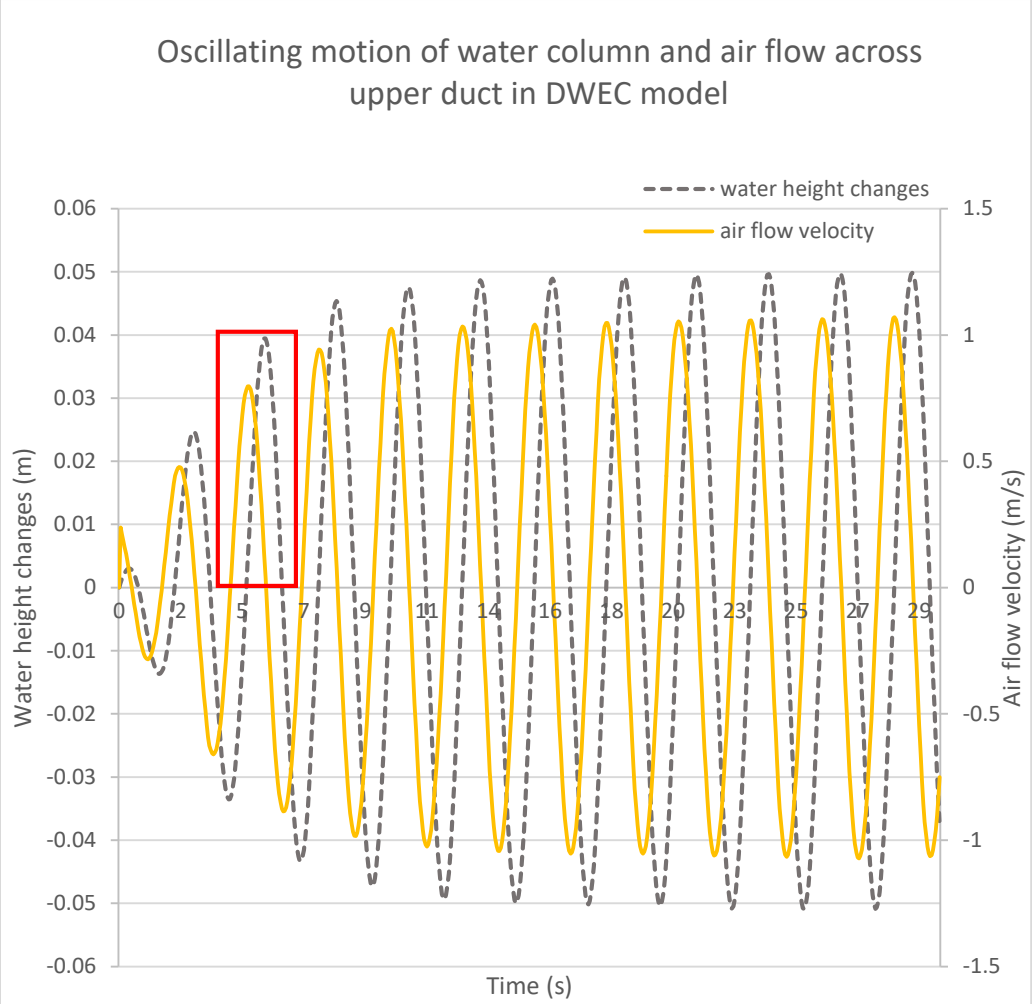

Figure 4.32: Graph of combined water height changes and air flow velocity across upper duct over time.

As observes, both the air flow velocity (gold-line) and water height changes (dashed-grey) data curves increases gradually during the initial transient period and eventually reaches their respective peak motions in the steady-state period around after 20s mark. During one half of the oscillating cycle as sampled in the red squared section, the air flow velocity reaches peak value about half way through the accelerating flow of sloshing water similar to that of a sine wave, and as the sloshing water reaches its peak height, the air flow velocity slows down closing to zero and began to accelerate in the opposite

direction as the water flow towards another side of the DWEC column in the next cycle. The average peak velocity of the air flow across the duct is measured at 1.066 m/s. As previously explained in the methodology, the air flow data will be applied as the inlet and outlet flow values for the second part of experiment where the well turbine is simulated.

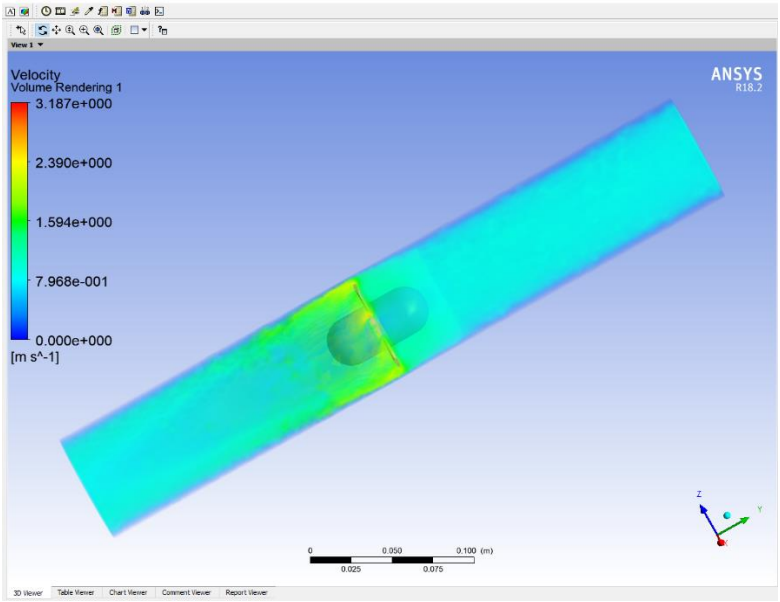

Figure 4.33: Air flowing through the air turbine in –y direction as illustrated in CFD post-processing.

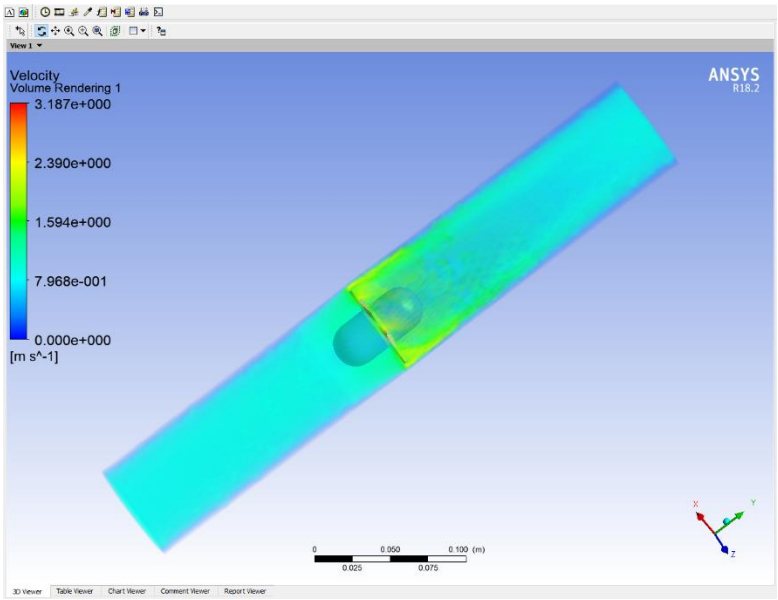

Figure 4.34: Air flowing through the air turbine in +y direction as illustrated in CFD post-processing.

In part 2, the modelled air turbine is simulated and the results obtained are compiled and studied here. The two way air flow through the air turbine can be observed in Figure 4.33 and Figure 4.34. The rotational motion of the air turbine is recorded every time-step and written to a motion history file. In the file, CG_X, CG_Y and CG_Z denote the rotational axis of the turbine motion (0, 1, 0) while THETA_Y represents the change in rotational angles of the air turbine about y-axis.

By converting the change in degree of the air turbine motion into radian, the rotational velocity (rad/s) of the turbine can then be calculated by dividing the change in radian between two consecutive time-steps by the time difference between the two steps. With that, the rotational velocity of the simulated air turbine is plotted as follow. As observed, the wave-like data curve indicates that the air turbine velocity oscillates as the air flow changes direction every half a cycle as the DWEC operates, while the general turbine rotational velocity accelerates over time and gradually slows down as time goes.

Although the simulated air turbine motion has yet to reach steady-state as it still slowly speeds up over time as shown in Figure 4.35, the maximum velocity can be predicted using extrapolation method by plotting a fitting curve based on the obtained data. Therefore, the maximum rotational velocity of the air turbine at steady-state measured is 62.57 rad/s or 597 rpm at time-step of about 100s.

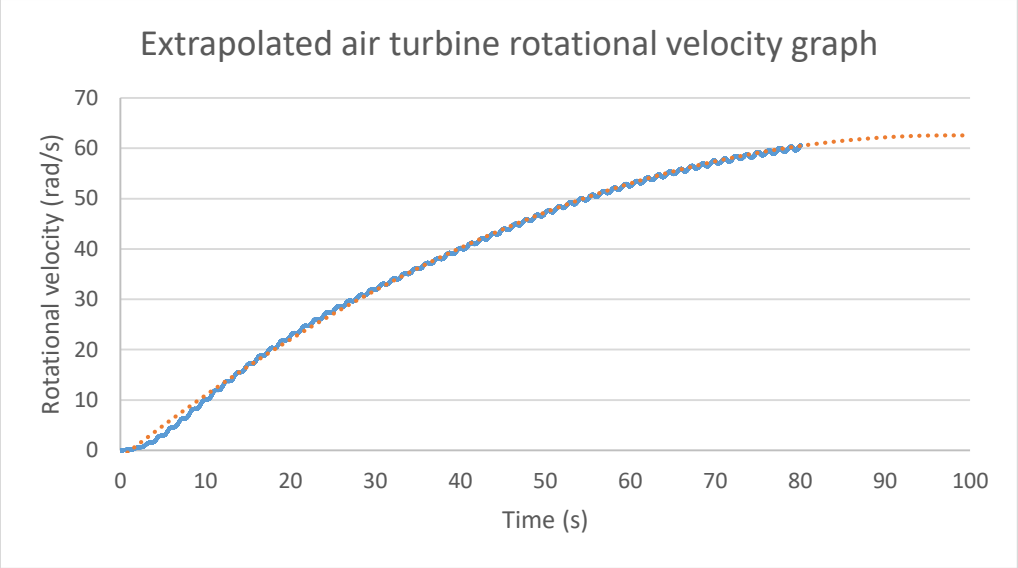

Figure 4.35: Graph of air turbine angular velocity over time (blue line) and the extrapolated angular velocity (dotted orange line).

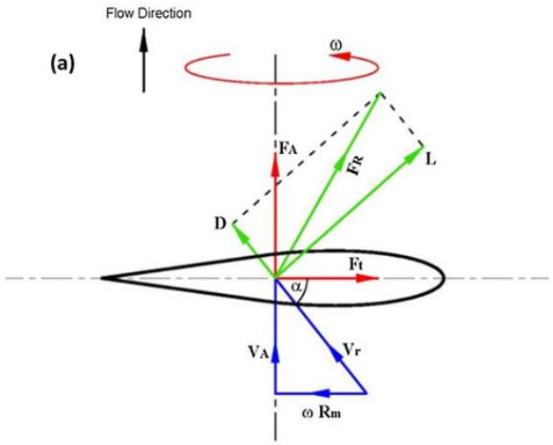

Figure 4.36: Aerodynamic forces acting on the turbine blade (Shehata et al., 2016).

To calculate the turbine power, the resultant tangential force, F_t exerted on the turbine blade as indicated in Figure 4.36, can be calculated using the equation:

$$F_t = L \sin \alpha - D \cos \alpha \qquad (4.7)$$

Where L is the lift force and D is the drag force generated on the turbine blade, and staggle angle, α = 90°. Thus, the maximum force acted on the turbine can be calculated by determining the lift force at the point where the air flow across the turbine reaches peak steady-state velocity after the 20s mark as previously discussed. To that end, the ANSYS Fluent provides the solution monitoring functions that can report and display the force values on the selected body or face. With that, the lift force of the turbine at peak air flow velocity is measured at 7.6 x 10^{-3} N. From here, the maximum turbine power is calculated using the similar equation from experiment Set 2 and the obtained value is as shown below:

$$P = F_t r_{turbine}\, \omega = 0.0076(0.015)(62.57) = 7.133mW$$

Therefore, a peak turbine power of 7.133mW is generated from the simulated air turbine model where the air flow is interchanging from one end to another as the DWEC oscillates from the induced vibration. In comparison to the result obtained in experiment set 2, the power generated by the simulated well turbine is ~2.5 times greater than that generated by the air turbine.

CHAPTER 5

CONCLUSION

5.1 Conclusion

In this study, a damping wave energy converter (DWEC) prototype is designed and constructed that adopts similar design from conventional tuned liquid column damper (TLCD) and integrated with operating mechanism of an oscillating wave column (OWC).

The DWEC prototype is tested for its ability to suppress externally induced vibration by mounting it to a moving structure and subjected to a series of vibration with a set frequency range using shaking table. The results shown that it is capable of reducing vibrating motion to a significant percentage of 49-58% within the frequency range of 0.36-0.46Hz about its operating frequency of 0.385Hz as designed.

In the experiments, three sets of DWEC energy generating mechanism designs are tested and studied for their feasibility. In the first design set, the hydro turbines installed along two sets of pipeline below the water level was not able to harness meaningful energy from the flowing motion of water in the DWEC during oscillatory motion due to insufficient water flow rate to drive the turbine. In the second DWEC design set, the drag-type vertical-axis air turbine

that is installed in a connecting duct that connects the top ends of the DWEC columns is capable of generating a maximum turbine power of 2.87mW at the peak operating frequency point 0.38Hz of the DWEC. Lastly, the third DWEC design set is simulated using commercial CFD software ANSYS Fluent in which a well turbine with round hub is installed along a cylindrical duct that connects the top ends of both the DWEC columns similar to the second design. The simulation result shown that the designed well turbine is capable of generating turbine power of 7.133mW at the peak operating frequency 0.38Hz of the DWEC. Therefore, the tested drag-type vertical-axis air turbine and the well turbine are capable of harvesting energy from the oscillatory motion of the water within the DWEC when subjected to externally induced vibration.

In summary, the DWEC prototype is capable of suppressing vibrating motion induced by external source effectively within its operating frequency range while energy can be harnessed from the resultant sloshing water motion within by means of installed air turbine that extract power from the driven air flow confined within the closed environment of the DWEC columns.

5.2 Limitation of Study

The study has some limitations in terms of boundary of work and tools availability. As of now, the study focuses only on the wave condition in Malaysia Waters for prototype design purpose. Without a wave tank facility, the prototype is tested using shaking table that is available within the campus facility and can only generate single degree of freedom motion. Whereas a wave

tank can generate 3D wave motion and simulates real wave conditions with selected amplitude, frequency and regularity.

5.3 Recommendation for Future Work

To further improve the project outcome and enhance the performance of the prototype. In future, the prototype experiments should be performed using proper laboratory-use wave basin. With that, realistic ocean wave motions can be simulated using wave basin to provide further insights to the development of the DWEC in terms of stabilization and energy generation performance under real wave conditions.

PUBLICATION

Wong, Y. H., King, Y. J., Lai, A. C., Chong, K.K. & Lim, B. H., 2017. Feasibility study of tuned liquid column damper for ocean wave energy extraction. *AIP Conference Proceedings, 1828.*

REFERENCES

Ahmed, Y. M., Mazukee, U. J. A., Yaakob, O. B., & Elbatran, A. H., 2014. Wells Turbine for Wave Energy Conversion for Malaysian Ocean. *Journal of Ocean, Mechanical and Aerospace*, 6.

Akmal, N., Zamri, M., Ibrahim, T., and Nor, N. M., 2016. Design and Modelling of Generator for Wave Energy Conversion System in Malaysia. *International Journal of Simulation Systems, Science & Technology,* 17, pp. 41.

Antonio F. O. and Joao C.C., 2015. Oscillating-water-column wave energy converters and air turbines : A review. *Renewable Energy,* 85, pp. 1391-1424.

Astariz, S., and Iglesias, G., 2015. The economics of wave energy : A review. *Renewable and Sustainable Energy Reviews,* 45 (2015), pp. 397–408.

Avril. T., 2007. *Water to tame wind atop new skyscraper* [Online]. Available at: http://articles.philly.com/2007-04-15/news/24993416_1_tallest-building-water-tanks-tame-wind [Accessed: 10 Aug 2016]

Blažauskas, N., Pašilis, A. and Knolis, A., 2015. Potential applications for small scale wave energy installations. *Renewable and Sustainable Energy Reviews,* 49, pp. 297-305.

Brito-Melo A., Neumann F. and Sarmento A.J.N.A., 2007. Full-scale Data Assessment in OWC Pico Plant. *Proceedings of The Seventeenth International Offshore and Polar Engineering Conference.*

Caineng, Z., Qun, Z., Guosheng, Z., and Bo, X., 2016. Energy revolution : From a fossil energy era to a new energy era. *Natural Gas Industry B,* 3(1), pp. 1–11.

Chen, A., and Laflamme, S., 2017. A novel tuned liquid wall damper for multi-hazard mitigation. *Civil, Construction and Environmental Engineering Conference Presentations and Proceedings*. Pp. 66.

Chiang. E. P., Zainal. Z. A., Narayana. A., & Seetharamu. K. N, 2003. Potential of Renewable Wave and Offshore Wind Energy Sources in Malaysia. *Marine Technology Seminar 2003*.

Colwell, S., and Basu, B., 2009. Tuned liquid column dampers in offshore wind turbines for structural control. *Engineering Structures,* 31(2), pp. 358–368.

Connor. J, 2003. Introduction to structural motion control. *Upper Saddle River, N.J.: Prentice Hall Pearson Education.*

Czech, B., and Bauer, P., 2012. Wave energy converter concepts : Design challenges and classification. *IEEE Industrial Electronics Magazine*, 6(2), pp. 4–16.

Di, A., Thomas, M., Adam, C., and Pirrotta, A., 2018. Optimal design of tuned liquid column dampers for seismic response control of base-isolated structures. *Acta Mechanica,* 229(2), pp. 437–454.

Drew, B., Plummer, A. R., and Sahinkaya, M. N., 2009. A review of wave energy converter technology. *Proceedings of the Institution of Mechanical Engineers, Part A: Journal of Power and Energy*, 223(8).

Ec.europa.eu., 2018. *Eurostat - Tables, Graphs and Maps Interface (TGM) table* [Online]. Available at: http://ec.europa.eu/eurostat/tgm/table.do?tab=table&init=1&language=en&pcode=t2020_31&plugin=1 [Accessed: 12 Jun 2018]

Falcao AFO and Gato L.M.C., 2012. Air Turbines. *Comprehensive Renewable Energy*, 8, pp. 111-149.

Gao, H., Kwok, K. C. S., & Samali, B., 1997. Optimization of tuned liquid column dampers. *Engineering Structures,* 19(6), pp. 476–486.

Glotmansimpson.com, 2016. *One Wall Centre – Glotman Simpson.* [Online]. Available at: https://glotmansimpson.com/project/one-wall-centre/ [Accessed: 10 Aug 2016]

Gunn. K., and Stock-Williams. C, Quantifying the global wave power resource. *Renewable Energy*, 44(2012), pp. 296-304.

Hanimann, L., & Mangani, L. (2018). Application of CFD in Indonesian Research : A review. *Journal of Physics: Conference Series*, pp. 1005.

Heath, T. V., 2012. A review of oscillating water columns. *Philosophical Transactions of the Royal Society A: Mathematical, Physical and Engineering Sciences*, 370(1959), pp. 235–245.

Ionut, C., 2015. CFD Simulation Approach for Semisubmersible Response in Waves Based on Advanced Techniques. *Applied Mechanics and Materials*, 772 (2015), pp. 108-113.

Jianbing, C., Youkun, L., and Xueyuan, B., 2015. Shaking table test and numerical analysis of offshore wind turbine tower systems controlled by TLCD. *Earthquake Engineering And Engineering Vibration*, 14(1), pp. 55–75.

Katsuhiko O., 2005. *System Dynamics*, 4th ed. University of Minnesota, pp. 617.

Lee, H. H., and Juang, H. H., 2012. Experimental study on the vibration mitigation of offshore tension leg platform system with UWTLCD. *Smart Structures and Systems 9*, 1 (2012), pp. 71-104.

Lee, H. H., Wong, S. H., and Lee, R. S., 2006. Response mitigation on the offshore floating platform system with tuned liquid column damper. *Ocean Engineering*, 33(8–9), pp. 1118–1142.

Lewis, A., Estefen S., Huckerby J., Musial W., Pontes T. and Torres-Martinez J., 2011. Ocean Energy. *IPCC Special Report on Renewable Energy Sources and Climate Change Mitigation.*

López, I., Andreu, J., Ceballos, S., Martínez de Alegría, I. and Kortabarria, I., 2018. Review of wave energy technologies and the necessary power-equipment. *Renewable and Sustainable Energy Reviews*, 27 (2013), pp. 413–434.

Melikoglu, M., 2018. Current status and future of ocean energy sources: A global review. *Ocean Engineering*, 148, pp. 563-573.

Mensah, A. F., and Dueñas-osorio, L., 2014. Improved reliability of wind turbine towers with tuned liquid column dampers (TLCDs). *Structural Safety*, 47, pp. 78–86.

Min, K. W., Kim, H. S., Lee, S. H., Kim, H., and Kyung Ahn, S., 2005. Performance evaluation of tuned liquid column dampers for response control

of a 76-story benchmark building. *Engineering Structures*, 27(7), pp. 1101–1112.

Mork, G., Barstow, S., Kabuth, A., and Pontes, M. T., 2010. Assessing the global wave energy potential. *Proceedings of the 29th International Conference on Offshore Mechanics and Artic Engineering*, pp. 1–8.

Muzathik, A. M., and Ibrahim, M. Z., 2011. Ocean Wave Properties of Terengganu for Renewable Energy Potential. *Journal of Applied Science,* 11 (11), pp. 1895-1903.

Muzathik, A. M., Nik, W. B. W., Samo, K. B., and Ibrahim, M. Z., 2011. Ocean Wave Measurement and Wave Climate Prediction of Peninsular Malaysia. *Journal of Physical Science,* 22(1), pp. 77–92.

Nasir N. and Maulud K. N., 2016. Wave power potential in Malaysian territorial waters. *IOP Conference Series: Earth Environment Science,* 37.

Nicole J. and Eric O. (2010). *What is an Oscillating wave column* [Online]. Available at: https://owcwaveenergy.weebly.com/ [Accessed: 16 Sep 2017]

Power Technology (2011). *Mutriku Wave Energy Plant* [Online]. Available at: https://www.power-technology.com/projects/mutriku-wave/ [Accessed: 18 Sep 2017]

Reiterer, M., Hochrainer, M. J., and Engineer, S., 2004. Damping Of Footbridge Vibrations By Tuned Liquid Column Dampers : A Novel Experimental Model Set-Up. *21st Danubia-Adria Symposium on Experimental Methods in Solid Mechanics.*

RWDI, 2016. Comcast Center [Online]. Available at: http://rwdi.com/en_ca/projects/comcast-center [Accessed: 18 Aug 2016].

Samrat, N. H., and Ahmad, N. Bin., 2014. Prospect of Wave Energy in Malaysia. *IEEE 8th International Power Engineering and Optimization Conference 2014*.

Shehata, A. S., Xiao, Q., Saqr, K. M., and Alexander, D., 2016. Wells turbine for wave energy conversion : a review. *International Journal Of Energy Research (2016)*

Shum, K. M., Xu, Y. L., and Guo, W. H., 2008. Wind-induced vibration control of long span cable-stayed bridges using multiple pressurized tuned

liquid column dampers. *Journal of Wind Engineering and Industrial Aerodynamics,* 96 (2008), pp. 166–192.

Tamboli. A., 2005. Manhattans Mixed Construction Skyscrapers with Tuned Liquid and Mass. *CTBUH Research Paper.*

Tu J., Yeoh G. and Liu C., 2013. *Computational Fluid Dynamics: A practical approach,* 2nd ed. Butterworth-Heinemann.

Tummala, A., Kishore, R., Kumar, D., Indraja, V., and Krishna, V. H., 2016. A review on small scale wind turbines. *Renewable and Sustainable Energy Reviews*, 56, pp. 1351–1371.

Ve, J., and Gaile, L., 2015. Overview of tuned liquid dampers and possible ways of oscillation damping properties improvement. *Proceedings of the 10th International Scientific and Practical Conference,* 1, pp. 233–238.

Xu, B. Y. L., Samali, B., Member, A., and Kwok, K. C. S., 2007. Control of along wind response of structures by mass and liquid dampers. *Journal of Engineering Mechanics,* 118(424), pp. 20–39.

Yaakob, O., and Ahmed, Y. M., 2013. Model Testing of an Ocean Wave Energy System for Malaysian Sea. *World Applied Sciences Journal,* 22 (5), pp. 667-671.